Physical Aspects of Arc Welding

Study Group 212

1 September 1993

Glasgow (UK)

Proceedings of seminar in honour of J.F. Lancaster

International Institute of Welding

Delftse Uitgevers Maatschappij

2342 6184

Physical Aspects of Arc Welding

Physical Aspects of Arc Welding

Proceedings of seminar in honour of J.F. Lancaster
1 September 1993, Glasgow (U.K.)

International Institute of Welding

Study Group 212 'Physics of Welding'

Editor: G. den Ouden

CIP-DATA KONINKLIJKE BIBLIOTHEEK, DEN HAAG

Physical

Physical aspects of arc welding : proceedings of seminar in honour of J.F. Lancaster,
1 September 1993, Glasgow (U.K.) / ed.: G. den Ouden. – Delft : Delftse Uitgevers Maatschappij. - Ill.
Publ. of the International Institute of Welding, Study Group 212 'Physics of Welding'. - With ref.
ISBN 90-6562-149-0
Subject headings: arc welding ; physical aspects.

Delftse Uitgevers Maatschappij b.v.
P.O. Box 2851, 2601 CW Delft, The Netherlands
Tel. 015–123725, telefax 015–143724

ISBN 90 6562 149 0

Preface

This volume contains the papers presented at a seminar held in honour of Prof. J.F. Lancaster on 1 September 1993 in order to mark the occasion of his retirement as Chairman of Study Group 212 (Physics of Welding) of the International Institute of Welding.

Prof. Lancaster was Chairman of Study Group 212 from 1965 to 1992.
During the long period of his chairmanship he was the driving force behind the many activities of the Study Group. He organised numerous meetings, stimulated many discussions on a variety of topics within the area of physics of welding and succeeded in bringing and keeping together a group of experts in the field from many different countries. He made Study Group 212 what it is today: a unique scientific forum for the physics of welding.

The theme of the seminar was 'Physical aspects of arc welding' and the papers presented cover the following topics: gas tungsten arc diagnostics, cathode phenomena in gas tungsten arc welding, the influence of ambient pressure on the arc welding process, arc ignition behaviour in gas metal arc welding, electrode melting in arc welding and weld pool behaviour.

The members of Study Group 212 offer this volume to Prof. Lancaster in recognition of his stimulating activities in the field of physics of welding over a period of many years.

G. den Ouden
Chairman Study Group 212
Delft, January 1994

Contents

The History of Study Group 212

J.F. Lancaster

The start

In 1962, as part of its annual Autumn Meeting, the Institute of Welding organised a Symposium entitled *Physics of the Welding Arc*. This meeting, held at the Institute's headquarters in London, was very successful and attracted a number of delegates from other countries. One of those attending from Russia was Professor N.N. Rykalin of the Baikov Institute in Moscow. Rykalin suggested that it would be profitable for the International Institute of Welding to provide means for continuing the work of this conference, and with commendable speed the secretariat of IIW set up Study Group 212, which had its first meeting in November 1962. The arrangements for this group differed from that of a commission; member societies were only entitled to appoint delegates if their country was actively engaged in the study of arc physics. Also, it reported to the Executive Council rather than to the Governing Council. The curious number 212 derived from the notion that we would provide a service to Commissions II and XII. In practice relations with Commission XII have been very close, but with Commission II almost non-existent. This is not surprising, since apart from some very useful observations by Dr. Becker, the Study Group has not done much work on welding with coated electrodes.

Initially the Group was well-staffed. We had an honorary Chairman, Professor Rykalin, a Chairman, L.F. Defize, Vice Chairman J.F. Lancaster, General Secretary J.C. Needham and Technical Secretary F. Dennery. Time, and the needs of employers, eroded this organisation quite rapidly. Mr. Defize resigned in 1965, the Secretaries found other work and for most of its life the Group has survived with (until his death in 1985) Professor Rykalin as Honorary Chairman and (from 1965 to 1992) the present writer as Chairman. Professor G. den Ouden became Chairman in 1992.

For the first few years of its existence the Group organised an intermediate meeting in the spring and a second meeting during the week preceding the Annual Assembly. We were not permitted to meet during the Assembly lest the work of the Commissions be disrupted. Thus it happened that at the Delft Assembly in 1966 the Chinese delegation attended our pre-assembly meeting. During the following weekend one member of the Chinese group died under curious circumstances, there was a diplomatic incident and

the remainder of the Chinese delegation failed to attend the Assembly. Thus we were the only IIW working group to welcome a Chinese delegation for some years to come. Subsequently we have had good contributions from China and in 1980 a course on physics of welding was organised by Tianjin University.

At a later date the Study Group was permitted to meet during the Assembly itself. No untoward incidents have occurred as a result of this change.

The Lausanne colloquium

The first project undertaken by the Study Group was to prepare for a Colloquium on Physics of the Arc which was held during the 1970 Annual Assembly in Lausanne. To this end we started work on the preparation of a film of metal transfer in arc welding. This was eventually compiled by the Welding Institute at Abington, using high speed sequences contributed by several member societies, including a historic shot of workers at the Institut de Soudure making a film of stick electrode transfer before World War I using a hand-cranked camera.

The IIW film was well-received on its first presentation at Lausanne, and subsequently numbers of copies were sold, particularly in France. Marketing a film was an innovation for IIW, and its production was a considerable success for the Study Group.

The other material presented at Lausanne consisted of four interpretive reports on different aspects of welding physics. These, with the exception of the presentation on the electric arc, were not so successful. The initial intention had been to put these contributions together and to arrange for their publication. Reviewing the material after the Colloquium, it became clear that understanding of some of the basic phenomena was very inadequate. For example, although welding experts talked knowingly about the 'pinch effect' as a cause of metal transfer, a proper analysis of this effect was not available. At the time there appeared to be no advance on the calculations of E.F. Northrup, which were first presented in 1907. The case of plasma flow in the arc column was similar. Maecker had predicted the existence of such flows over twenty years earlier, but the fluid dynamics of the plasma jet had not yet been explored. Not surprisingly, in view of the lack of basic knowledge, the mechanism of metal transfer remained a mystery. So it was felt inadvisable to prepare any of the Laususanne material for publication, and the immediate endeavours were directed towards understanding the basic physics of fluid flow in welding.

Plasma flow

In fact we had already started work on plasma flow before the Lausanne meeting. This was clearly a magnetohydrodynamic phenomenon, so help was sought from

J.A. Shercliffe, who was the author of a textbook on the subject.

Professor Shercliffe attended some of our meetings and discussed the welding problem. As a result he published a paper in which the mechanics of flow due to a point source of current at the surface of a semi-infinite fluid was examined for the case where the viscosity was zero. Although this condition is unrealistic, it was a start, and the problem was then picked up by C. Sozou and his colleagues. As a consequence, during the period 1971 to 1975, the character of electromagnetically-induced flow was determined for a point source of current, for a distributed source, and for the case where the flow occurred inside a hemispheroidal container. These results make it possible to obtain a sound basic understanding of the nature of electromagnetically-induced flows. They also show that where the surface flow is directed inwardly towards the origin (i.e. the axis of the jet) it may become unstable, whereas if it is directed outwards across the surface it is stable for all values of the driving force. This conclusion is important in relation to the problem of variable penetration in stainless steel TIG welds.

The pinch effect

During the same period (the early 1970s) Professor Herlofson of the Technical University, Stockholm joined the group, and introduced us to the work of his colleagues on instabilities in liquid cylinders carrying an electric current. This work had been initiated by H. Alven, an astrophysicist, with the object of modelling certain celestial processes – the condensation of matter to form stars in the spiral arcs of galaxies being a possible example. Experiments were made with falling columns of mercury, whilst at the same time the theory of instabilities in liquid cylinders carrying an electric current was developed by Murty, an Indian physicist who worked for a period in Stockholm. Murty ended Rayleigh's analysis of capillary instabilities to the case where there are electromagnetic forces. For such conditions there is a hierarchy of unstable modes, designated by $m = 0, 1, 2$ etc. The simplest mode ($m = 0$) is the cylindrical pinch, where constrictions form at intervals along the cylinder, which eventually disperses into drops. Higher modes are promoted by a higher current density and by the presence of a longitudinal magnetic field. The theory provides a good qualitative description of the various transfer modes in GMA welding. The pinch instability dominates in the spray arc transfer mode, where drops are detached individually and projected across the arc; also in pulse-arc welding. The kink instability ($m = 1$) in which the cylinder collapses into a rotating spiral, occurs in 'rotating' welding and in the plasma-MIG process. The flute instability ($m = 2$) occurs when a longitudinal magnetic field is applied to high-current MIG; the rotating spiral disappears and instead the liquid drop at the electrode tip splits longitudinally and two drops detach simultaneously. A quantitative result is not to be expected, firstly because the Rayleigh-type analysis is an approximation that only applies to small displace-

ments, and secondly because there are many complicating factors; for example, the arc root tends to spread over the whole surface of the drop in the spray transfer mode. Nevertheless, Murty's work was felt at the time to provide a firm basis for understanding the various metal transfer modes in MIG welding, and subsequent experience has reinforced that view.

Physics of welding

The notion of producing a book on welding physics was a natural result of all this theoretical activity. Work started in 1972, but progressed rather slowly until 1979 when increased confidence in the analytical work together with an accumulation of research data made it practicable to finalise the text. We were fortunate in having A.E. Guile to write the chapter on the Electric Arc. Alan Guile is an electrical engineer who has made important contributions to knowledge about the mechanism of non-thermionic arc cathodes, as well as being a recognised expert on problems associated with switchgear arcs. Another contribution was the compilation of data on physical properties of fluids which was due to Dennery and his colleagues at Air Liquide in Paris. The first edition of the book was published in 1984 and sold well, such that the publisher asked for a second edition, which appeared in 1986. Then the Japanese members of the Study Group undertook the onerous task of translating the text, and eventually produced a Japanese edition. This was particularly appropriate because Japanese workers had made a major contribution to basic knowledge about the electric arc in welding and the behaviour of weld pools.

Change of name

As noted earlier, the Group was originally given the name 'Physics of the welding arc'. However, we very soon extended our field of study to other aspects of welding; metal transfer and weld pool behaviour for example. In 1978 therefore it was decided that the name should be changed to 'Physics of Welding' and the terms of reference were modified accordingly. There was some concern at first that the work of the Group might overlap that of some Commissions but this did not prove to be a problem. For example, the subject of variable penetration in GTA welds was of interest to Study Group 212 and also Commissions IX an XII. These Commissions were kept fully informed of the progress of our work and accepted the final report without comment.

Variable penetration in GTA welds

This project was undertaken with the object of producing recommendations for the avoidance of variable penetration. It was carried out in co-operation with VAMAS and with the National Physical Laboratory (UK). The final report was approved by the Group and recommended for publication, and this is now scheduled for late 1993.

It is interesting to recall that Professor Ishizaki predicted that surface tension gradients would cause circulation in the weld pool, and demonstrated this effect by melting a pool of paraffin wax with a soldering iron. The circulation was made visible by particles of aluminium. A film of this experiment was shown at the 1966 meeting in Delft, and caused a great deal of interest at the time. However, later work by Andersson appeared to show that in the case of hot liquid mercury such flow would only occur in vacuum and was inhibited by the presence of an oxide layer on the metal surface. Therefore we failed to pursue the subject until Heiple and Roper raised the possibility of surface-active agents reversing the direction of flow. In more recent years the tide has turned again, and it is generally thought that the effect of surface-active agents is to nullify surface tension induced flow and produce a weld pool in which any flow is irregular and confused. Thus, the shape of the weld pool is little affected by flow and is more or less semi-circular in section.

Other recent work

Three other subjects have been of interest in recent years: spatter, undercut and precipitation in the weld pool. The spatter problem exists because calculations predict that the interface temperature when a drop strikes the metal surface should be below the melting point, therefore it should not stick. A proportion of spatter does stick, however, and Professor Rehfeldt has shown that such spatter is indeed fused to the metal surface. This condition can only be accounted for if there is flow in the spatter drop, such that its effective conductivity is high. It is possible that such flow could be induced by surface tension gradients associated with temperature gradients in the drop.

Interest in undercut arose because tests on the surface melting of cast iron disclosed that the effect of surface active elements in reducing surface energy was much greater in solid iron than in liquid iron; thus the liquid weld pool might under some circumstances tend to draw away from the solid. No progress has been made here.

It was suggested some time ago that the micron-sized oxide precipitates seen in steel weld metal may form in the weld pool and that they could be removed by increased circulation. However, the size of the oxide particles is such that they are more likely to be precipitated either in the more stagnant part of the boundary layer of the pool, or in the solidified metal.

Documents and discussions

It is inevitable that most of the time at meetings of the Group is spent in the presentation and discussion of research papers. The average number of documents per year (obtained for example by dividing the current document number, 830, by 31) is about 27, and allowing 7 for minutes and the like leaves a mean figure of 20. This

number has not changed very much over the years, which is rather surprising in view of the general increase in research activity. It has varied greatly from year to year as has the attendance at Annual Assembly meetings: for example at the Kyoto Assembly we had over fifty participants (admittedly students for the most part), whereas in Tel Aviv there were just three, including the chairman. The average number of attendances has been half-way between these two extremes, about twenty-five. Again there has not been much change but my general impression is that there has been a slight increase in recent years. Intermediate meetings, on the other hand, which were well supported at one time, have in the last few years either been poorly attended or have not been held.

Conclusions

There is no doubt that it was correct to widen the terms of reference of the Study Group and it may well be possible to continue this trend in the future. The Group has always benefited from the interest that senior figures in IIW have shown in its work, and from support of the Secretariat in publishing ventures such as Physics of Welding. On the negative side the current lack of interest in the intermediate meeting poses a problem. Lack of funds is an obvious cause and this situation is likely to continue at least in the immediate future. However, the main activity of the Group has always centred around the Annual Assembly meeting, and provided that there is no undue competition (such as that provided by all-day meetings of Commission XII) there is good reason to expect continued and possibly increased support.

Gas Tungsten Arc Diagnostics – *a review*

S. Albrecht, G. Forster, A. Koch, K. Landes, G. Seeger, and W. Tiller

University of the German Army,
Munich, Germany

Abstract

In this paper a review is given of the various methods which can be used to measure the physical parameters of the welding arc.
After a brief introduction, attention is given to emission spectroscopy, laser scattering, thermography and particle velocity measurements.

1. Introduction

Nearly two hundred years ago the physicists Davy and Ritter struck the first electric arc and gave it its name because the light phenomenon they observed between the two horizontally located carbon electrodes was curved upwards due to the thermal ascending force. It was a long way from that time to the modern welding technology of today.
Initially, the arc was applied for lighting purposes and for melting materials. Succesful applications in welding started about hundred years later. Today the welding arc is used extensively in the metal industry.
Diagnostics of the welding arc started in the sixties and was stimulated by the use of the laser as diagnostic tool.

2. Emission spectroscopy

One of the first developments in the area of arc diagnostics was the investigation of the temperature distribution of a TIG arc by means of emission spectroscopy. A scheme of the experimental set-up for this measurement is given in Figure 1.

A necessary assumption in using this technique is the rotational symmetry of the arc. An image of the arc is generated on an observation layer by a lens. In the optical path there are a pin diaphragm (telecentric projection) and an interference filter (selection of the spectral line wavelength). A system of crossed slits in the observation layer forms a very small quadratic measuring window. The arc image can be scanned by moving

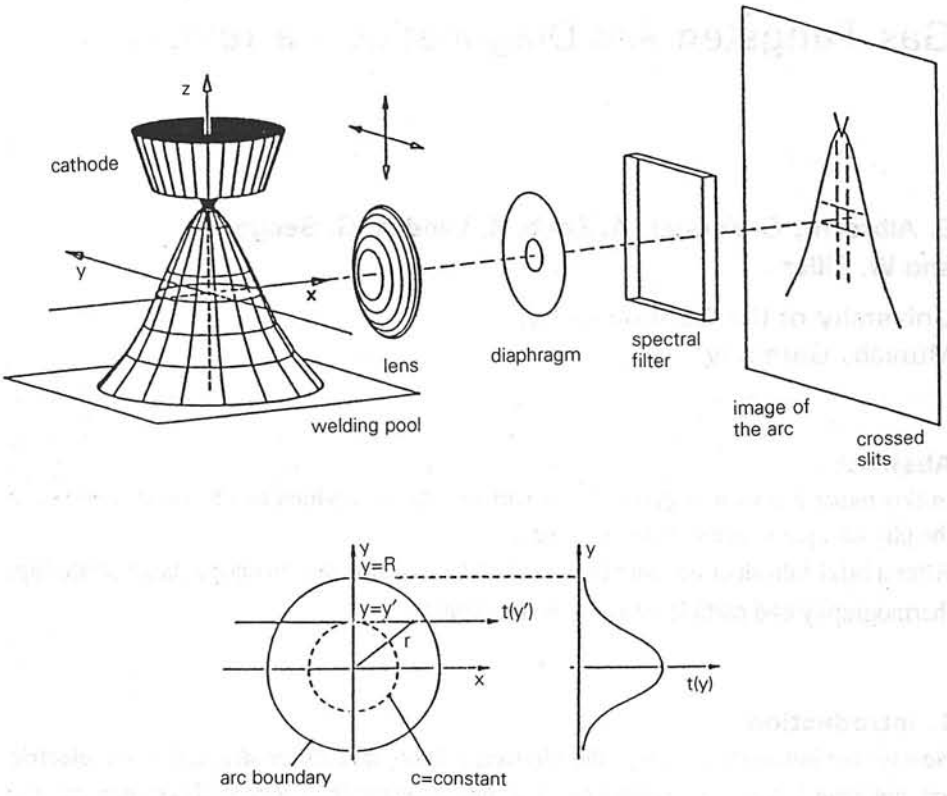

Figure 1. Spectroscopic temperature diagnostics in a TIG arc by integral measurements.

the lens in z-direction (definition of a cross-sectional area) and in y-direction (measurement of the integrated spectral intensity profile). The plasma in a volume element of the arc emits radiation depending on the local temperature. The relation between the local line emission coefficient $\varepsilon_{\text{line}}$ and the temperature T is known via the particle density n:

$$\varepsilon_{\text{line}} = \frac{h \cdot \nu_{mn}}{4\pi} \cdot A_{mn} \cdot n_m(T)$$

with h the Planck constant, A_{nm} the Einstein coefficient and ν_{mn} the frequency of the transition mn.

The complete theoretical procedure which is necessary to obtain the temperature from the emission coefficient is described in [1]. In a first step, however, one has to calculate the local emission coefficient $\varepsilon_{\text{line}}$ from the measured integral intensity $I(y)$. This procedure is called Abel inversion. The integral

$$I(y) = 2 \cdot \int_{x=0}^{x=\sqrt{R^2-y^2}} \varepsilon(x,y) \cdot \mathrm{d}x$$

is inverted to

$$\varepsilon(r) = -\frac{1}{\pi} \cdot \int_{r}^{R} \frac{\frac{\mathrm{d}I(y)}{\mathrm{d}y}}{\sqrt{y^2 - r^2}} \cdot \mathrm{d}y$$

The coordinate system is shown in Figure 1. $I(y)$ is measured, the derivative $\mathrm{d}I(y)/\mathrm{d}y$ can be calculated, thus the integral yields the temperature distribution for every arc cross-sectional area via $\varepsilon_{\text{line}}(T)$. The calibration is done by means of a tungsten strip lamp. Figure 2 shows the result for an argon TIG arc with 100 amps current and 5 mm arc length.

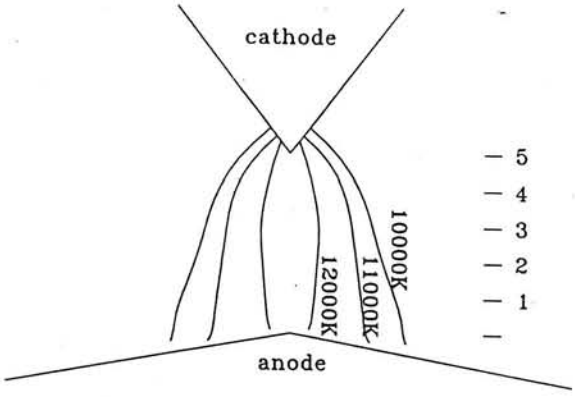

Figure 2. Temperature distribution in a TIG arc.

The specification of the standard TIG arc as defined by Study Group 212 is given in Figure 3.

If there is no rotational symmetry in the arc, a modified Abel-procedure must be applied. It is of interest to note that this modified procedure developed in 1968 [2] has led to the well known computer tomography.

3. Laser scattering

A serious problem in spectroscopic measurements is the integral character of this method. This problem has been overcome by application of lasers. Laser light scattering offers a powerful tool for the investigation of plasma parameters with an active technique providing a good spatial resolution. Furthermore, this technique can

arc length	3 mm	5 mm	cathode configuration
current	100 A	300 A	tip axially ground
argon flow rate	6 ℓ/min	18 ℓ/min	
nozzle	13 ∅ mm	16 ∅ mm	

argon	99,995
anode	≥ 50 ∅ mm plain copper plate (water cooled)
cathode	3,2 ∅ mm Tungsten, 2% (±1%) thoriated cathode tip bearing 5 mm out of the nozzle

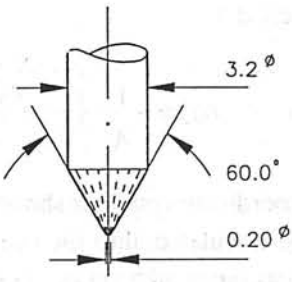

Figure 3. Standard TIG arc.

be considered a non perturbative probe in most cases. Laser light is coherent (i.e. strictly monochromatic) and very intensive. It can be focused on a minimum measuring volume. The laser light is scattered by electrons, ions, atoms and molecules passing this volume. (The scattering process is not an effect of reflection!) An explanation of this phenomenon is given in Figure 4.

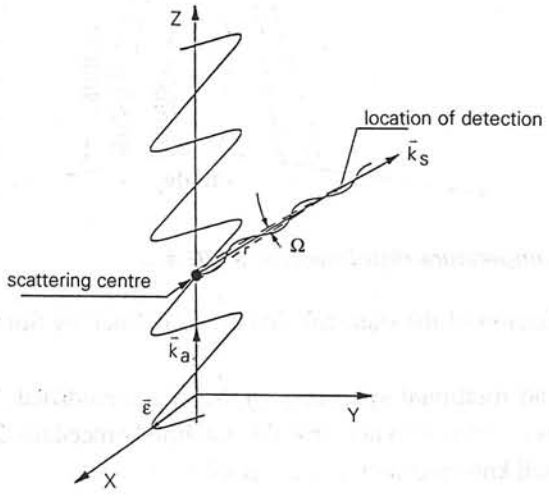

Figure 4. The Laser scattering effect.

A laser wave with the electric field vector $\vec{E}$ propagating in the direction of the wave vector $\vec{k}$ excites the *free* electrons in the scattering volume. The electrons oscillate in the wave field of the laser and emit dipole radiation with the laser frequency. This effect is called Thomson scattering. A far radiation field depending on the laser intensity, the fluctuation of electron density and the solid angle Ω is measured in the

direction of observation at the distance r. This signal is transformed by a photomultiplier into a photocurrent i_s proportional to the power of the detected scattering radiation i.e. the electron density in the measuring volume.

A second scattering phenomenon is Rayleigh scattering. It is caused by the oscillation of bounded electrons in the atoms or ions respectively. In this case the laser frequency must be very close to a spectral line, but not too close, in order to avoid a transition effect. The atoms act like dipoles emitting scattered light with the laser frequency.
The theory of Thomson and Rayleigh scattering is briefly explained in [3]. Via the scattering cross section the densities of the free electrons and the neutral atoms and therefore their temperature can be evaluated. The calibration is provided by a cold gas measurement based on the known cold gas Rayleigh scattering cross section. The advantage of the scattering method is an optimum spatial resolution.
The experimental arrangement of an application to a TIG-arc is shown in Figure 5.

Although this array looks quite simple it is nevertheless very complex. Using a pulsed laser, it is also possible to measure the time resolved behaviour of a pulsed TIG arc!

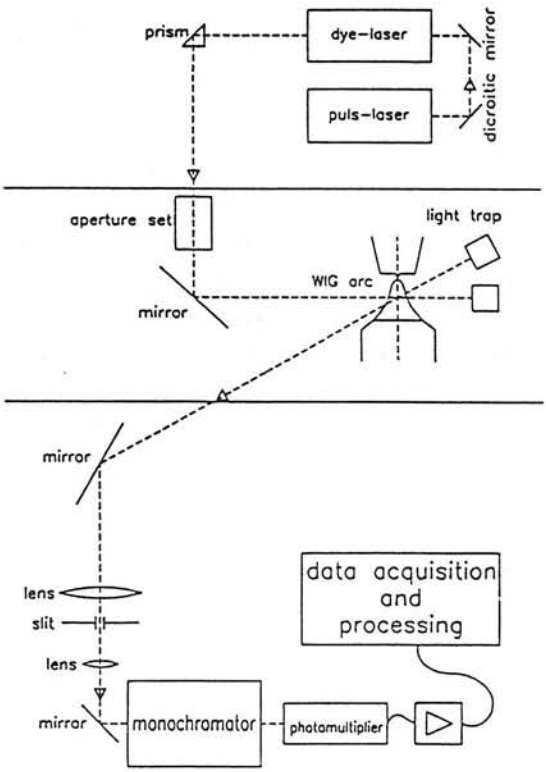

Figure 5. Experimental set up for laser scattering measurements.

Figure 6 gives the results for the spatial and time resolved distributions of the temperature for pulsed arc currents of 60/120 amps and an arc pulse frequency of 150 Hz, as reported in [4].

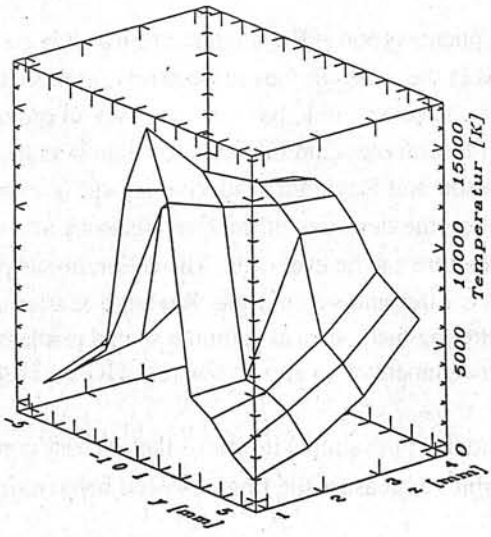

Figure 6. Temperature distribution in a pulsed TIG arc, measured by laser scattering.

4. Thermography

Thermography represents a new and very successful development within the field of spectroscopic methods. The image of the whole arc is recorded by means of a high resolving and high sensitive CCD-array. The spectral resolution is provided by different interference filters. This method is already applied to low temperatures, but there are still problems at the much higher plasma temperatures .

In the meantime the first results were obtained with this technique. Figure 7 gives the intensity distribution of the arc measured in less ten milliseconds. A new time saving analysis method allows for the compution of the temperature distribution in about 100 milliseconds, i.e. this investigation gives a quasi real-time response of the arc behaviour.

5. Measurement of particle velocity

Another interesting plasma parameter is the *velocity* of the different plasma components. First investigations were done in the middle of the seventies [5]. Small particles (< 10 μm) of aluminium oxide (Al_2O_3) were added to the shielding gas and after entering the arc, their velocity was measured by laser anemometry.

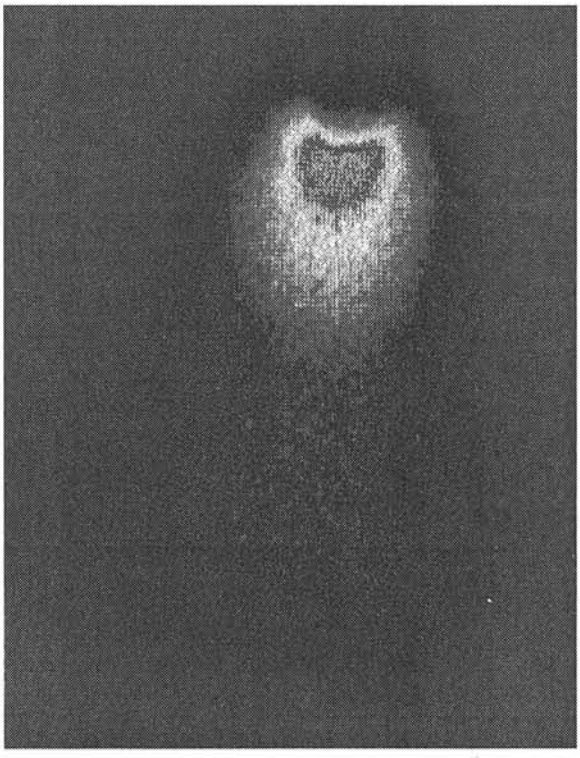

Figure 7. Intensity distribution in a TIG arc at the wavelength of 4300 Å

The experimental arrangement is shown in Figure 8. The beam of a dye laser is divided into two beams of equal intensity which are focused on the measuring volume in the arc. Thus, an interference pattern is generated in the measuring volume consisting of light and dark stripes, the separation of which can be calculated from the geometry and the laser wavelength. A test particle, which flies through this pattern, causes a set of scattered light pulses, the frequency of which is proportional to the velocity component in the axial direction. By means of a photomultiplier the signal is converted into a photocurrent which can be observed by an oscilloscope. A typical oscillogram is shown in Figure 8. This experimental method (anemometry) has hitherto in particular been used with liquid fluids and cold gases.

As an example of the results obtained the distribution of the axial particle velocity component as a function of radius, r, and axial coordinate, z, are shown in Figure 9.

It must be mentioned, that because of the slippage of the particles this results have only the character of an approximation.

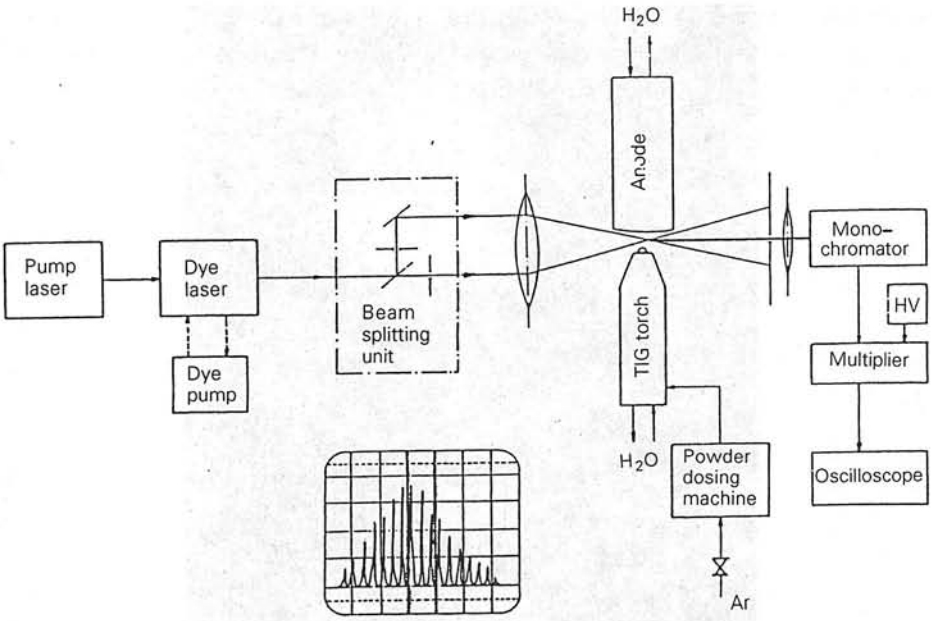

Figure 8: Anemometry of particles in a TIG arc

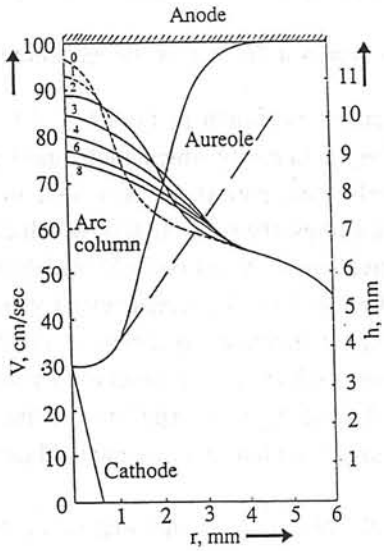

Figure 9. Particle velocity in a TIG arc at different positions in the arc.

By the application of high power pulse lasers an improved method for the velocity measurement of ions, electrons and atoms in a plasma was developed. First investigations were done with a plasma jet used in plasma spraying techniques. At the

moment this method is adapted to the TIG arc. The principle of the method is a combination of laser scattering and laser anemometry. Figure 10 shows the experimental set up, as extensively described in [6].

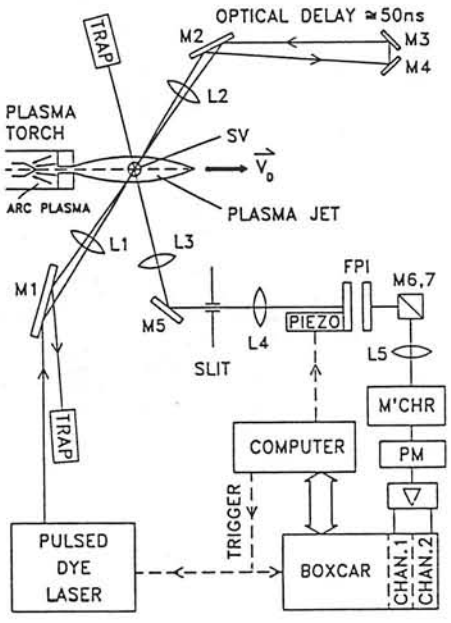

Figure 10. Experimental set up for the velocity measurement of plasma components.

A laser pulse is sent through the plasma producing scattered light. In the case of electrons this leads to Thomson scattering and in the case of ions and atoms to Rayleigh scattering, respectively. The movement of the scattering plasma components results in a Doppler shift of the scattered light, depending on the direction and the magnitude of the velocity. The frequency shift of the Doppler effect can be doubled by reflecting the laser pulse in the measurement direction backwards. There are two problems connected with this technique:

1. The spectral resolution of the Fabry-Perot interferometer used for the measurement must be very high.
2. The data acquisition must be fast enough to store the two pulses with a time distance of 50 nanoseconds. Figure 11 shows a time-frequency-diagram of the two scattered light pulses.

Up to now, only measurements have been carried out with a plasma jet. However, as mentioned above it is the aim to apply the technique also to a TIG arc.

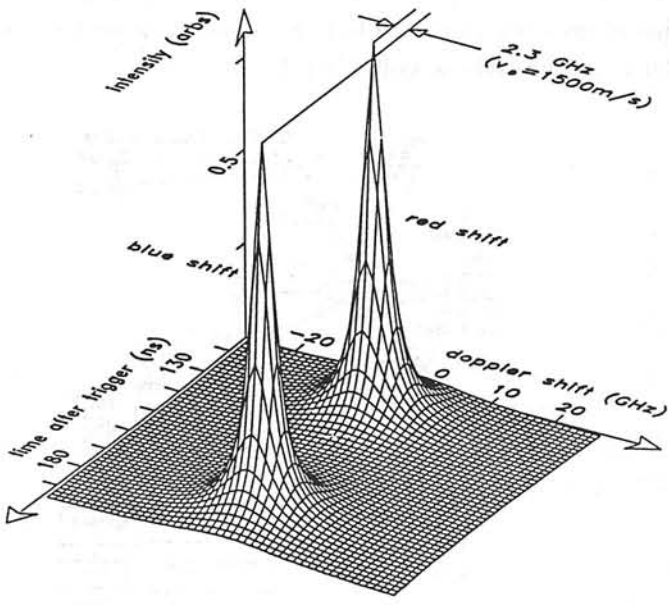

Figure 11. Velocity measurement by Doppler shifted scattered laser light pulses.

6. Conclusions

This brief survey describes the development in TIG-arc diagnostics of the last twenty years. By starting laser diagnostics the investigation of welding arcs has become more interesting because this new tool enables spatial- time- and spectral-resolved informations of the arc interior. The lack of a robust measuring set up applicable under manufacturing conditions, however, will lead to a preference of the spectral measuring method with CCD-arrays in the next future.

References

1. Forster G., Seeger G., Tiller W., IIW Doc. 212-747-90, 1990.
2. Maldonadow C., Olsen H., ARL-Report 66-0016, 1966.
3. Koch A., Landes K., Seeger G., Tiller W., IIW Doc. 212 -706-88, 1988.
4. Albrecht S., Forster G., Seeger G., Tiller W., IIW Doc. 212-814-92, 1992.
5. Tiller W., Welding Institute Reprint, London, 1979.
6. Forster G., ICPIG, Barga, Italy, 1991.

Cathode Phenomena in GTA Welding

M. Ushio, K. Tanaka, F. Matsuda

Welding Research Institute,
Osaka University, Japan

Abstract

The performance of tungsten electrodes used in GTA welding are discussed through a comparative study on arc properties, oxide behavior in the electrode, electrode temperature and erosion phenomena, consumption of electrode material due to evaporation, for several types of electrodes.

The work was carried out with one standard electrode (W-ThO_2) and other electrodes developed by the addition of rare earth metal oxides, La_2O_3, CeO_2 or Y_2O_3. It is shown that the newly developed electrodes have superior properties compared with thoriated tungsten. The experiments make it clear that the behavior of rare earth metal oxides contained in the tungsten electrode have decisive effects on arc properties and durability of the electrode tip, and that this is governed by the temperature distribution of the electrode tip.

Consumption of electrode material due to evaporation, effect of oxygen on the evaporation and rim formation phenomena are also discussed.

1. Introduction

In GTA welding, the arc burns between a tungsten electrode and the workpiece within a shield of inert gas, argon or helium, which excludes the atmosphere and prevents contamination of electrode and molten metal. Unlike the electrode in the gas metal arc welding process, the tungsten is not transferred to the work and evaporates extremely slowly. The gas tungsten arc provides a stable heat source of welding and a filler metal wire is generally fed into the molten pool to fill the weld groove. A very wide range of wire feed rates is applicable under fixed arc conditions, which is the most important advantage of GTA welding.

Because of the greater heat liberated at the anode, a tungsten electrode is used as the cathode. If the tungsten electrode is used as the positive pole of the arc, the electrode will easily be molten and the arc will be unstable. For this reason tungsten arc welding with electrode positive is practically only used for the welding of Al, Mg and their alloys. The cathode phenomena in electrode-positive GTA will be treated in a separate paper.

Guile made an extensive study of the arc electrode phenomena and published an

important review paper [1]. In the review, he explained the mechanism of thermionic emission and classified many elements into the material which could work as hot cathode (thermionic cathode). After that, Ecker also presented an eloquent theoretical model of the arc cathode mechanism. However, this model is mainly focused on the non-thermionic cathode [2]

The cathode phenomena of oxide-activated or rare-earth-metal-activated tungsten have not been treated precisely, so far. The interest of this paper is the phenomena occurring in this activated-tungsten cathode of inert gas shielded welding.

Usually tungsten electrodes are used after grinding to a point to obtain a strong stiffness of the arc, and consequently to fix and stabilize the heat transfer to the work. However, it is very difficult to keep a sharp cone during long periods of arc burning. The thoriated tungsten electrodes have improved electron emission, thus, give easier starting, a more stable arc and less weld contamination with tungsten particles due to electrode tip melting. In addition they have a greater current-capacity for a given diameter than pure tungsten [3-6].

However, modern technology, particularly the automatic or robotic welding industry, demands more stable and reliable performance of the electrode for a longer time of operation. Also the radio-activity contained in the thoriated tungsten electrode is considered to be undesirable from the view point of health.

In view of these circumstances, various types of new electrodes have been developed, which contain a small amount of rare earth metal oxide, La_2O_3, CeO_2 or Y_2O_3, in place of ThO_2 (see Table I). They result in satisfactory properties, namely, high stability of the arc and durability of the electrode tip. Many phenomena of the tungsten cathode have been made clear through the study of the behavior of oxide inside the electrode. It is shown that the behavior of rare earth metal oxide contained in the tungsten electrode, i.e. the formation of compounds of low melting temperature, melting and migration of the compound, and the balance between migration and evaporation of the rare earth metal and its oxide, has decisive effects on the arc properties and durability of the tip of the electrode. This may lead to a better insight into the possibility to control the arc root.
In this paper, based on research work [7–10] carried out in our laboratory some recent results related to the cathode of gas tungsten arc are reviewed.

Table I Electrodes used

Electrode		Oxide	Content (%)
Pure-tungsten	(P-W)	—	0
Thoriated tungsten	(Th-W)	ThO_2	1 to 3
Yttriated tungsten	(Y-W)	Y_2O_3	1 to 3
Ceriated tungsten	(Ce-W)	CeO_2	0.5 to 2
Lanthaniated tungsten	(La-W)	La_2O_3	0.5 to 2

2. Arc properties with oxide-activated tungsten electrodes

a Arc starting performance

The criterion for evaluating starting performance was the minimum open circuit voltage required for reliable starting with a superimposed high frequency spark. As the best electrode was considered that electrode which required the smallest starting voltage.

An example of comparison of successful starts as a function of open circuit voltage for these electrodes is shown in Figure 1A. Conventional high frequency current is applied in 10 sec between the tungsten electrode with a 45 degree cone and a water cooled copper under the pre-set open-circuit voltage. The successful arc starting percentages are shown in the figure. The follow-up arc current was adjusted to 20-30 A in each case.

The La-W electrode was found to start and maintain an arc at the lowest voltage values, followed by Y-W, Ce-W, and Th-W electrodes in that order. The minimum starting voltages for both La-W and Y-W are fairly definite, while those for pure W are much more random.

It may be significant to note that the order of the increasing starting voltage of the electrodes corresponds to the order of the effects on electrode work functions caused by rare earth metal oxide additives, as will be discussed later.

b Arc voltage-current characteristics

The voltage-current characteristics for GTA with pure tungsten and oxide containing electrodes have been investigated and are shown in Figure 2. The differences between the voltage-current characteristics of the various tungsten electrodes containing oxides are essentially negligible, except with that of the Zr-W electrode which shows a comparatively large deformation due to melting.

The observed changes in total arc voltage are believed to be due to the changes in the cathode potential drop, which depends on the changes in work function and tip geometry when all other factors are fixed. Consequently, this is related to the role of the contained oxide and its effect on the tip geometry, see Figure 6.

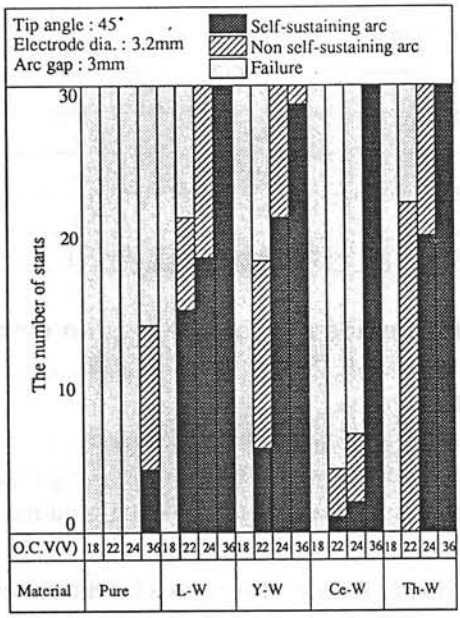

Figure 1. Arc starting characteristics evaluated by open circuit voltage (O.C.V.) tests.

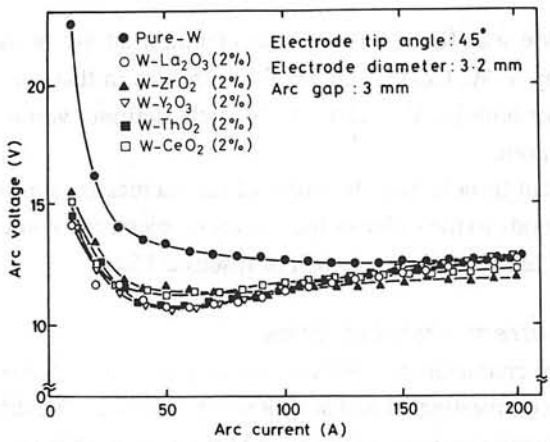

Figure 2. Comparison of voltage-current characteristics.

c Arc force

The arc force distribution at the water cooled copper anodes are measured by a semiconductor transducer, as shown in Figure 3. The arc force as a function of arc current is illustrated in Figure 4. Figure 5 shows the maximum arc force at various radii of electrode-truncation related with arc current for a La-W electrode as an example.

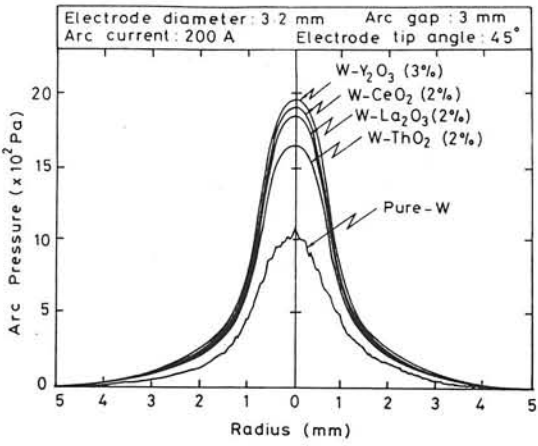

Figure 3. Arc pressure distribution measured at the anode. The irregular oscillation in case of pure W shows the unstable behavior of the arc during the measurement.

The arc force originates mainly by the induced flow of plasma gas due to the expansion of the current path from the electrode to the gaseous arc space. Therefore, the truncation or the deformation due to melting must change the current distribution near

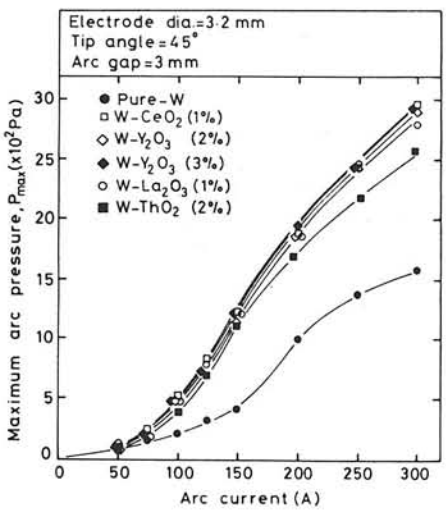

Figure 4. Arc pressure as a function of arc current.

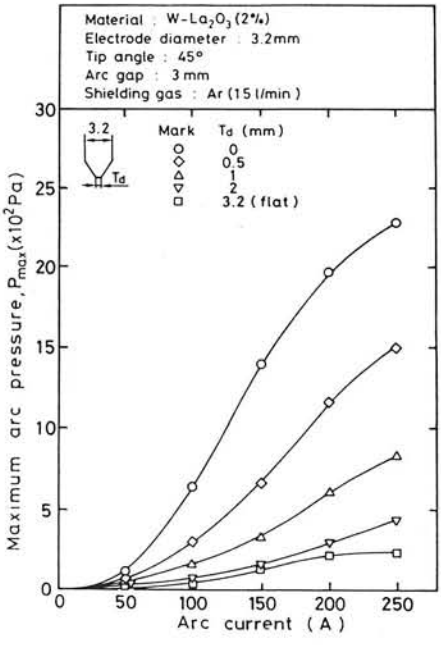

Figure 5. Effect of truncated electrode diameter on maximum arc pressure.

the cathode and also the impedance for induced flow, consequently leading to the change in arc force acting on the anode.

d. Durability of electrode tip

A comparison of the metallurgical micro-structures after 1 hour burning is shown in Figure 6. The pure tungsten tends to recrystallize and form large grains, while some activated electrodes, such as Th-W and Zr-W, tend to lose the oxides and start forming large tungsten crystals at the tip, as in the case of Th-W, or experience severe melting as in the case of Zr-W. However, the La-W, Ce-W and Y-W electrodes showed more stable structures.

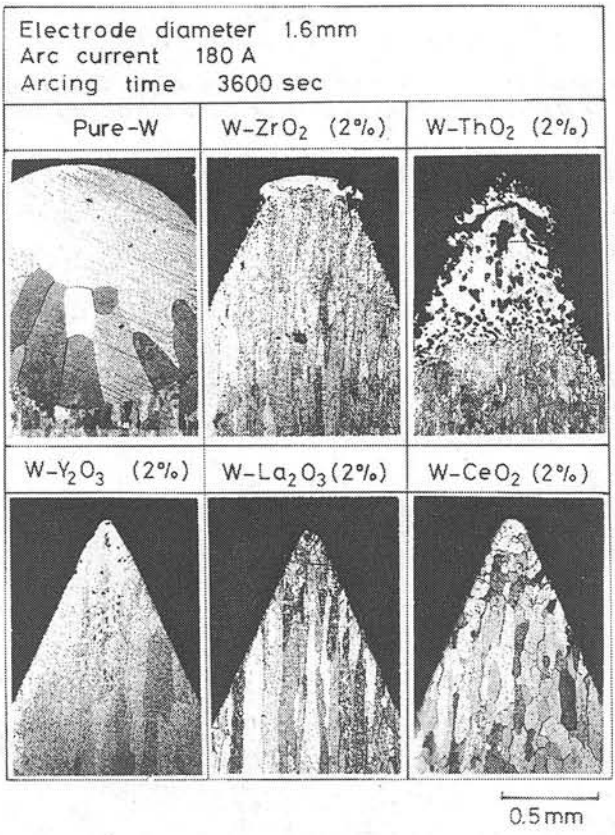

Figure 6. Microstructure of cross section of electrode after heavy loading.

These metallurgical changes affect electrode erosion, consequently changing operating characteristics and temperature distribution. In other words, the loss of oxides leads to a decrease in the electron emission and an increase in the temperature, because the tip operates as pure tungsten at that time.

The arc characteristics and the metallurgical structure, show that the La-W, Ce-W and Y-W electrodes have at least the same performance as the normal thoriated tungsten electrodes.

3. Behavior of rare-earth metal oxides

During arc burning, the oxide contained in the electrode changes its morphology due to melting and moves to the higher temperature zone near the arc root area, as shown in Figures 7-9 [7, 10, 12]. Figure 7 shows the oxide redistributions on the tip surface after 30 minutes and 60 minutes of arc burning. The concentration of oxide just outside the arc root area is observed clearly. For the Y-W, it is difficult to discriminate the Y-line from the W-line in the EDX line analysis. Ce has a nearly uniform distribution throughout the electrode tip without the localized concentration peaks, suggesting that the migration and vaporization rates of Ce or Ce-oxide are much higher than those of other oxides.

In Figure 8, the results of X-ray diffraction analyses of oxide particles inside and near the electrode surface are shown. The rare earth metal oxides react with tungsten and form tungstates or oxy-tungstates in general. The melting points of those tungstates and oxy-tungstates are lower than those of oxides and tungsten.

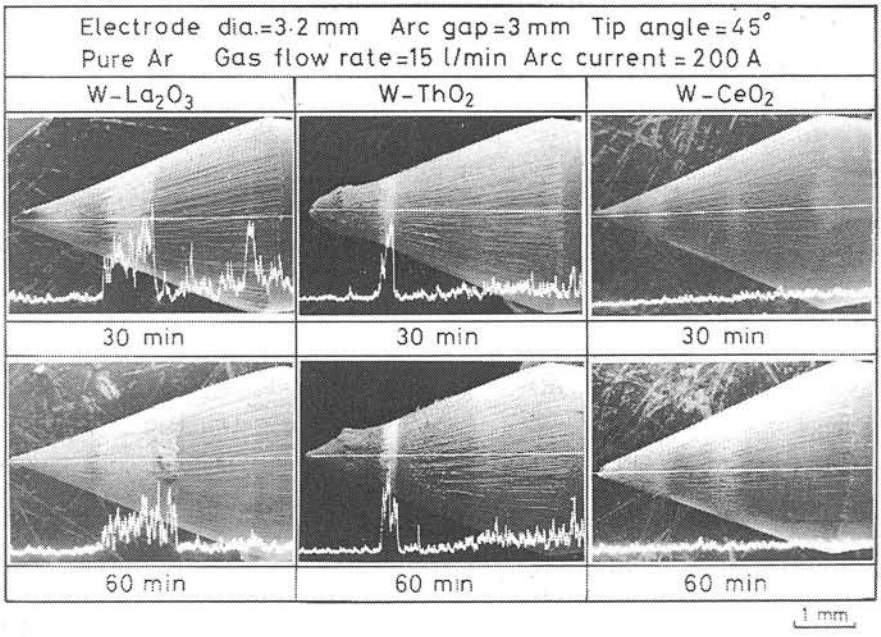

Figure 7. Appearance of electrode surface and EDX line analysis of La, Th and Ce, respectively.

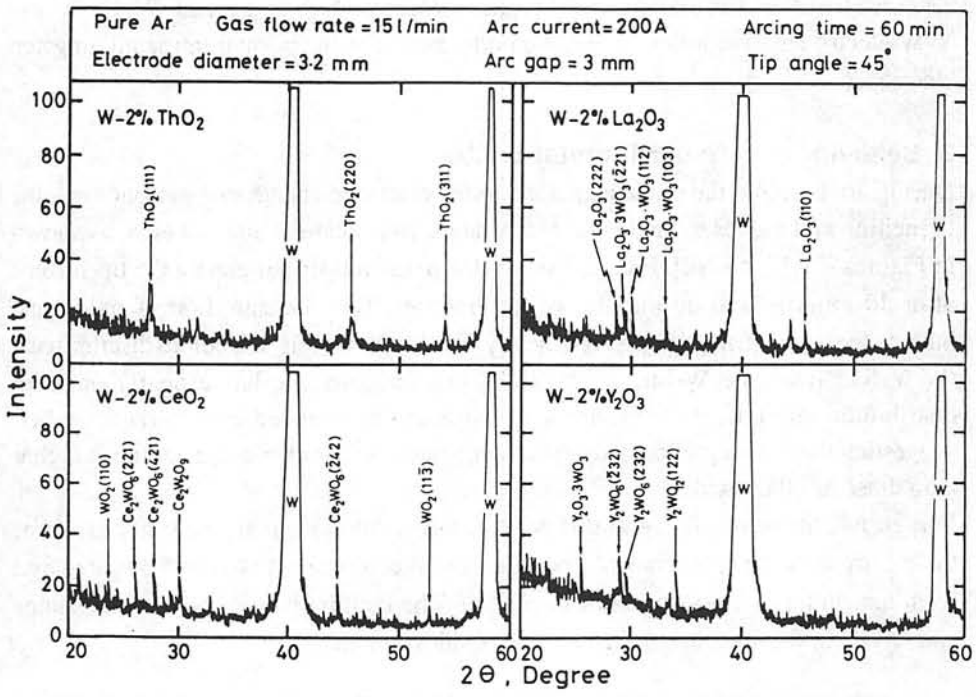

Figure 8. X-ray analysis of particles inside electrode.

In the case of Th-W electrodes, no tungstate and oxy-tungstate is detected. Thus the ThO_2 is supposed to react with tungsten, forming only Th during arc burning. The collected data of thermodynamic properties and estimated behavior of the oxides are listed in Table II and Figure 9. Note that only CeO_2 was reduced to Ce_2O_3 in the sintering process in hydrogen atmosphere.

A schematic illustration of the suggested migration and the different behavior of the oxides accompanied by the temperature field are shown in Figure 9. In the case of rare earth metal oxides their tungstates and oxy-tungstates melt and migrate from the lower temperature zone to the higher temperature zone along the grain boundaries (tungsten grains have usually a longitudinal shape) probably due to capillary action. The migration rate increases considerably with increasing temperature gradient. This is supported by the lower melting points of tungstate and oxy-tungstate. Also, as the migrating particles travel up the temperature gradient, they are accelerated and increase in size [7].

The highest migration rate among the different oxides is shown by CeO_2, whose tungstate has the lowest melting point. This tungstate easily migrates and it is continuously fed to the electrode tip. Thus, the oxide consumption of Ce-W is much higher than that of the other oxides.

Table II Summary of oxide behavior

Type of oxide	ThO_2	La_2O_3	CeO_2	Y_2O_3
Melting point K	3323 (Th: 2028)	2490 (La: 1193)	2873 (Ce: 1071)	2708 (Y: 1799)
Heat of decomposition, (kJ)	1227.6	1244.7	(523.4)	1271.1
Type of oxide after sintering	ThO_2	La_2O_3	Ce_2O_3 (m.p.: 1883 K)	Y_2O_3
Reaction with tungsten	reduction of ThO_2 by W occurs forming pure Th	forms tungstate (m.p.: 2073 K) and oxytungstate (m.p. > 1773 K)	forms tungstate (m.p.: 1363 K)	forms tungstate (m.p.: 1743 K) and oxytungstate (m.p. > 2473 K)
Oxide behavior	1. diffusion of Th atoms to the electrode surface 2. vaporization of Th from the electrode surface	1. migration of La_2O_3 occurs from the center to the electrode tip 2. vaporization of La_2O_3 from the electrode surface	1. migration rate throughout the electrode edge is higher than from the center to the electrode tip 2. vaporization of CeO_2 from the electrode surface	1. very low migration and vaporization
Stability of oxide	low	high	reasonable	high

The rather stable behavior of La-W can be related to the slightly higher melting point of La_2O_3 as well as its oxy-tungstate compounds. Also, migration provides a reasonable compensation for evaporation loss. Due to the higher melting point of Y_2O_3 and its tungstate or oxy-tungstate and the shape of the tungsten grain boundaries (which exhibit granular shape), the migration rate along the grain boundaries will be decreased and it takes much more time to reach the electrode tip.

Because of the high melting point of ThO_2 and the temperature range at which ThO_2 may be reduced by tungsten, the feeding and diffusion rate are much lower than the vaporization rate. Thus, the electrode tip will lose the ThO_2 and act as pure tungsten. From above observations, it was deduced that the balance between the evaporation of the rare-earth metal at the surface and its feed from inside through migration of compounds is essential to achieve stable and long life operation and that this balance is governed by the temperature field of the electrode.

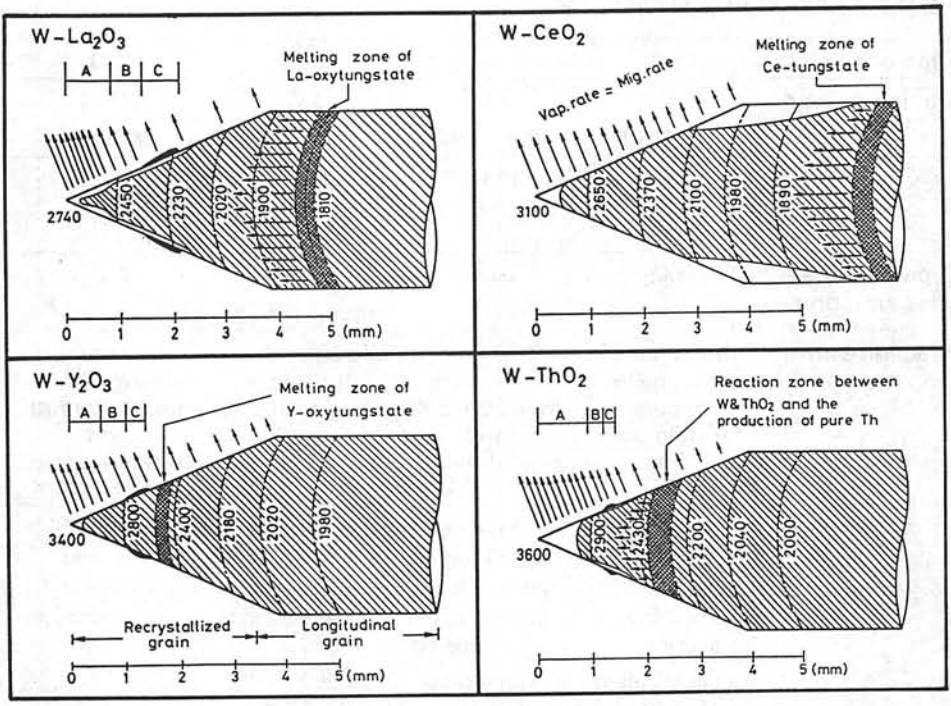

Figure 9. Schematic illustration of oxide distribution and temperature distribution along electrode axis. Dashed area represents oxide remaining after arc burning and arrows show the vaporization.

Sometimes excess migration was observed, see Figure 10. This occurs in the case that the tip cone angle is very sharp or high current is applied. The electrode tip is overheated locally and lack of rare earth metal oxide or the formation of gaseous holes occur. The latter may be due to gasification of the oxide. If the temperature field has no such a steep gradient, these phenomena were not observed. This may suggest that a low content of rare earth metal oxide in combination with a high current by which a sufficiently large portion of the electrode is heated to the high temperature, could give the appropiate conditions for keeping the electrode shape unchanged.

4. Electrode temperature and apparent work function

It is difficult to measure the electrode tip temperature, because of its high value, obviously above 2000 °C. As shown in the preceding section, the spectral radiation emissivity of the surface is not constant due to the redistribution of rare earth metal or its oxide and also due to the change in surface morphology.

In this experiment, electrode temperatures during arc burning were determined by measuring the radiation from the graphite powder that was inserted in a groove in the electrode. An electrode of 2.4 mm in diameter was machined to contain a V shape

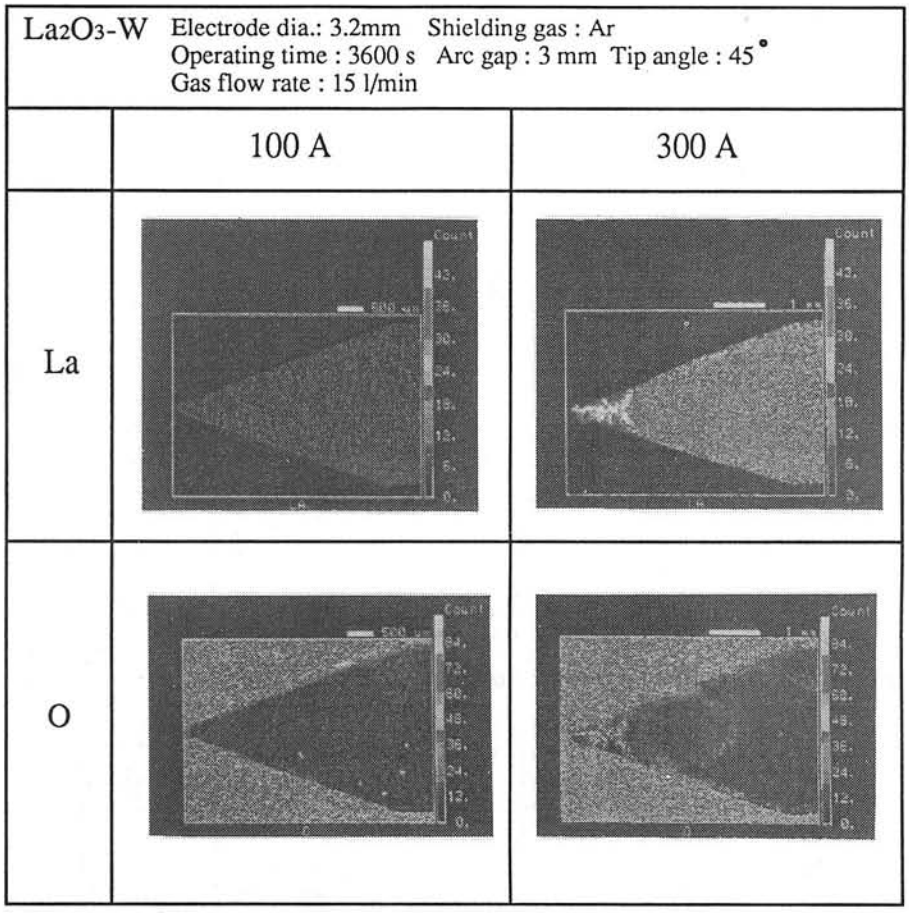

Figure 10. EPMA analyses of cross-section of La-W electrode after arc burning.

groove, which was then filled with graphite powder under extreme pressure to avoid its loss during arc burning. The graphite powder has a known emissivity.

The temperature distribution along the electrode axis was measured using an infrared thermometer. It collects the infrared radiation ranging from 1.8 to 5.0 microns in wave length from a target area 0.65 mm in diameter. Figure 11 is an example of the measured temperature distribution.

When the electrode is used with a current above the recommended standard value, the temperature distribution curve changes from a smooth and monotonical curve to one that has a peak at some point along the electrode extension. Figure 12 shows the change in temperature distribution with changes in arc current. The temperature gradient near the tip changes sign, and also the tip temperature decreases with increase in current mainly due to electron emission cooling and geometrical effects.

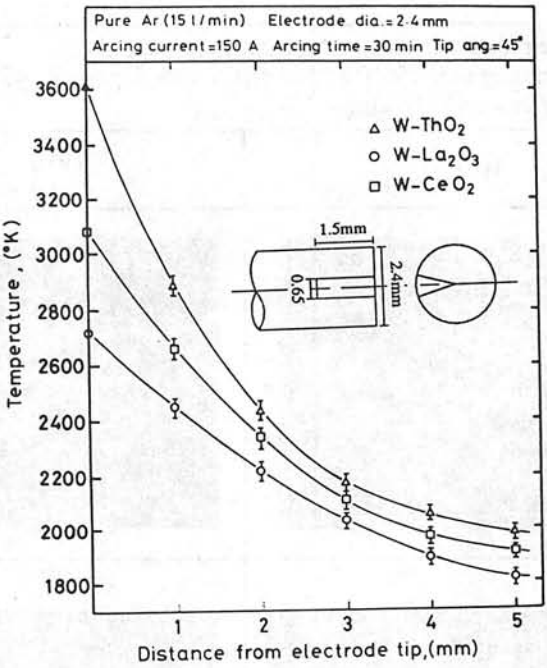

Figure 11. Temperature distribution along the electrode axis.

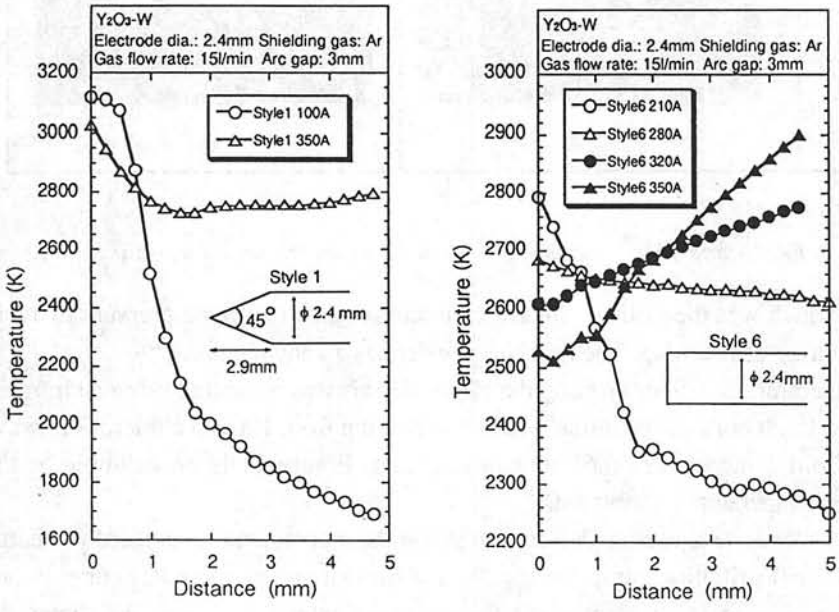

Figure 12. Electrode temperature near the tip for various arc currents.

As shown in Figure 13, the electrode tip surface exhibits three characteristic zones: the pointed end zone (A), a smooth surface zone (B) corresponding to the arc boundary, and a rather rough surface zone (C) whose edge shows a higher oxide concentration.

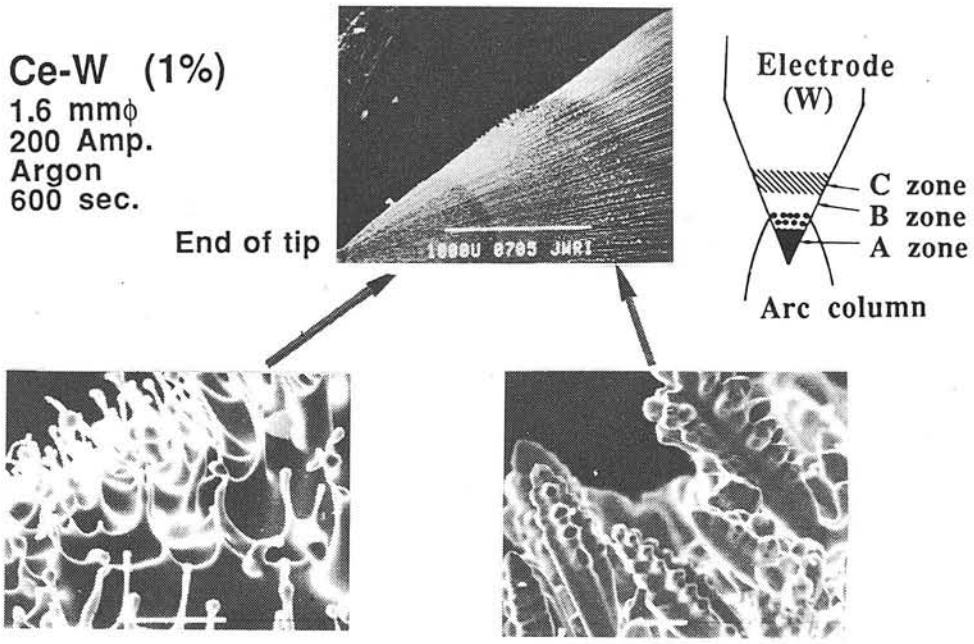

Figure 13. Microstructure of electrode tip surface after arc burning.

Assuming that the electron emission occurs in zone A, the current density at this zone and the apparent work function could be estimated using the measured values of temperature and the Richardson-Dushman equation,

$$J_s = AT^2\exp(-e\Phi/kT),$$

where J_s = current density, A = a constant, k = Boltzmann constant, T = temperature, Φ = work function.

The results are plotted in Figure 14, which shows that in the case of La-W the change in work function is rather small and can be considered to have a constant value (about 2.1 eV). This may explain the good balance between the migration and feeding of rare earth metals or their oxides during arc burning. On the other hand, the apparent work function of thoriated tungsten increases with arc burning time, which can be considered as an indication of the lower migration rate of Th-oxide to the electrode tip.

5. Electrode consumption and rim formation

A simple measurement of electrode consumption in steady state of arc burning shows a severe weight loss by introducing a small amount of oxygen in the gas atmosphere, while nitrogen and hydrogen have little effect as shown in Figure 15.

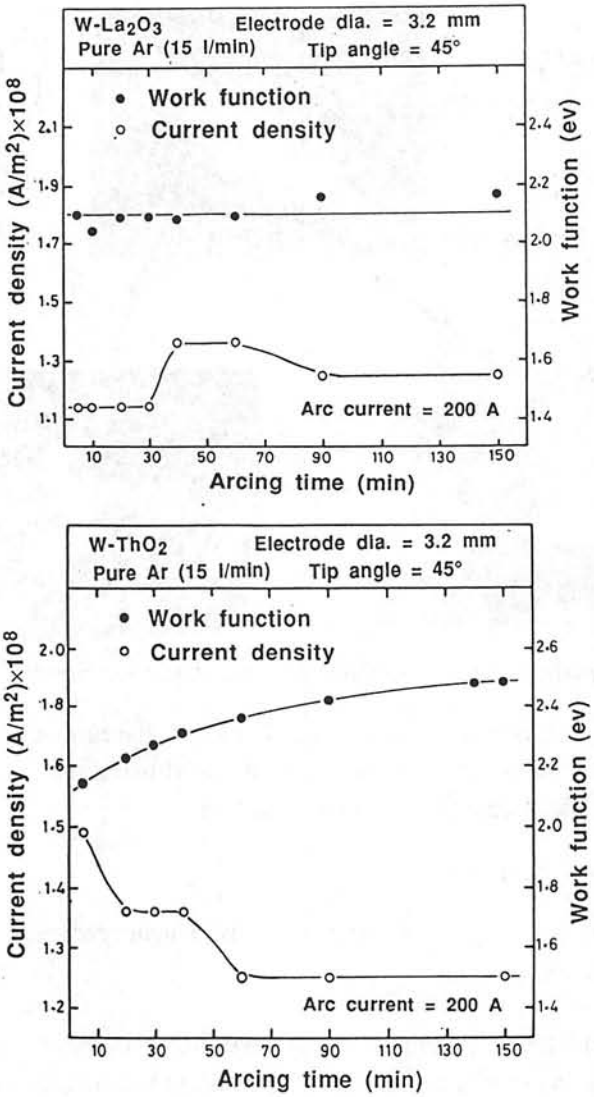

Figure 14. Change in work function and current density.

Figure 16 shows the weight loss as a function of arc current in steady state. Figure 17 shows the weight loss rate under rather high current conditions in pure argon shielding.

Theoretical treatment shows that the erosion rate is related to the physical condition of the arc cathode region. The temperature field of the cathode is the most influential factor of the evaporation and the temperature field of the electrode is estimated by the heat balance of the cathode-arc boundary. However the cathode region is not

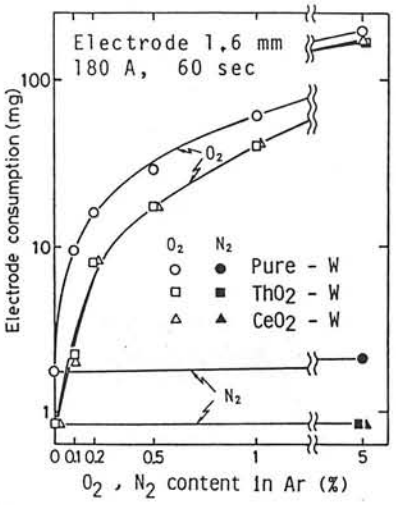

Figure 15. Effect of oxygen and nitrogen introduced into the argon gas on the weight loss of the electrode.

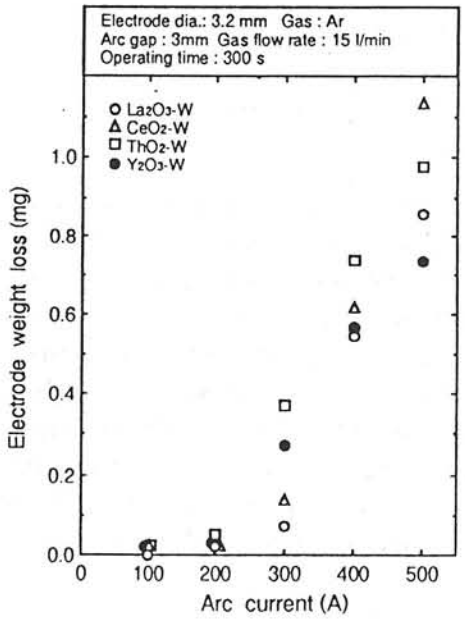

Figure 16. Electrode weight loss as a function of current.

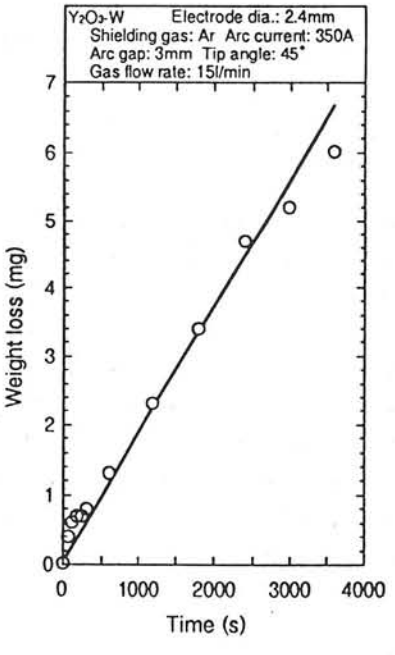

Figure 17. Electrode weight loss as a function of operation time.

homogeneous and the behavior of the oxide provides a complicated effect on the temperature distribution.

The introduction of oxygen into the inert shielding gas promotes strongly the growth

of tungsten dendrites in the zone C and resuls in the formation of a rim, like the brim of a hat as shown in Figure 18. It causes unstable arc behavior and consequently large fluctuations in arc voltage and arc pressure as shown in the same figure. The size and shape of the rim depend on the arc burning time at a given current. The rim is formed a small distance away from the tip end. According to the X-ray diffraction analysis the rim is formed by the deposition of pure tungsten on the electrode surface where the situation is suitable for crystal growth.

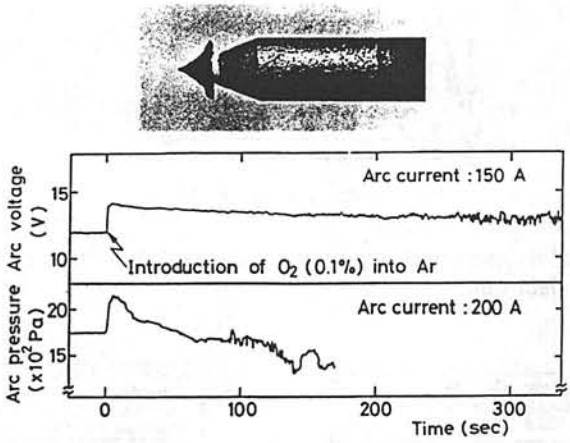

Figure 18. Unstable arc behavior due to formation of a rim. The appearance of the rim is also shown.

Figure 19 gives a schematic illustration of the vaporization and the motion of volatile tungsten oxides along the electrode surface. There is a change in vaporization rate along the electrode surface, as shown in the calculation. Under the effect of a gas stream, oxides from the regions of high vaporization rate move along the electrode. Decomposition of tungsten oxide and condensation of tungsten occur on the electrode surface at the point where the conditions are favorable for crystal growth. This consideration makes clear the distinctive features of the three characteristic zones: zone A is defined as emitting zone due to its high temperature, zone B is defined as the higher vaporization rate zone of rare earth metal and has a smooth surface, but electron emission is lower than that in A, zone C is the only zone which has a suitable temperature for crystal growth.

6. Conclusions

The performance of tungsten thermionic cathodes are discussed through a comparative study of arc properties, oxide behavior in the electrode, cathode temperature and erosion phenomena, consumption of electrode material due to evaporation, for several types of electrodes.

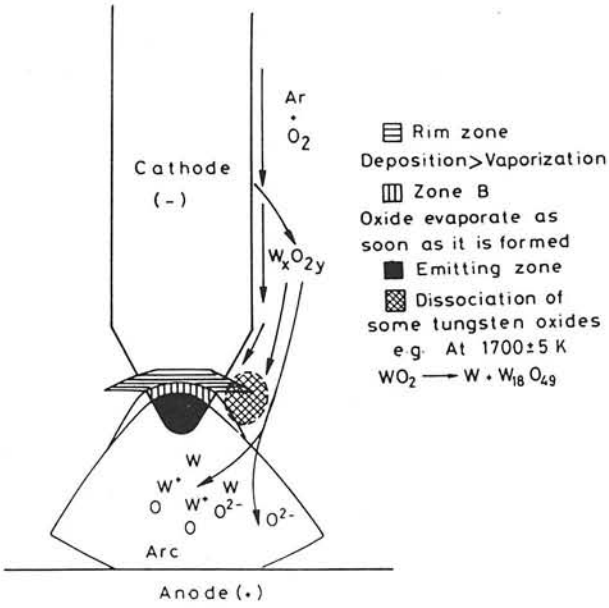

Figure 19. Schematic illustration of the rim formation mechanism.

The work was carried out with one reference electrode (W-ThO_2) and other electrodes activated by rare earth metal oxides, La_2O_3, CeO_2 and Y_2O_3. It was shown that these newly developed electrodes have superior properties compared with those of thoriated tungsten. On the basis of the results of this study the following conclusions can be drawn.

1. ThO_2 may react with tungsten, forming pure Th. The Th is considered to diffuse away from the bulk to the tip surface and then to evaporate.
2. Rare earth metal oxides react with tungsten, forming tungstate and oxytungstates. These tungstates or oxy-tungstates melt and migrate from the lower temperature zone to the higher temperature zone. The difference in their migration rates may be attributed to their melting points and to the tungsten grain morphology.
3. The behavior of rare earth metal oxides during arc burning is the most important factor in determining the operating properties of the electrode, that is, electrode temperature, work function, electron emission, and stability of the tip shape.
4. The balance between the migration rate and the evaporation rate of the oxide has a decisive effect on the operational stability and durability.
5. At high current, the temperature of the tip of a sharp cone increases and severe concentration of oxide sometimes occur. This is due to the excess migration in a high temperature gradient. These oxides may decompose and gasify.
6. The behavior of oxides is governed by the temperature and its distribution, which are different for various tip shapes. When the evaporation of the oxide material from the surface and its feed from inside is well balanced, the electrode gives the most superior durability. This consideration suggests that an optimum amount of

oxide can be determined by estimating the temperature field of the electrode.

7. The formation of the rim at the periphery of the emitting area of the cathode is a serious problem for the arc stability during long time operation. The rim was shown to consist of tungsten dendrites and is considered to originate from the oxidation of tungsten.

Acknowledgment

The authors would like to express their appreciation to Dr. A.A. Sadek for valuable contributions, and to TOHO KINZOKU Co., Ltd. for production of many electrodes.

References

1. A.E. Guile: IEE Rev., 118 (1971), p.1131.
2. G. Ecker: Z. Naturf., 28a (1973), p.417.
3. A.C. Davies : THE SCIENCE AND PRACTICE OF WELDING 7th Ed., Cambridge Univ. Press (1977), p.373.
4. L.P. Winsor and R.R. Turk : Weld. J., 36 (1957), p. 113.
5. N.A. Chapin, J.D. Cobine and C.J. Gallagher: Weld. J., 30 (1951), p. 529.
6. D. Flemming: Schweiszen und Schneiden, 18 (1966), Heft 5, p. 220.
7. A.A. Sadek, M. Ushio and F. Matsuda: Metallurgical Trans. 21A (1990), p. 3221.
8. Committee on Weld. Process J.W.S.: IIW Doc.XII-1047-87.
9. M. Ushio, A.A. Sadek and F. Matsuda: IIW Asian Regional Welding Congress, Australia (1988), Vol. 2, p. 989.
10. M. Ushio, A.A. Sadek arid F. Matsuda: Plasma Chem. and Plasma Processing 11 (1991), p. 81.
11. M. Ushio, A.A. Sadek and F. Matsuda: Proc. Int. Conf. Plasma for Industry and Environment, Paper 6.3, Oxford, BNCE (1990).
12. M. Ushio, F. Matsuda and A.A. Sadek : Proc. Int. Conf. of Int. Trends in Welding Science and Technology, Gutlinburg, Tennessee (1992), p. 405.

The Influence of Ambient Pressure on Arc Welding Processes – *a review*

I.M. Richardson

Cranfield Institute of Technology,
Cranfield, Bedfordshire, UK

Abstract

Ambient pressure has a profound influence on arc stability, process characteristics and energy transport properties. Many features are common to all welding processes, although detailed behaviour has been found to depend critically on local environmental conditions and is therefore process dependent.

This paper presents a review of some of the pressure dependent effects on basic arc structure, principally for the TIG welding arc for which significant quantities of data are available. Attention has also been paid to recent research concerning the MIG, Flux-cored and Plasma welding processes at elevated pressures. Several groups have shown that these processes exhibit levels of overall stability essential for welding in very deep waters (below 500 m sea depth). For many aspects of reported process behaviour, little or no understanding of the physical relationships and governing principles exist at the present time. Several such instances have been discussed together with recommendations for further research.

1. Introduction

High pressure arcs are used in a variety of industrial applications including furnaces, high power shock tubes, rail guns, power interrupt systems (fuses and circuit breakers) and as standard spectral sources, in addition to applications in areas such as chemical production and materials processing (welding, cutting, surfacing etc.) [1,2].

In general the term high pressure refers to arcs which are collision dominated such that conditions in the plasma column tend (very approximately) toward local thermal equilibrium, in contrast to the low pressure and vacuum arcs for which significantly greater electron temperatures are observed [3]. The behaviour of a high pressure discharge depends to a large extent on the arc configuration and power supply characteristics. High pressure conditions may also be created in low or medium pressure environments by the action of the discharge. Large pressure differentials occur in high current (kA) arcs (e.g. heaters and furnaces) due to the interaction

between the current flow and the self generated magnetic field [4]. These may be associated with pressure increases of the order of a few bar to a few tens of bar for both confined [5,6] and free burning [7–9] arcs.

Arcs associated with welding operations must provide continuous, controllable sources of heat. This generally imposes stability requirements on the discharges which become critical at high operating pressures.

This paper is concerned with the operation of welding arcs in high pressure environments with currents of the order of a few tens of amps and small induced pressure changes (compared with ambient pressures). A full review of the physical concepts associated with hyperbaric welding arc behaviour is considered to be outside the scope of the present work; indeed, such a work would require a substantial book despite (or because of) the fact that so little of the physical detail is understood, even in a qualitative manner. The purpose of this review is to highlight some of the most important aspects of hyperbaric welding arc behaviour and to indicate areas where further research efforts are required.

2. General

A large body of literature exists on the exploitation of arc welding techniques in connection with the offshore construction and repair industry [4, 10–22]. The majority of publications consider the influence of environmental conditions on the behaviour of the welding processes and the resultant influence on weld metal properties [14–17]. During the 1970's and 1980's considerable research effort was expended to improve operating performance and develop suitable control strategies for the various welding processes.

The influence of pressure on process performance and requirements is governed to a large extent by changes in arc properties. The structure of the arc column is controlled by the material properties of the plasma, environmental conditions and the required current flow. Equilibrium operating conditions occur when the rate of electrical energy supplied to the discharge is balanced by the energy losses to the electrode, workpiece and surrounding media. As the ambient pressure is raised above one atmosphere the physical properties of the plasma are altered and particle densities increase (approximately) in proportion to the absolute pressure [23]. Convective and radiative heat losses increase with pressure and are associated with a rise in arc voltage.

A self consistent explanation of many of the observed phenomena may be made by appeal to the minimum energy loss principle. Enhanced energy transport constrains the arc to contract and adopt a new minimum energy loss configuration, resulting in a

smaller cross-sectional area of the conducting core. Electrical conductivity rises with pressured [24] (> 12,000 K) such that the reduced arc column is capable of sustaining the required current flow at similar core temperatures. Increased radiative energy loss occurs as a result of a re-distribution of the arc energy (which may be inferred from the form of the enthalpy term in the energy balance equation [4]).

This general behaviour is common to all types of welding arcs presently used offshore. Each welding process however, creates unique environmental conditions, a detailed description of arc behaviour is therefore process dependent.

3. Arc voltage

The potential drop across an arc may be subdivided into a number of components related to physical regions in the welding arc. In its simplest form, this subdivision includes components for the anode and cathode fall regions and the plasma column. At one atmosphere, the majority of the power generated in the welding arc occurs in the fall regions, the column contributing only 20 to 30% of the total power.

3.1 The column component

As pressure increases the arc voltage rises resulting from an increased power dissipation, with voltage changes being almost entirely associated with an increased column component. For welding arcs whose behaviour is dominated by the physical properties of the shielding gas, this rise is approximately proportional to the square root of pressure. The mean voltage (V) is often expressed in the form [4, 25–27]

$$V = V_0 + E_1 \ell \left(\frac{P}{P_0}\right)^n \tag{1}$$

where V_0 is the sum of the fall voltages, E_1 is the one bar electric field strength, ℓ the arc length, P the operating pressure and P atmospheric pressure (P_0 is often implicitly assumed in the literature when the pressure is measured in bar).

The value of the exponent n is generally reported to be about 0.5. Allum [2] notes that values as low as 0 and as high as 1 have been quoted under extreme conditions. The value of the exponent may be regarded as an indication of the energy exchange processes taking place in the arc, greater values being associated with increased energy losses [28]. Thus, the value of the exponent depends on the operating conditions, including shielding gas flow rate, current and plasma composition. Values of n in the range 0.1 to 0.25 have been found for low current (few amperes) arcs [29], whereas for conditions normally encountered in welding arcs n is often reported [4, 30, 31] in the range 0.3 to 0.6 (Figure 1).

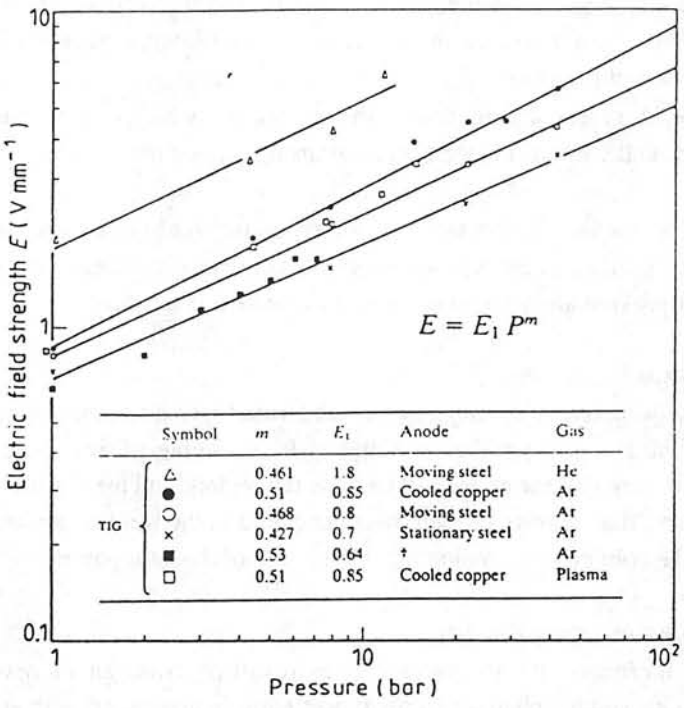

Figure 1. Illustration of the influence of pressure on arc column electric field strength for a range of operating conditions [31] (†-ref. [25]).

More detailed forms for the electric field strength term have been published which provide greater accuracy over a limited range of operating conditions [21, 27]. For example, Sugar reports that n is dependent on arc length and takes the form

$$n = 0.53\ \ell^{-0.31} \tag{2}$$

valid for both helium and argon arcs over the range of pressure 1 to 50 bar and arc lengths 1.5 to 6 mm.

Equation (1) and its variants are generally applicable to TIG type arcs. More complicated expressions for the constricted plasma arc have been derived for a given welding torch geometry and limited parametric ranges, although the final pressure dependence differs little from the $P^{0.5}$ relationship given above [32]. A summary of the influence of welding parameters on TIG arc voltages is given in reference [32].

There are no reported results concerning the measurement of voltage as a function of arc length and pressure for the MIG or Flux-cored welding processes. However, empirical models produced for process stability control suggest that the column is dominated by the properties of the shielding gas [33]. It is therefore reasonable to

suppose that the column properties will be similar to those of the non-consumable processes with electric field strength approximately proportional to $P^{0.5}$.

Unlike the welding processes mentioned above, the arc column during MMA welding is dominated by properties of the materials evolved from the flux coating surrounding the metallic electrode core. These consist primarily of CO_2, iron, sodium, potassium, calcium etc. which are easily ionisable. It has been reported on a number of occasions that pressure has only a small influence on arc voltage (Figure 2), with the dependence related to the composition of the flux coating [34–36]. There are few publications providing quantitative data on arc length/voltage/pressure relationships; however, recent work by Ogawa [37] concerning the effect of iron vapour on electron densities at elevated pressures provides an initial step toward understanding the behaviour of hyperbaric arcs dominated by metal vapours.

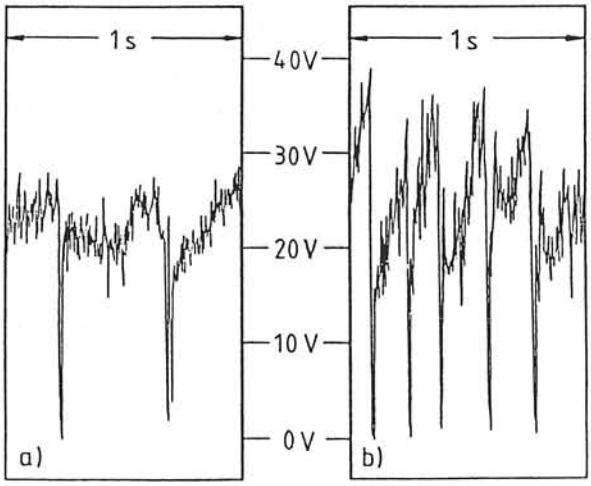

Figure 2. Arc voltages for MMA welds at (a) one atmosphere and (b) 150 m water depth for nominally identical operating conditions [16].

3.2 The fall voltage

The majority of published results concern the TIG arc, for which the sum of the anode and cathode fall voltages V_0 is thought to be substantially unaffected by pressure. Some reports of a pressure dependent fall voltage have been published [25, 29, 28] in which V_0, for an argon arc burning on a water cooled copper anode, increased by between 1.5 and 5 V over the pressure range 1 to 14 bar. Matsunawa and Nishiguchi [25] suggested that the increase in V_0 occurred due to contraction of the arc root on the cathode surface with a subsequent rise in electrode surface temperatures. However, no experimental evidence was offered to support this view. An alternative explanation has been offered by Allum who attributed such results to errors arising from the problems associated with extrapolating the voltage – arc length curves to zero arc length, due to

non-linear behaviour at short (< 1 mm) electrode separations [2] (similar to behaviour at one atmosphere [39]). A different technique for the determination of V_0 has been applied by Suga [26] and Dijk et al [30] whereby the arc gap was reduced until short circuiting took place. V_0 was equated with the voltage immediately prior to collapse. In both cases V_0 was observed to fall slightly with pressure. Suga reported no change above 6 bar and up to 60 bar (consistent with the observations of Dijk et al), with the combined fall voltage for an argon TIG arc operating on a cooled copper or mild steel anode [40, 41] being of the order 9±1 V.

Similar pressure dependence is observed for the consumable welding processes, although fall voltages are significantly greater [16, 33], typically 14 to 16 V due to the different electron emission mechanism (field domination cf. thermionic domination for the non-consumable processes).

The limited influence of pressure on the combined fall voltage is not surprising when the structure and purpose of the fall zones are considered. The potential drop in these regions occurs as a result of the imbalance of charged particles close to the electrode surfaces. This in turn is related to the energy requirements for electron liberation and capture, which are primarily dependent on the physical properties and conditions occurring at the electrode surfaces.

4. Stability

The stability of all arc welding processes is found to deteriorate with increasing ambient pressure. This may be explained in terms of the gas flow behaviour in the arc column, together with changes in conditions occurring at the arc roots.

An arc may be regarded to first order as behaving like an electromagnetically driven plasma jet whose origin lies in the interaction between the current flow and the self generated magnetic field [42]. This behaviour is modified by consideration of the plasma viscosity and compressibility [43, 44]. Plasma flow velocities for a wider range of gas shielded processes and operating conditions have been shown to result in a laminar gas flow at atmospheric pressure [4, 32].

Allum et al [21] have shown that the transition from laminar to turbulent flows in the cooler outer regions of the arc occurs at pressures of only a few bar (typically < 5 bar) in argon TIG arcs. The exact point of transition depends somewhat on the shielding gas flow rate, occurring at lower pressure for greater gas flow rates. At low flows, this criterion is superseded by the flow rate generated as a result of mass entrainment. Turbulent behaviour in the outer regions of the arc generates instabilities which propagate inward toward the arc core, resulting in a decrease in arc stability with rising pressure. It has been reported that the current carrying inner region of the arc contracts

at a faster rate with increasing pressure than the hot, essentially non-current carrying luminous boundary region [4]. Buoyancy forces will therefore dominate in the outer region (in the absence of the Lorentz force) resulting in the development of turbulence which opposes the flow of the plasma jet in downhand welding (Figure 3) [40].

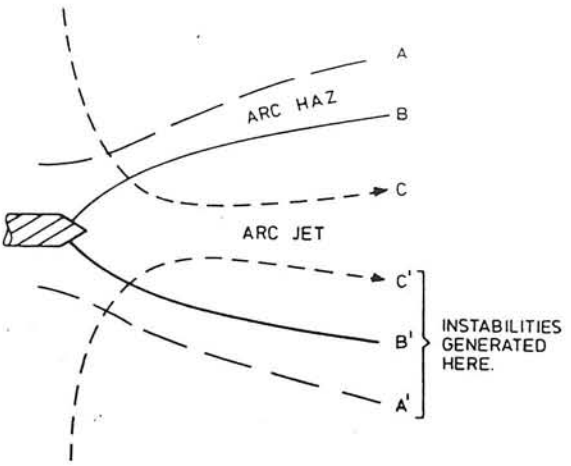

Figure 3. TIG arc structure illustrating strong mass entrainment close to the rod electrode with a strong plasma flow within CC'. Current is carried through BB' and arc heating extends to AA' [40].

Quantitative data on stability has been derived from the oscillation amplitude and frequency of an arc operating close to the split plane of adjacent isolated water-cooled copper anodes. Both the frequency and maximum amplitude are found to increase with increasing shielding gas (volumetric) flow rate and ambient pressure. Stability is reported to be directly linked to the mass flow rate of the shielding gas [4]. Over the pressure range 1 to 14 bar, mass flow rates of 0.5 g/s or less result in Reynolds numbers < 2,000 and minimal arc oscillation independent of ambient pressure (Figure 4). Maintenance of a constant mass flow rate requires that the volumetric flow rate must vary with pressure according to P^{-1}, unfortunately this leads to an unacceptable reduction in shielding efficiency. Allum et al have shown that for an arbitrary 5% stability criterion (the ratio of maximum oscillation to arc radius) gas flow is always turbulent at high operating pressures. With a constant volume flow rate of 10 l/min laminar flow limits are exceeded at pressures below 2 bar and the 5% limit at less than 4 bar. Alternatively, if the shielding gas mass flow rate is increased in proportion to the mass flow through the space occupied by the arc (proportional to $P^{0.66}$) [21] then the laminar limit occurs near 4 bar and the 5% limit at 37 bar. This behaviour indicates that for any given stability level an upper pressure limit will be reached for which arc oscillation exceeds the given criteria. The upper limit is likely to be reduced by additional requirements for efficient shielding [45].

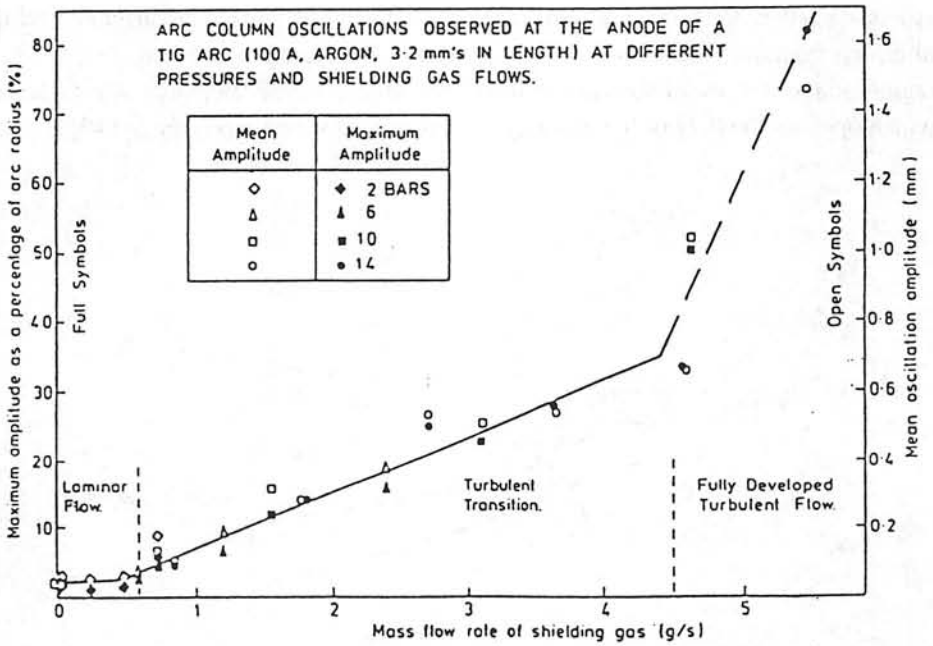

Figure 4. The influence of shielding gas mass flow rate on the amplitude of oscillation of a TIG arc [40]. Note: 1 gs^{-1} corresponds to a Reynolds number of 4.525.

The stability of the gas flow may be assessed in terms of the Reynolds number (Re) which is related to the velocity of the flow u_z, the plasma density ρ and the viscosity η by

$$\mathrm{Re} = \frac{\rho u_z L}{\eta} \tag{3}$$

where L is a characteristic length related to the geometry of the system (arc diameter).

For temperatures below 10,000 K, viscosity rises linearly with temperature and is virtually independent of pressure [46]. Density increases approximately linearly with pressure [47] and u_z falls with pressure according to $P^{-0.36}$ for the TIG arc [45] and between $P^{-0.46}$ and $P^{-0.75}$ for weakly and strongly constricted plasma arcs respectively [2]. From experimental measurements, the radius of the arc column is observed to fall with increasing pressure according to $P^{-0.17}$ for the TIG [47] arc and $P^{-0.16}$ for the constricted arc, although the exponent for highly constricted arcs [32] falls to -0.23. Hence the Reynolds number of the gas flow increases approximately according to $P^{0.5}$ for the free burning arc and $P^{0.39}$ for the weakly constricted plasma arc, whereas only a small pressure dependence ($P^{0.02}$) is predicted for the highly constricted arc [32], suggesting that stable arcs may be maintained at very high

ambient pressures.

The behaviour in the inner core of the arc is somewhat more complicated due to the temperature and pressure dependence of viscosity at temperatures above 10,000 K [46]. Nevertheless, the reduction in density at elevated temperatures ensures that flow in the hot current carrying core remains laminar to pressures of at least several tens of bar [32].

Turbulence in the arc results in increasing random fluctuations in arc voltage (mirroring the random influence on energy losses). Such behaviour has been observed for all hyperbaric arc welding processes, including MMA [4, 11, 32, 33, 48] (see Figure 2).

Electrode erosion is reported to increase with increasing pressure [12, 19, 25]. This is often associated with an observed decrease in the cathode root area and an increase in cathode surface temperature due to electron emission requirements. Allum reports that the radius of the cathode root R_0 for a 3.2 mm long, 100 A argon arc follows the relationship

$$R_0 = 0.46\ P^{-0.11}\ [\text{mm}] \tag{4}$$

over the pressure range 1 to 14 bar. The associated mean current density then follows a $P^{+0.22}$ relationship. Greater electrode surface temperatures lead to increased erosion rates and a deterioration in arc stability. Edmonds et al [29] noted that erosion rates increased with pressure and depended on electrode size and vertex angle. Erosion was found to be reduced with large diameter electrodes at a vertex angle of 30°. Hoffmeister [19] also reports reduced erosion with larger diameter electrodes. Replacement of the conventional thoriated tungsten by a lanthanum oxide doped electrode and the use of efficient water cooling also helped to reduce erosion.

The deterioration in arc stability with increased electrode erosion has been attributed to cathode root instabilities. Huismann et al [49] report three stages of erosion at high pressure:

I - tip detachment, where the sharp point of the electrode is melted and vaporised or transferred as a tungsten droplet
II - electrode melting covers the end of the truncated cone, erosion related to vaporisation only (by implication the arc root covers the entire truncated surface)
III - the truncated surface is larger than the melt zone, the cathode root precesses due to the action of the induced $\underline{J} \times \underline{B}$ force.

Significant instabilities are observed in the third stage. The influence of erosion on arc stability is difficult to assess on the basis of electrode mass loss. Huismann et al therefore measured the diameter of the truncated cone surface (d_e) and found that this gave more consistent indications of arc behaviour. These authors found that d_e was a minimum at an electrode vertex angle of 30° for thoriated electrodes and 35° for ceriated electrodes (Figure 5). Tip diameter was found to increase with increasing additions of thorium oxide and with increasing material resistivity. Resistivity varied depending on electrode manufacturer and appeared to be associated with electrode homogeneity, a lower value corresponding to a more uniform distribution. Erosion rates are reported to increase rapidly with increasing arc current and are more severe in helium environments [26, 40].

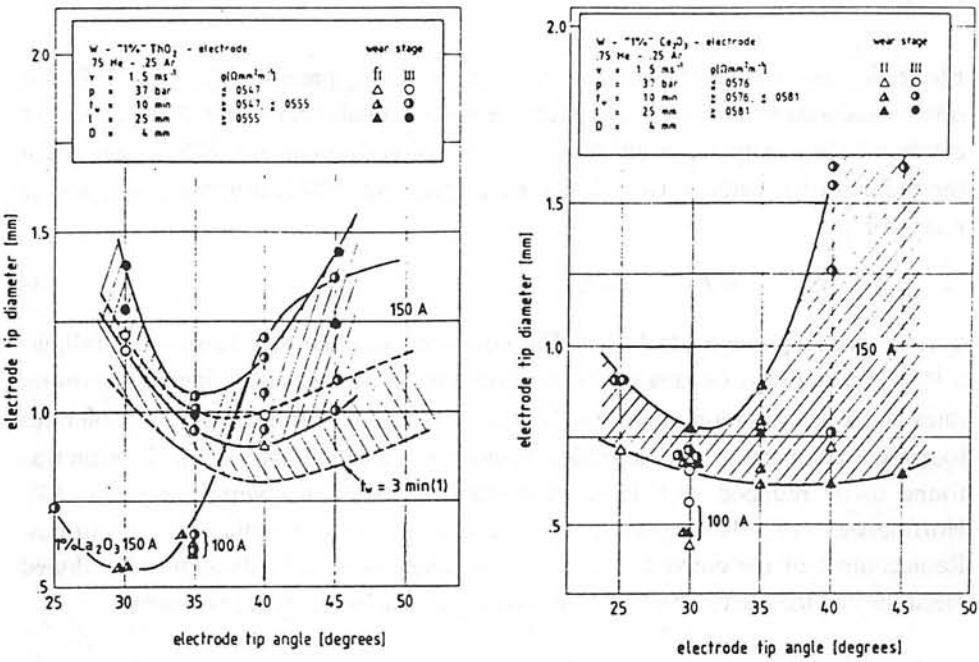

Figure 5. Effect of electrode tip angles on tip diameters of thoriated (left) and ceriated (right) tungsten electrodes after 10 min. arcing time at 37 bar [49].

5. Energy transport

Allum has considered the energy balance of the free burning arc in some detail [4, 31, 50]. Based on measurements of electromagnetic radiation, the radiation leaving the arc has been found to be (approximately) linearly dependent on arc length and current ($I > 75$ A). The radiated power Q_R in agreement with the one atmosphere observations of Goldmann [51], is shown to be dependent on arc column power and is proportional to $P^{0.5}$. Similar results have been reported for the constricted (Plasma) arc operating over a wide range of conditions [32] (see section 6.1). Recent work at

Cranfield has shown that the ultra-violet subset of the electromagnetic spectrum also obeys a $P^{0.5}$ relationship, where integrated intensities in the wavelength region 170 to 260 nm have been measured (Figure 6). This has important implications for the safety of welder/divers.

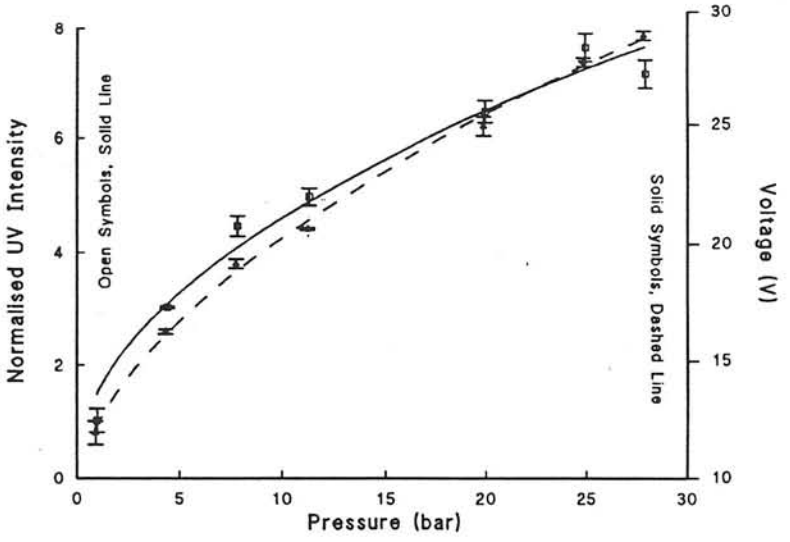

Figure 6. The relationship between pressure and integrated UV radiation intensity (170 to 260 nm) for a 3 mm long, 100 A argon TIG arc on a water cooled copper anode (data normalised to 1 bar).

Conductive power losses Q_κ from the arc column (neglecting end effects) have been estimated [52] using the expression

$$Q_\kappa = 2\pi\kappa \cdot \Delta T \cdot \ell \tag{5}$$

where κ is the thermal conductivity, ΔT the temperature difference across the arc boundary and ℓ the arc length. Thermal conductivity is reported to decrease with pressure at moderate temperatures and increases at high temperatures. For the pressure range typically associated with hyperbaric welding (up to 100 bar), the change over occurs in the temperature range 13,000 K to 16,000 K [46]. Conductive losses are thought to be only weakly influenced by pressure [4]. The importance of this term is therefore reduced as pressure increases due to the overall increase in arc column power.

Convective power dissipation Q_{cv} is dependent on the mass flow through the arc $\dot{m}$ given by

$$\dot{m} = \int_0^\infty \rho u_z \, 2\pi r \, \mathrm{d}r \tag{6}$$

and the enthalpy H (dependent on the arc temperature field)

$$Q_{cv} = \dot{m}\, H \approx \rho \cdot A \cdot \bar{u} \tag{7}$$

where the mean velocity $\bar{u}$ (for a magnetically driven arc jet) is found from the momentum flux expression [44] to be

$$\bar{u} = \left(\frac{\mu_0 I^2 \ln (R/R_0)}{4\pi\rho A}\right)^{0.5} \tag{8}$$

R is the mean arc radius and R_0 the radius at the cathode, I the current, A the arc cross sectional area and ρ the density. Equation (7) may then be written as

$$Q_{cv} = \frac{1}{2} H\, IR\, (\mu_0 \rho \ln \frac{R}{R_0})^{0.5} \tag{9}$$

and exhibits a pressure dependence slightly weaker than $P^{0.5}$. Alternatively for buoyancy dominated arcs $\bar{u}$ is given by

$$\bar{u} \approx \left(\frac{\rho_\infty g_z \ell}{\rho}\right)^{0.5} \tag{10}$$

and

$$Q_{cv} \approx \pi H R^2 (\rho \rho_\infty g_z \ell)^{0.5} \tag{11}$$

where ρ_∞ is the density of the cool gas in the surrounding atmosphere and g_z the acceleration due to gravity. In this case Q_{cv} is approximately proportional to $P^{0.66}$. For buoyancy forces to be significant (greater than 10%) Allum [53] has shown that arc current must be less than some critical value I_c given by

$$I_c = 2\pi R_i \left(\frac{10 \ell \rho(R_i) g_z}{\mu_0 \ln(R/R_0)}\right)^{0.5} \tag{12}$$

where R_i represents the radius of an isothermal boundary such that $\rho(R_i) \rightarrow \rho_\infty$.

Examination of the expressions given in equations (8) and (10) indicate that mean arc velocity for a magnetically driven arc falls according to $P^{-0.33}$ and is independent of pressure for the buoyancy dominated arc. Similar results have been predicted from gas flow behaviour models [44,50].

A number of authors have observed that heat transfer (process) efficiency decreases with increasing ambient pressure [2, 4, 31, 54], the larger percentage change occurring over the first few bars of pressure. At high pressures little change in process efficiency is observed [21]. Over the first 40 bar of pressure Allum indicates a decrease in efficiency from 80% to 60% on water cooled copper anodes and 75% to

40% on molten steel anodes [40]. The difference between the two materials may be explained in terms of the shielding effect of the molten weld pool and depends on the mechanisms involved in heat transportation in the molten anode. Slightly lower values of process efficiency have been reported for constricted plasma arcs falling from 70% to 60% over the first 16 bar of pressure and remaining virtually constant thereafter [32].

Melting efficiency is observed to increase over the first few bars of pressure [4, 54] followed by a slow decrease at high pressures (>15 to 20 bar) [4]. Efficiency increases with current and decreasing arc length and has been shown to be of the order 10% at 100A, rising to 30% at 210A for an argon arc in the pressure range 8 to 20 bar. The decreasing melting efficiency reported by Allum [4] was not observed with the 100A TIG welds or with welds made using the plasma process [32]. It seems probable that this behaviour (seen at 75A and 150A) may be due to arc induced weld pool turbulence. Plasma arc melting efficiencies are generally lower than those for the equivalent TIG arc and decrease with increasing arc constriction, due to greater column energy losses. Values are reported to be typically between 6 and 8% and virtually independent of pressure for pressures above about 8 bar.

6. Process dependent behaviour

The majority of the information on which the preceding sections are based is concerned primarily with the TIG welding process which has received significant attention in the literature; primarily due to its present employment both for manual root welding and for fully automated applications. Recently, interest has been expressed in the consumable wire processes and the Plasma welding process because these appear to offer stable operating conditions at high pressures (in excess of 50 bar) together with the potential for full automation.

6.1 The plasma process

Plasma welding is often considered to be a modified form of the TIG process in which a physical constriction is placed co-axial to the arc around the cathode. Physically, this introduces additional boundary conditions to the set of equations describing the structure of the arc column. The basic arrangement and nomenclature is illustrated in Figure 7. The major difference between the free burning TIG arc and the constricted plasma arc may be attributed to the influence of the plasma forming gas. The plasma gas acts to protect the constricting nozzle from the hot arc plasma by providing a thin layer of cool gas close to the nozzle wall. The plasma gas also supplies additional mass to the arc, plasma gas flow rates being typically one to two orders of magnitude greater than the mass flow due to self entrainment. The forces exerted by the cooler outer gas flow are found to dominate buoyancy induced behaviour, resulting in arc

stabilisation [32, 55, 56]. As pressure is increased the Reynolds number of the outer gas flow is expected to rise resulting in turbulent flow. However, over the range of pressures 1 to 64 bar these effects are found to be small compared with buoyancy generated forces of the free burning arc. Results indicate that a significant improvement in stability may be achieved with relatively large constrictions and low plasma gas mass flow rates leading to voltage increases of less than 10% above those of equivalent TIG arcs.

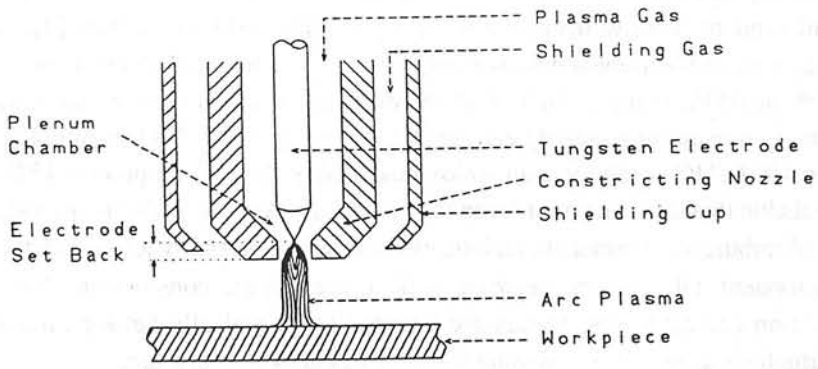

Figure 7. Scheme of the main features of the plasma welding process [32].

The constriction of the arc acts to limit radial expansion close to the point of arc generation, resulting in a more columnar arc (compared to a similar TIG arc). Arc velocities depend on a large number of factors; however, for moderate operating conditions, the plasma arc velocities are of the order 2 to 3 times greater than those of the equivalent free burning arc.

One consequence of the limited radial expansion of the plasma arc is the rise in radiative output. The pressure dependence of radiation may be understood in terms of the energy balance of the arc. As pressure is increased the arc takes on an even more columnar appearance, contracting to minimise energy losses. Expanding the convective term of the energy balance equation (see for example reference [23]), leads to

$$\rho \underline{u} \cdot \nabla H \rightarrow \rho C_P \left(u_r \frac{\partial T}{\partial r} + u_z \frac{\partial T}{\partial z} \right) \tag{13}$$

where H is the enthalpy, ρ the density, C_p the specific heat capacity at constant pressure, u the velocity and T the temperature.

For columnar arcs both $\partial T/\partial z$ and u_r are small, the significance of the enthalpy term therefore decreases as the arc column contracts due to constriction or increased pressure. Conduction is limited by the surface area of the arc which is reduced; therefore radiative transfer must increase to account for the observed rise in energy

loss implied by the increased arc voltage.

The dependence of arc radiation on current and arc length was found to be similar for free and constricted arcs although absolute levels are greater for the plasma arc. Both arc forms exhibit a linear relationship between radiated power and arc length, although this breaks down at long arc lengths with the TIG process.

The percentage of column power radiated is also found to be greater for the plasma arc than for the TIG arc. Allum [4] quotes values of 18 to 25% for pressures of 1 to 41.6 bar ($I > 75$A), compared with ~30 to 40% for similar constricted arcs (1 to 32 bar). Radiative output from a 100 A argon plasma arc column at 32 bar ranges from 250 W for a 2.1 mm long arc to > 1kW for an 8.1 mm long arc [32], equivalent to between 6 and 18% of the total process power (Figure 8). For plasma arcs it was found that the percentage column contribution increased significantly with current at low pressures and became virtually independent of current, orifice diameter and plasma gas flow rate at pressures in excess of 16 bar. For higher current arcs, the percentage column power radiated reached saturation at lower pressures. This indicates that for high pressure or high current arcs, other energy loss mechanisms are required to account for the increased process power (i.e., increased arc voltage). It is thought that these additional energy losses may be accounted for by turbulent transfer from the arc column.

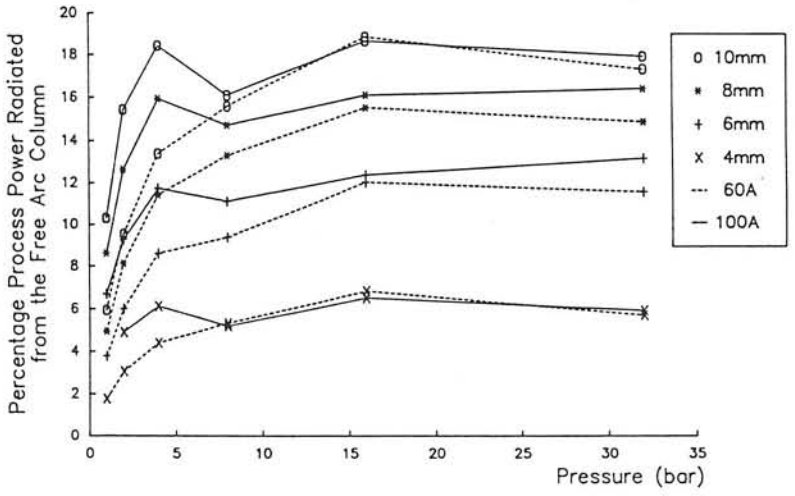

Figure 8. The effect of pressure on the fraction of total process power radiated from the free column of a plasma welding arc (4.75 mm orifice, 2 mm tungsten set back, argon plasma at a flow rate of $0178P^{0.5}$ g/s) [32].

The contribution to anode heating from arc column radiation is expected to be comparatively small. It is difficult to calculate with any accuracy because the distribution of energy within the arc column is unknown. Fifty percent of the power

radiated travels away from the anode. A significant percentage of the remainder strikes the anode outside the pool boundary. Of the radiation incident on the pool surface at least 50% is reflected from the surface. It is therefore unlikely that more than ~10% of the radiated column power is absorbed by the molten pool (and probably a much smaller fraction). This accounts for < 2% of the power appearing in the anode at high pressures and a smaller percentage as pressure approaches one atmosphere.

Although in many instances, the TIG and plasma arcs show similar characteristics and behaviour, the plasma arc differs in several important respects [4, 32]. Notable among these is the influence of arc constriction on the pressure exerted at the anode by the arc. It is well known that the plasma process offers the capability of keyhole welding at one atmosphere; however, little relevant research has been reported in the literature until comparatively recently [32].

The total excess pressure on the arc axis P_a may be written as the sum of a gas dynamic term P_g and an electromagnetic term P_{em} where [42]

$$P_g = \tfrac{1}{2}\rho u_z^2 \tag{14}$$

and

$$P_{em} = \frac{\mu_0 I J}{4\pi} \tag{15}$$

J is the mean current density and u_z the axial component of plasma velocity away from the anode surface.

The excess arc pressure for constricted argon plasma arcs is found to fall with increasing ambient pressure. This is in direct contrast to the behaviour of the free burning TIG arc for which P_a has a $P^{+0.28}$ dependence [40]. Intermediate behaviour has been found for weakly constricted arcs. This may be explained in terms of the differing pressure dependence of the arc radius (see section 4) and hence the relative contributions of P_{em} and P_g. The electromagnetic term has a pressure dependence of $P^{+0.31}$ and the relative contribution to the TIG arc is typically of the order 35±5% of the total measured pressure, independent of ambient pressure.

During plasma welding at one atmosphere, the gasdynamic term dominates and P_{em} is found to contribute typically around 5% to the measured pressure. However, as u_z falls rapidly with pressure (see section 4) for the constricted arc, the relative importance of P_{em} increases, and the term dominates at high pressures [32].

It has also been reported that P_a increases with increasing plasma gas mass flow rate; however, beyond a critical flow rate P_a remains constant [32, 57] (Figure 9). The

mass flow at which the arc pressure attains its maximum value is virtually independent of ambient pressure though strongly dependent on orifice diameter, being greater for the smaller nozzles. The reason for this is obscure.

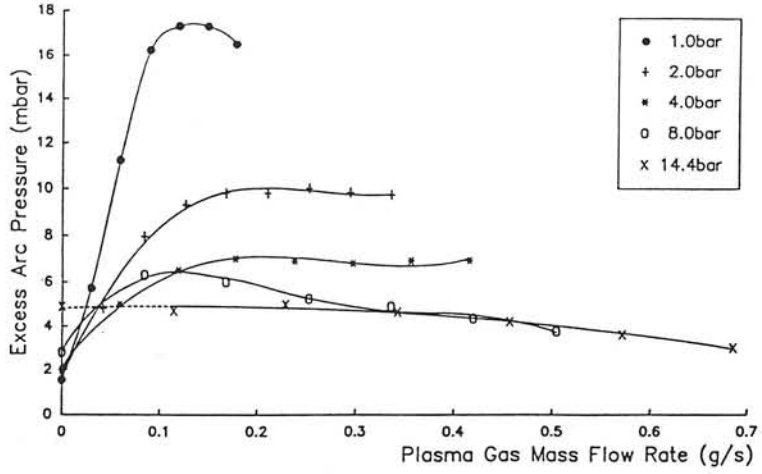

Figure 9. The influence of plasma gas mass flow rate on excess arc pressure for a range of ambient pressures (100 A, 4 mm orifice, 8 mm arc length, 2 mm tungsten set back) [32].

Measured values for the cold gas flow suggest that the pressure in the absence of the arc is small compared with P_a. The cold flow must therefore act to accelerate the plasma within the constriction nozzle, effectively changing the boundary conditions. Increasing plasma flow will eventually lead to nozzle clogging which results in a reduced effective nozzle area. Close to the arc axis temperatures are high and densities significantly lower than exist near the arc boundary or outside the arc. The majority of mass therefore passes around the arc which acts as a barrier restricting the cold flow [9, 58]. In terms of the arc energy balance, arc structure will adjust to minimise convective losses due to excess mass transport. The net effect will be to divert excess mass away from the arc core whilst minimising structural changes. This explains qualitatively the observation that axial arc velocity tends toward a constant value at high flow rates. The mechanism is supported by the observations of Edels on high current constricted arcs [9] who noted increasing flow rate caused a reduction in the arc thermal radius with minimal influence on axial plasma temperatures.

The net result indicates that high arc pressures cannot be achieved at high ambient pressures for an argon plasma arc and this has been confirmed experimentally [32]. Recent research concerned with the use of mixed gas plasma have shown that high arc pressures can be achieved with the addition of helium to the plasma forming gas and keyhole welds over a range of pressures up to 32 bar have been demonstrated [59].

The mechanism responsible for the increase in arc pressure with the addition of helium at high ambient pressures is obscure.

6.2 The MIG and Flux-cored processes

By their nature, the MIG and Flux-cored processes exhibit a time dependent behaviour related to the melting of the wire, and the transfer of metal from the wire to the weld pool. At one atmosphere, this may be achieved either by an open arc process or dip process. In open arc operation, the molten metal droplet is formed, detached and transported through the arc due to the jet like flow of the plasma. Conversely, in dip transfer, the molten droplet periodically bridges the gap between the wire and the weld pool resulting in a short circuit. Despite considerable differences in the methodology of metal transfer, both process variants are governed by similar operational considerations at high pressures.

Investigations involving the open arc (pulsed current) mode of metal transfer [33, 60, 61] indicate that the MIG arc is significantly influenced by pressure. The arc is observed to contract as pressure increases over the first few bars in a similar manner to the free burning TIG arc. It has also been found from photographic evidence that the droplet transfer velocity decreases with increasing pressure, suggesting a decrease in the plasma velocity [33]; this is also in accord with the behaviour of the TIG arc.

At one atmosphere, the MIG arc generally operates with a wire positive polarity. At pressures of a few (4 to 5) bars, contraction of the arc and of the cathode root on the weld pool surface leads to the formation of one or more cathode spots, with associated plasma jets. The spots are highly mobile on the weld pool surface and individual spots may exist for long periods (> 1 s). The plasma jet forms as a result of electromagnetic pumping (identical to the primary arc jet mechanism), creating a plasma force acting normal to the weld pool surface and outward into the arc column.

The formation of these spots is highly dependent on the chosen welding conditions, and the onset of spot formation may be postponed by selection of large amplitude, short duration current pulses; however, increasing pressure inevitably leads to their generation. Further increasing pressure tends to result in the formation of a single cathode spot and associated plasma jet which acts to oppose the anode jet and disrupt the transfer of the metal from the wire to the weld pool [33, 60, 61] this is illustrated schematically in Figure 10. Spot formation is associated with an increase in arc voltage of the order 2V, and is significantly influenced by the chemistry of the consumable and the shielding gas.

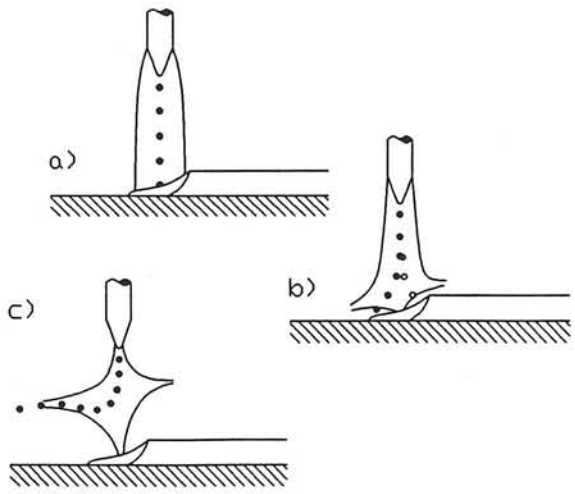

Figure 10. Influence of arc root constriction on plasma column and metal transfer behaviour; a. and b. dominant anode jet, b. with multiple (small) cathode spots and jets, c. equal anode and cathode jets, single cathode spot [32].

The force exerted by the cathode jet has been found to increase with pressure until it approximately balances the force of the anode jet. This behaviour disrupts the metal transfer, often retarding transfer by suspending the droplet in the region where the electromagnetically driven jets collide (Figure 11) and expelling the droplets sideways from the arc column.

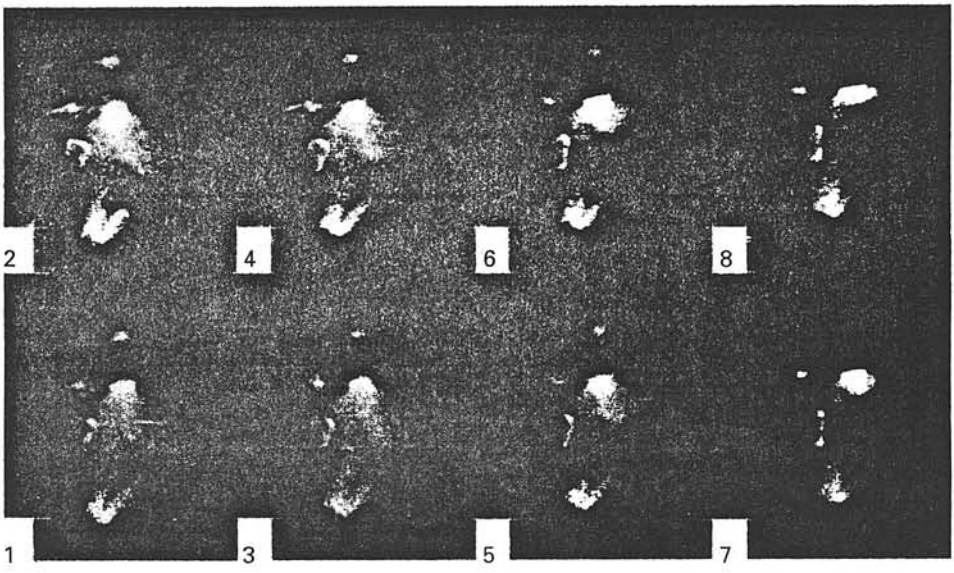

Figure 11. Anode and cathode jet formation during pulsed MIG welding in an argon atmosphere at 4 bar. Photo sequence with 0.1 ms between exposures.

At high pressures, the influence of the opposing jet structure in the arc column may be minimised by welding with a relatively short arc (typically < 1 mm) and small diameter consumable (≤ 1 mm). Under such conditions, some short circuiting is inevitable, although the majority of the metal is transferred around the arc column. Positional welding is feasible provided close control of the arc length is maintained. This suggests that the metal droplets are initially accelerated after detachment by the plasma jet acting from the wire, and subsequently expelled from the arc column. However, detailed behaviour for such short arcs is difficult to observe at high pressures due to diffraction effects.

Behaviour in the dip transfer mode shows similar arc structures, although disruption of the metal transfer does not occur [62, 63]. This has significant advantages at moderate pressures (10 to 15 bar) where, due to the balance of forces, pulsed operation does not provide adequate stability for positional welding [33, 61].

The key to maintaining process stability for the MIG and Flux-cored processes lies in the control of the welding power source. Due to the disrupting influence of the metal motion, operating with a constant current power source characteristic rapidly leads to voltage spikes in excess of the supply capability of the power source, with subsequent loss of control of the operating current and arc extinction. It has also been observed that the arc rooting mechanism is influenced by the power source output characteristic, resulting in a strong cathodic jet at moderate pressures (4 to 5 bar) when operating in a constant current mode.

Voltage control may be achieved using a sloping power source output characteristic, such that the arc operates in a self adjusting mode [17] (Figures 12 and 13). In the control model developed at Cranfield, it was found that the degree of self adjustment (i.e., the slope of the power source) was pressure dependent. Optimum control requirements (determined empirically) indicate that for a given consumable, the current change per unit change in arc length should be constant, independent of pressure. Hence, the pressure dependence of the power source slope (k measured in V/A) is determined by the arc length/voltage/pressure relationship. This follows the same behaviour as the TIG arc (see equation 1) for solid wires for which the column component is determined by the properties of the shielding gas. Thus,

$$k = \text{const.} E_1 \, P^{0.5} \tag{16}$$

Any power source output characteristic may be defined by the slope and a set point. The set point is usually hardware dependent; however, in general

$$V_{set} = m \, I_{set} \tag{17}$$

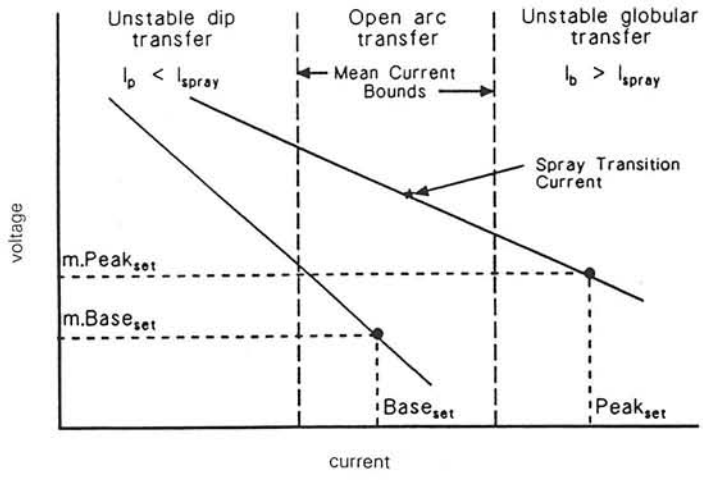

Figure 12. Relationship between power source set points and output characteristic for a pulsed current self adjusting arc [33].

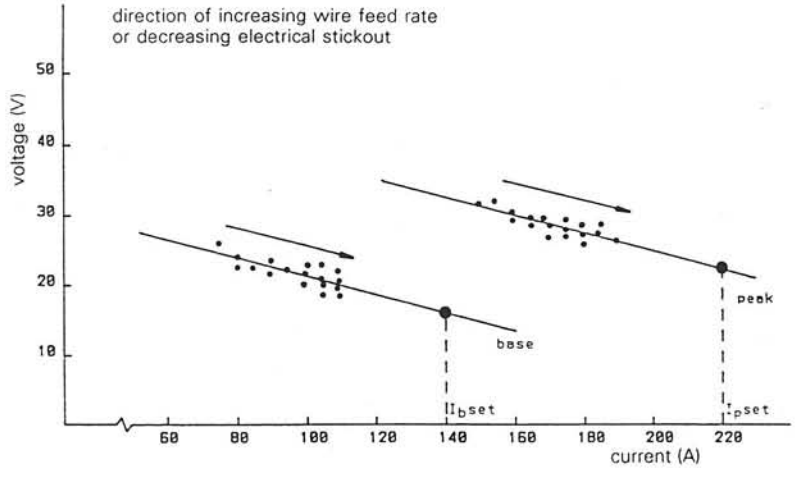

Figure 13. Power source output characteristics for a pulsed, self adjusting arc. Points represent values for a stable argon shielded arc at 30 bar [33].

where m is a constant. The voltage anywhere on the characteristic is then related to the mean current by

$$V = k(I_{set} - \overline{I}) + mI_{set} \tag{18}$$

It is notable that the mean process power is now dependent on a negative I^2 term; the current at which the maximum power occurs $I_{\Phi max}$ is therefore given by

$$I_{\Phi max} = I_{set}\left(\frac{k+m}{2k}\right) \tag{19}$$

At one bar $I_{\Phi max}$ is typically around 1,000 A. However, at high pressures (above 20 bar) the power maximum occurs at mean currents typically employed for pulsed welding. Operating with a mean current close to the power maximum ensures that total power generation is little influenced by inherent process instabilities (Figure 14).

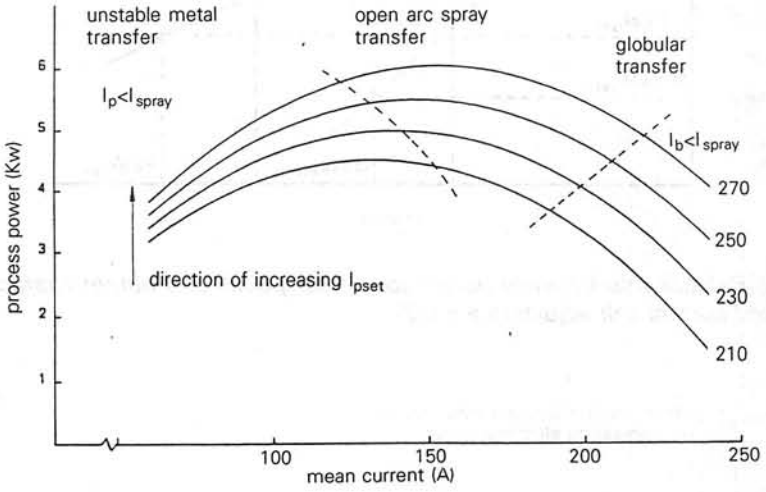

Figure 14. Illustration of process power as a function of mean current, parameters are based on stable operating conditions for helium arcs at 36 bar [33].

It has been reported that for solid wires and most flux cored consumables, acceptable process stability can only be achieved by control of power source dynamics. Details differ between the dip and pulsed current process variants; however, current rise and fall rates must be controlled during all parts of the operating cycle. During pulsed welding, if the rise rate is too slow, droplet detachment often fails to occur, resulting in the build up of molten material on the wire tip. Conversely, if the rise rate is too fast, large quantities of very fine spatter are produced. This is thought to be associated with the dispersion of the molten droplet due to a physical shock imparted by the rapidly expanding plasma. Similar observations have been made for the dip transfer mode where spatter levels and dip frequencies have been shown to be highly dependent on the dynamics of the current during the dip cycle [48].

In general, parametric envelopes decrease in size with increasing pressure and are larger for the flux-cored wires than the solid wires, due to the influence of the chemical arc stabilisers which have a significant influence on the arc rooting behaviour, reducing the strength of the anode and cathode jets (i.e., the current densities at the arc roots).

7. Summary

This paper provides a review of some aspects of hyperbaric welding arcs. The majority of the information available is concerned with the free burning TIG arc, although it is evident that most welding arcs with plasma columns dominated by the properties of the shielding gas behave in a similar manner.

The plasma welding process appears to offer the potential for welding at pressures well in excess of those of the free burning arc due to its inherent stability. Initial research has proved promising; however, further work is required to develop a complete understanding of the influence of arc constriction and enforced gas flow on arc structure and behaviour.

The MIG and Flux-cored processes have also been reported to produce stable welds at very high pressures. These processes work essentially by limiting the degree of arc instability to lie within acceptable bounds, usually by operating with very short arc lengths. High quality welds can therefore be made even though the arc itself is highly mobile and unstable at quite moderate pressures. Arc forces are controlled either chemically (as in the case of flux-cored wires) and/or electrically. Virtually nothing is known about the interaction between power source dynamics and arc behaviour at the present time; further research would therefore be of significant interest.

References

1. Jones, G.R. 'High Pressure Arcs in Industrial Devices' Cambridge University Press, 1988.
2. Allum, C.J. 'The Effect of Pressure on Arcs' Proc. IIW Int. Conf., 'Underwater Welding' Trondheim, Norway, 27-28 June, 1983, pp. 171 to 178, Pergamon Press.
3. Hoyeaux, M.H. 'The Physics of the Electric Arc' High Temp. High Press., Vol. 2, pp. 17 to 30, 1970.
4. Allum, C.J. 'Characteristics and Structure of High Pressure (1-42bars) Gas Tungsten Arcs' Ph.D Thesis, Crarfield Institute of Technology, 1982.
5. Marlotte, G.L., Cann, G.L. and Harder, R.L. 'A Study of the Interactions Between Electric Arcs and Gas Flows' USAF Report ARL 68-0049, Task 7063, Aerospace Research laboratories, Wright-Patterson Alr Force Base, Ohio 45433, USA, March 1968.
6. Kovitya, P. and Lowke, J.J. 'Theoretical Predictions of Ablation Stabilised Arcs Confined in Cylindrical Tubes' J. Phys. D: Appl. Phys., Vol. 17, pp. 1197 to 1212, 1984.
7. Bowman, B. 'Measurements of Plasma Velocity Distributions in Free-Burning DC Arcs up to 2160A' J. Phys. D: Appl. Phys., Vol. 5, pp. 1422 to 1432, 1972.
8. Ramakrishnan, S., Stokes, A.D. and Lowke, J.J., 'An Approximate Model for High Current Free-Burning Arcs' J. Phys. D: Appl. Phys., Vol. 11, pp. 2267 to 2280, 1978.
9. Edels, H., 'Properties of the High Pressure Ultra High Current Arc' Proc. 11th Int. Conf. on 'Phenomena in Ionized Gases', Prague, Czechoslovakia, Vol. 2, pp. 9 to 59, Sept. 10-14, 1973.
10. Stalker, A.W. and Salter, G.R. 'A Review of the Literature on Underwater Welding and Cutting to June 1984' Weld. Inst. Report RR/SMT-R-7405, 1975.
11. Nixon, J.H. and Billingham, J. 'A Survey of Underwater Welding Techniques' Endeavour, New Series, Vol. 11, No. 3,1987.
12. Lythall, D.J. and Gibson, D.E. 'Report on the Effect of Depth on Underwater Code Quality Gas Metal Arc Welding' Offshore. Tech. Conf., Paper 2643 Dallas, Texas, 1976.

13. Richardson, I.M. 'Underwater Arc Welding – A Survey of Process Behaviour' Weld. Rev. pp. 11-20, Feb. 1989.
14. Christensen, N. 'The Metallurgy of Underwater Welding' Proc. IIW Int. Conf., Trondheim, Norway, 27-28 June, 1983.
15. Pandey, R.K. and Swetnam, D. 'Dry Hyperbaric MMA Welding, The Effect of Water Depth on Welding of BS 4360 50E Structural Steel' Weld. & Met. Fab., pp. 232-236 Sept. & pp. 278-281 Oct. 1985.
16. Allum, C.J. 'Hyperbaric SMAW: Cold Cracking' American Gas Association Report No. PR-147-135, 1982.
17. Richardson, I. M. and Nixon, J.H. 'Open Arc Pulsed Current GMAW: Application to Hyperbaric Welding Operations' Proc. ASM Int. Conf., Toronto, Canada, 15-17 Oct. 1985.
18. Ibarra, S., Olsen D.L. and Grubbs, C.E. 'Underwater Welding of Higher Strength Offshore Steels' Proc. 21st Annual OTC Conf., Texas, pp. 67-76, 1989.
19. Hoffmeister, H. 'The Effect of Pressure on Process Parameters and Mechanical Properties in Hyperbaric Underwater Welding' State of the Art Report on Underwater Welding Pt.2, IIW Doc CREAU 87-86, 1986.
20. Knagenhjelm, H.O. and Ovland, S. 'Deep Ex 81' Norsk Hydro Report No. 47/82 Oct. 1982.
21. Allum, C.J., Pinfold, B.E. and Nixon, J.H. 'Some Effects of Shielding Gas Flow on Argon Tungsten Arcs Operating in High Pressure (1 to l4bar abs.) Environments' Weld. J. Res. Sup. 59, (7), pp. 199s – 207s July 1980.
22. Bauder. U.H. and Bartelheimer, D.L. 'Spectroscopic Studies of High Pressure Argon Plasmas' IEEE Trans. Plasma Sci. Vol. PS-I, pp. 23 to 30, Dec. 1973.
23. Lancaster, J.F. 'The Physics of Welding' 2nd Edition, IIW, Pergamon Press, 1986.
24. Devoto, R.S. 'Transport Coefficients of Ionised Argon' Phys. Fluids, Vol. 16, No.5, pp. 616 to 623, May 1973.
25. Matsunawa, A. and Nishiguchi, K. 'Arc Characteristics in High Pressure Argon Atmospheres' Proc. Int. Conf. 'Arc Physics and Weld Pool Behaviour', Weld. Inst., London, paper 8, May 1979.
26. Suga, Y. 'On the Arc Welding under High Pressure Argon and Helium Atmosphere' Proc. IIW Int. Conf., 'Welding Under Extreme Conditions', Helsinki, Finland, 4-5 Sept. 1989, pp. 207 to 214, Pergamon Press.
27. Dynachenko, V.V. and Olshanskii, A.N. 'Effect of Controlled Atmosphere Pressure on Welding Process Variables' Weld. Prod., No. 11, pp. 5 to 9, 1968.
28. Guile, A.E. 'The Electric Field in the Column of High-Pressure Argon Arcs' Proc. 2nd Int. Conf. on 'Gas Discharges' IEE Conf. Publ. No.90, London 1972.
29. Edmonds, T.G., Allum, C.J., Pinfold, B.E. and Nixon, J.H. 'The Effects of Pressure on the Tungsten Argon welding Arc' Proc. Int. Conf. 'Arc Physics and Weld Pool Behaviour', Weld. Inst., London, paper 46, May 1979.
30. Dijk, O. and den Ouden, G. 'The Effect of Pressure on the TIG Welding Process' Proc. IIW Int. Conf., 'Underwater Welding' Trondheim, Norway, 27-28 June 1983, pp. 155 to 161, Pergamon Press.
31. Allum, C.J. 'Mechanisms of Power Dissipation in the Columns of High Pressure Argon-Tungsten Arcs' Weld. J. Res. Sup., pp. 35~s to 3~s, December 1983.
32. Richardson, I.M. 'Properties of the Constricted Gas Tungsten (Plasma) Welding Arc at Elevated Pressures' Ph.D. Thesis, Cranfield Institute of Technology, 1991.
33. Richardson, I.M. 'Hyperbaric Open Arc Pulsed GMAW at Pressures 20 to 100bar' Final report for SERC MTD Ltd and Industrial Sponsors, May 1988.
34. Stalker, A.W. and Salter, G.R. 'A Preliminary Study of the Effect of Increased Pressure on the Welding Arc' Report RR-SMT-R-7504, The Welding Institute, 1975.
35. Groves, D. 'Hyperbaric Welding', Underwater Construction Technology Conf., Cardiff, April 1975.
36. Gaudiano, A . 'A Summary of 26 Underwater Welding Habitat Jobs', OTC 2302, Houston, Texas, May 1975.

37. Ogawa, Y. 'The Effect of Iron Vapour on Electron Density of Hyperbaric Arc Plasma', Proc. 121h OMAE Conf., Vol 3, ptA, p147-154, Glasgow, 1993.
38. Levin, M.L. 'Some Observations on the Effect of Pressure on the Tungsten Inert Gas Arc' Proc. 9th Int. Conf. on 'Phenomena in Ionised Gases' Bucharest, 1-6 Sept. 1969. Publ. Editura Akademiei Republicii Socialistic Romania.
39. Lancaster, J.F. 'Energy Distribution in Argon Shielded Welding Arcs' Brit. Weld. J., Vol. 1, pp. 412 to 426,1954.
40. Allum, C.J. 'Underwater Welding with TIG' IIW Doc. 212-522-82,1982.
41. Allum, C.J. 'FIG's Underwater Role: Present and Future' Weld. and Met. Fab., pp. 124 to 132, April 1982.
42. Maecker, H. 'Plasmastromungen in lichtbogen infolge Eigenmagnetischer Kompression' Z. Phys., Bd. 141, pp. 198 to 216,1955. Eng. trans. AEI Research labs., Manchester. Doc. No. AEI/T/895, July 1955.
43. Lancaster, J.F. 'The Dynamics of the Plasma Jet in a Free-Burning Arc' IIW Doc. 212-87-66,1966.
44. Allum, C.J. 'Gas Flow in the Column of a TIG Welding Arc' J. Phys. D: Appl. Phys., Vol. 14, pp. 1041 to 1059,1981.
45. Allum, C.J., Pinfold, B.E. and Nixon, J.H. 'High Pressure Inert Gas Shielded Arcs' IIW Doc. XII-B-28&80, 1980.
46. Kannappan, D. and Bose, T.K. 'Transport Properties of a Two Temperature Argon Plasma' Phys. Fluids, Vol. 20, No. 10, pp. 1668 to 1673, Oct. 1977.
47. Brahinsky, H.S. and Neel, C.A. 'Tables of Equilibrium Thermodynamic Properties of Argon, Volume II: Constant Pressure' Von Karman Gas Dynamics Centre, Arnold Engineering Development Centre, Tennessee, USA. Report No. AEDCTR-69-19, March 1969.
48. Olsen, J.M. 'Effect of Metal Transfer on Process Parameters on Metal Transfer and Arc Stability of Hyperbaric GMA Welding of Duplex Stainless Steels' M.Sc Thesis, Cranfleld Institute of Technology (work undertaken at GKSS, Germany) 1993.
49. Huismann, G., Hoffmeister, H. and Knagenhjelm, H.O. 'Effects of TIG Electrode Properties on Wear Behaviour under Hyperbaric Conditions of 37 to 40bar' Proc. IIW Int. Conf., 'Welding Under Extreme Conditions', Helsinki, Finland, 4-5 Sept. 1989, pp. 239 to 246, Pergamon Press.
50. Allum, C.J. 'Power Dissipation in the Column of a TIG Welding Arc' J. Phys. D: App]. Phys., Vol. 16, pp. 2149 to 2156, 1983.
51. Goldman, K. 'Electric Arcs in Argon: Heat Distribution' Brit. Weld. J., Vol. 10, pp. 343 to 347, July 1963.
52. Quigley, M.B.C., Richards, P.H., Swift-Hook, D.T. and Gick, A.E.F. 'Heat Flow to the Workpiece from a TIG Welding Arc' J. Phys. D: Appl. Phys., Vol. 6, pp. 2250 to 2258, 1973.
53. Allum, C.J. 'The Stability of Argon Tungsten Arcs Operating on Water Cooled Copper Anodes at Pressures up to 14.8 Atmospheres' Proc. IEE Conf. on 'Gas Discharges', Sept. 1980.
54. Zijp, J.P. and den Ouden, G. 'Effects of Ambient Pressure on GTA Welding of Ferritic Steel' IIW Doc. 212-71&8B, 1988.
55. Digre, N.O. 'Hyperbarisk Sveising med Innsnevret Lysbue' Internal report on project No. 341217, Division of Metallurgy, SINTEF, N-3704 Trondheim NTH, Norway, 15th January 1985 (in Norwegian).
56. Waldie, B. 'Effects of Increasing Ambient Pressure on Cutting Characteristics and Heat Transfer in Plasma Cutting' Proc. 6th Int. Conf. on 'Gas Discharges and their Applications', Edinburgh, pp. 82 to 85,8-11 September 1980.
57. Stepanov, V.V. and Nechaev, V.I. 'On the Pressure of the Plasma Arc' Weld. Prod., No. 11, pp. 6 to 8, 1974.
58. Lowke, J.J. and Ludwig, H.C. 'A Simple Model for High Current Arcs Stabilised by Forced Convection' J. Appl. Phys., Vol. 46, No.8, pp. 3352 to 3360, August 1975.
59. Richardson, I.M. and Cave, W.F. 'Plasma Welding at Pressures 1 to 100bar', MTD Grant Ref. GR/G25917, Presentation to sponsors, July 1993.
60. Abas, S.H.K. 'Hyperbaric Controlled Transfer GMAW: Process Stability at Pressures 1 to 10bar', M.Sc Thesis, Cranfield Institute of Technology, 1987.

61. Malkin, A. 'The Effect of Pressure and Shielding Gas Composition on the Hyperbaric GMAW Process in the Pressure Range 1 to 10bar absolute' M.Sc Thesis, Cranfield Institute of Technology, 1988.
62. Dos Santos, J.F., Szelagowski, P. and Schaftstall, H.G. 'Properties of Hyperbaric Flux Cored Arc Welds: Weld Metal Chemistry', 21st Offshore Technology Conference, OTC5893, Houston, Texas, 1-4 May 1989.
63. Dos Santos, J.F., Szelagowski, P., Schatstall, H.G. and Dobernowsky, A., 'Preliminary Investigations of the Effect of Short Circuit Variables on Metal Transfer Above 60bar abs.', 22nd Offshore Technology Conference, OTC6212, Houston, Texas, 7–10 May 1990.

Arc Ignition Behaviour in Gas Metal Arc Welding

D. Rehfeldt and C. Bremer

Joining of Materials – Welding Technology,
University of Hannover, Germany

Abstract

The ignition cycle with touch starting in metal inert gas welding of aluminium alloys and the reignition behaviour in short-arc welding of steel are studied on a microprocessor controlled, mechanized welding set-up. High-speed photographs of the ignition process as well as current-time signals and voltage-time signals are evaluated.

1. Introduction

The fully mechanized or automatic gas metal arc welding requires spontaneous ignition of the arc when using touch starting and reignition after short-circuits, together with high reproducibility of the ignition process. Disturbed ignition causes lack of fusion, spatter, flying wire end pieces and a non-uniform welded joint, which makes weld finishing necessary and thus limits the economic effectiveness of capital-intensive, fully mechanized welding equipment. To optimize this critical phase in gas metal arc welding it is necessary to know the physical sequence of events during the arc ignition.

The ignition with touch starting was investigated in metal inert gas welding of aluminum alloys where the ignition is difficult due to the material properties.
The reignition of the arc in short-arc welding with dip transfer was investigated in welding of steel.
The tests help to clarify the physical phenomena taking place during ignition and reignition in gas metal arc welding.

2. Measurement and test set-up

Figure 1 shows the basic measurement and test set-up. A microprocessor controlled, fully mechanized welding set-up was used for the tests. The welding voltage-time signals and welding current-time signals were recorded by various digital storage oscilloscopes (sampling rates: 20 MS/s, 400 MS/s, 800 MS/s and 1.6 GS/s). For the oscilloscopes the welding voltage signal was sensed directly between the contact tube and the workpiece by a well adjusted probe (division factor 10 : 1). The sensing of the

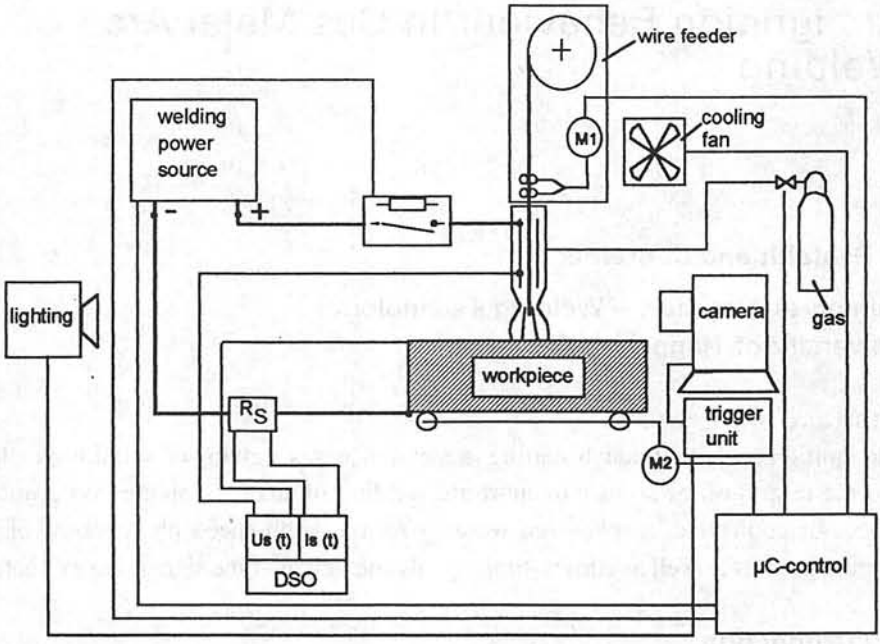

Figure 1. Measurement and test set-up.

measurement signal proportional to the welding current took place on a high frequency coaxial shunt.

The arc formation was recorded by the backlighting method with an ultra-high-speed image-converter camera at a recording speed of 1 MHz (max. recording speed: 50 MHz). The back light source was a xenon flash bulb. The welding voltage was used for triggering the camera and the digital storage oscilloscope.

In addition, the ignition process and the stationary welding process were observed with a high-speed-film camera. The camera was started shortly before the beginning of ignition by the microprocessor control of the welding set-up. The welding current and voltage were recorded with a digital storage oscilloscope synchronously with the camera recording. On the film and the oscillograms time marks at a frequency of 1 kHz and event marks at a frequency of 10 kHz were imposed, which made it possible to allocate the pictures to the electrical signals.

For high-contrast representation of the wire electrode here again the backlighting technique was used. The source of light was a helium-neon laser with an output power of 15 mW and a wavelength of 632.8 nm.

To avoid disturbances in the wire feeding a four-roller drive was mounted directly above the water cooled torch. The wire feed length was thus only 0.5 m.

For the ignition and welding tests typical combinations of AlMgSi0.5 were used as the base metal and S-AlMg5 (DIN 1732, Part 2) as the wire electrode (diameter: 1.2 mm). The dimensions of the plate were 300 mm × 30 mm × 15 mm. The shielding gas was commercially available Argon 4.6. The gas flow rate was 20 ℓ/min and the welding speed 58 cm/min. Before each welding operation the electrode end was cut off perpendicularly to the axis and the plate surface was cleaned with a wire brush made of stainless steel.

To examine the reignition in short-arc welding steel St 37 with ground surface was used as the base metal and SG 2 (DIN 8559) for the wire electrode (diameter: 1.2 mm, wire speed: 5,4 m/min). A mixed shielding gas (82% Ar , 18% CO_2) was used (gas flow rate: 15 ℓ/min). The welding speed was 35 cm/min. The mean welding voltage was 16 V and the mean current 160 A.

Two different power sources were used (a silicon-bridge rectifier and a secondary chopped transistor power source).

3. Experimental results

3.1 Ignition tests with touch starting in metal inert gas welding of aluminum alloys

In the tests, two different ignition processes occurred from the short-circuit.
Figure 2 represents a typical ignition in which, after creating the short-circuit, the short-circuit voltage rises, first of all linearly and then super-proportionally up to about 8 V approximately 3 µs before the voltage peak.

The resistance of the short-circuit increases during the heating up of the metal and the constriction of the softening wire electrode at the contact point due to the pinch forces. This is followed by a steeper voltage rise. The resistance heating leads to lengthening and bending of the wire electrode, blocked in the axial direction. The point of contact with the workpiece melts, overheats and evaporates spontaneously from the inside [1]. It burns through in an explosive manner like a fuse in fractions of microseconds [2]. As a result a shock wave is generated, which sprays the molten metal droplets away [3]. By breaking off the short-circuit a voltage is induced from the stored magnetic energy in the whole current circuit which superposes the open-circuit voltage up to a peak of approximately 83 V, Figure 2. In some tests maximum values above 160 V were measured at a short-circuit current of approximately 900 A.

From the highly heated metal droplet cloud and the metal vapor a non-stationary, high-voltage / high-current gas discharge is ignited between the workpiece and the wire electrode. This generates a second shock wave. These shock waves can be detected

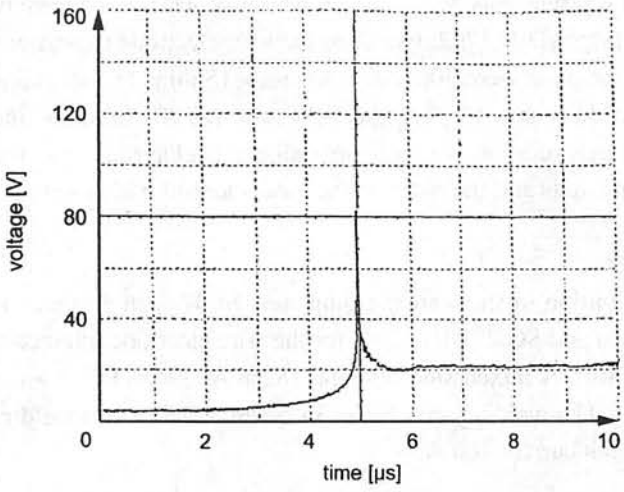

Figure 2. Ignition after a short circuit.

acoustically as the 'ignition bang'. The non-stationary gas discharge then changes over into a stationary welding arc.

With an ultra-high-speed image-converter camera pictures of a touch ignition with an image frequency of 1 MHz were produced. The high recording frequency and the short recording duration of 8 µs caused difficulties in triggering the camera by the ignition process. Figure 3 shows that the gas discharge ignites in less than 1 µs between pictures 1 and 2.

In other ignition sequences, after the first ignition voltage peak a second induction peak follows from a level of between 35 and 40 V and currents around 780 A, Figure 4.
First of all, the ignition process as described above begins and a non-stationary arc burns for approximately 600 µs. The not so high voltage peak values recorded in Figure 4 can be explained by the fact that the sampling frequency of the digital storage oscilloscope was much lower during this test.

Figure 5a shows such an ignition process in a high-speed film taken at about 9.000 pictures per second. The resistance heating leads to lengthening and bending of the wire electrode, blocked in the axial direction, Figure 5a, pictures 1 to 3. The point of contact with the workpiece melts, overheats, evaporates spontaneously and an arc ignites. Electromagnetic forces act on the conducting loop consisting of the softened wire electrode and the arc and cause the electrode end to rotate around the original electrode axis (spiral in stability). Reaction forces on the anode due to the emission of

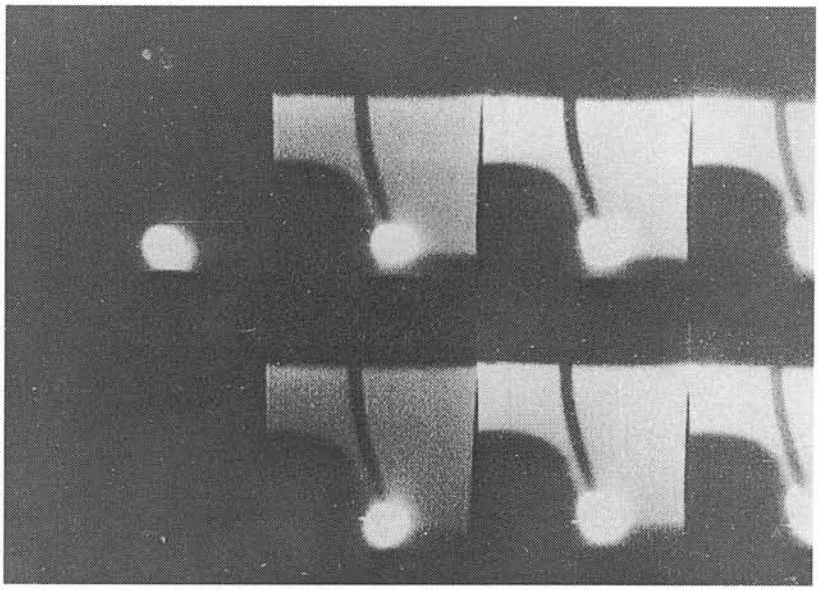

Figure 3. Ultra-high-speed recording of an arc formation 2 4 6 8. 1 3 5 7

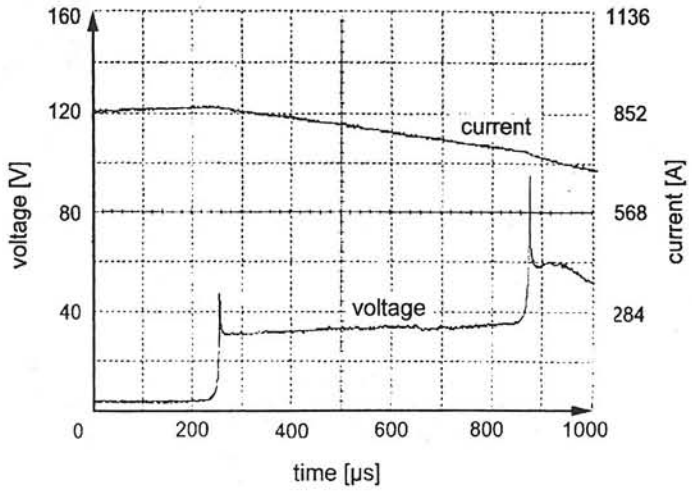

Figure 4. Ignition after a short circuit with jumping of the arc.

metal vapor (repulsion) and the starting plasma jet increase the bending and rotation, Figure 5a, pictures 3 to 15. The arc between the rotating wire electrode and the workpiece becomes longer. The softened wire end bends at the contact tube and is ejected out of the electrode axis by electromagnetic forces and centrifugal forces. At about 5 mm under the gas nozzle, the electrode cross-section contracts due to bending and the pinch forces, Figure 5a, pictures 13 to 15. The constricted electrode melts and

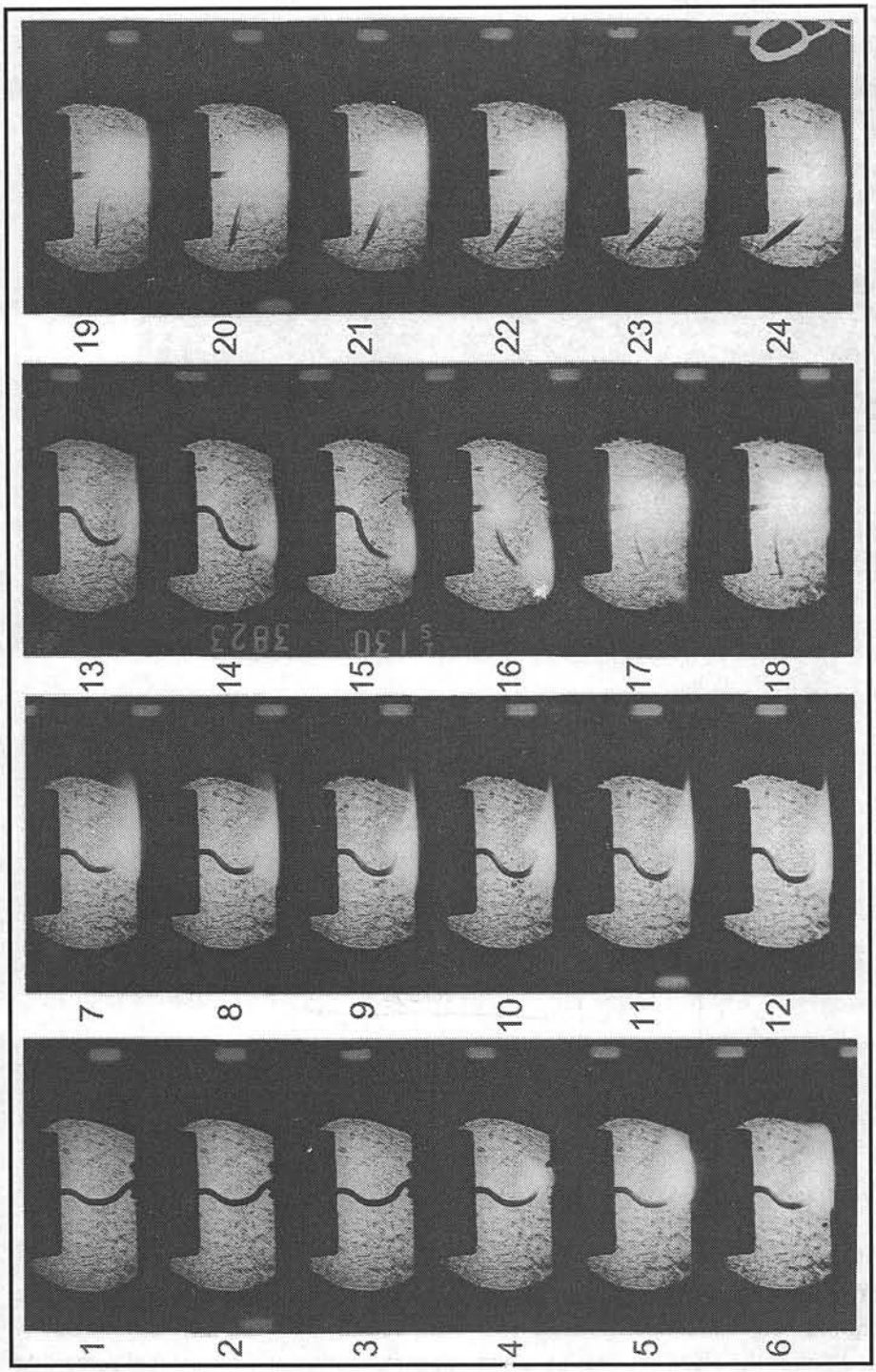

Figure 5a. High-speed film records (about 9000 pictures per second) of an ignition with two serial arcs.

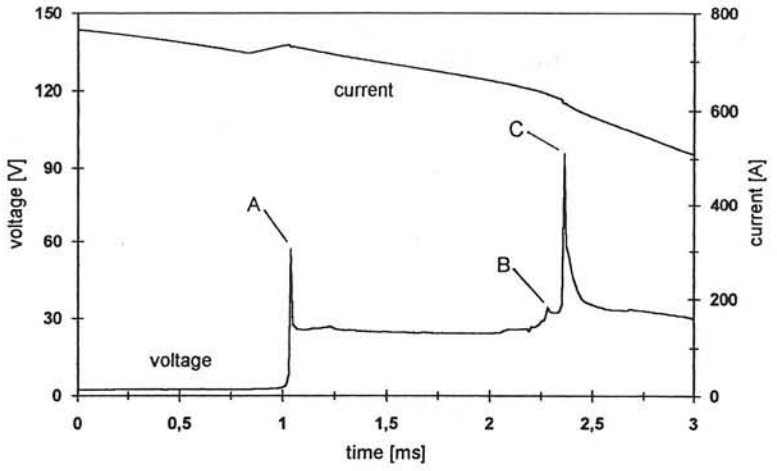

Figure 5b. Oscillogram of welding voltage and current corresponding to the high-speed film (Figure 5a) of an ignition with two serial arcs.

a second arc ignites, Figure 5a, picture 16, and then the arc jumps from the workpiece directly to the electrode projecting from the contact tube, Figure 5a, pictures 17. The detached wire is ejected from the arc region, Figure 5a, pictures 17 to 24.

The oscillogram of the welding voltage and current recorded synchronously is reproduced in Figure 5b.

The first arc ignition corresponds to the induction peak at point A (t = 1.05 ms). Nearly 1 ms later, after t = 2.01 ms the voltage increases exponentially causing the constriction of the electrode until at point B (t = 2.29 ms), with ignition of the second arc a small voltage peak occurs. The two serial arcs, Figure 5a, picture 16, burn for about 80 µs, Figure 5b, between point B and C. The jumping of the arc from the workpiece directly to the electrode projecting from the contact tube induces a voltage that leads to the third voltage peak at point C (t = 2.37 ms).

3.2 Reignition behavior in short-arc welding

The explosion of the molten metal bridge at the end of metal transfer in short arc welding generates a very fast and high voltage peak. The reignition was studied with fast digital storage oscilloscopes, sampling rates up to 1.6 GS/s. All measuring cables were as short as possible.

Different waveforms of the voltage signal occur during the fast short-circuit resolution when the molten bridge breaks in an explosive manner and the arc reignites.

Figure 6 shows a voltage peak of about 155 V after opening the short-circuit at the end of metal transfer. The trigger level of the digital storage oscilloscope was about 100 V. The voltage increases exponentially from about 50 V, 200 ns before the maximum peak, up to 80 V, 30 ns before the maximum of about 155 V. The molten short-circuiting bridge between electrode and workpiece is highly heated and pinched with increasing short-circuit time till explosion of the very thin metal bridge will occur. Figure 7 shows ten pictures of arc reignition of a short-arc process picked up by the ultra-high-speed camera with an image frequency of 1 MHz. On the first picture, 5 µs before arc reignition, a thin metal bridge can be seen with a decreasing diameter up to picture 5. The arc reignition occurs at picture 6 and the arc column grows up to the stable arcing phase.

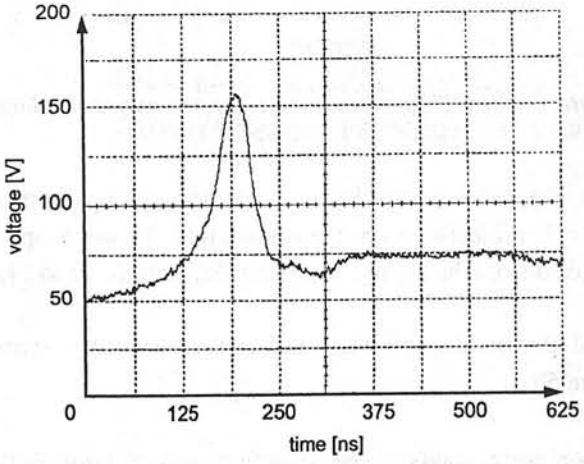

Figure 6. Reignition after a short circuit in MAG welding.

Another voltage waveform at the end of the short-circuit is shown in Figure 8. After the voltage has increased up to 180 V, there is an inflexion in the slope as it continues to rise. An extension of the time base (Figure 9) shows that the voltage persists for approximately 12 ns on 180 V and then rises up to its maximum of nearly 193 V.

Figure 10 shows a voltage peak and the light signal recorded with a photo diode. The light intensity rises with the first inflexion on the voltage curve. It can be assumed that the inflexion on the voltage curve is caused by the ignition of the first gas discharge.

Conclusions

Under the given test conditions, in metal inert gas welding of aluminum a high-current/high-voltage gas discharge ignites in less than 1 µs at the electrode-workpiece contact point as a result of the touch. A non-stationary arc then burns for a short time in this discharge area with high current and high voltage.

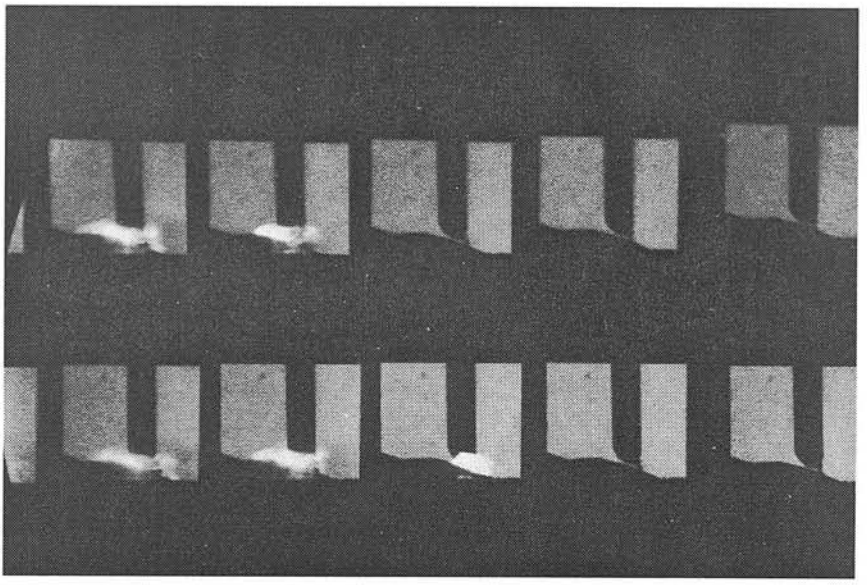

Figure 7. Ultra-high-speed recording of a reignition in MAG welding 9 7 5 3 1. 10 8 6 4 2

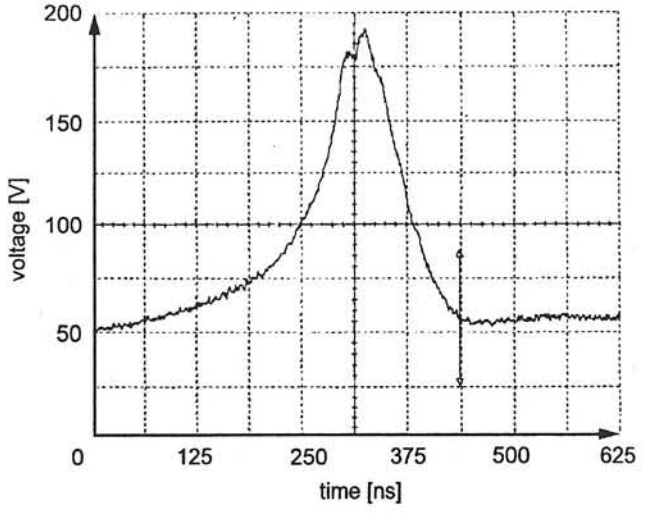

Figure 8. Reignition with an inflexion in slope before the voltage maximum.

After some hundred microseconds the softened and partially molten wire electrode often bends at the contact tube. It was observed that frequently the free wire end still existing is melted through by a second arc near the current contact tip. For a short time two serial arcs burn. The arc then jumps from the workpiece directly to the electrode projecting from the contact tube. The detached wire end is ejected from the arc region.

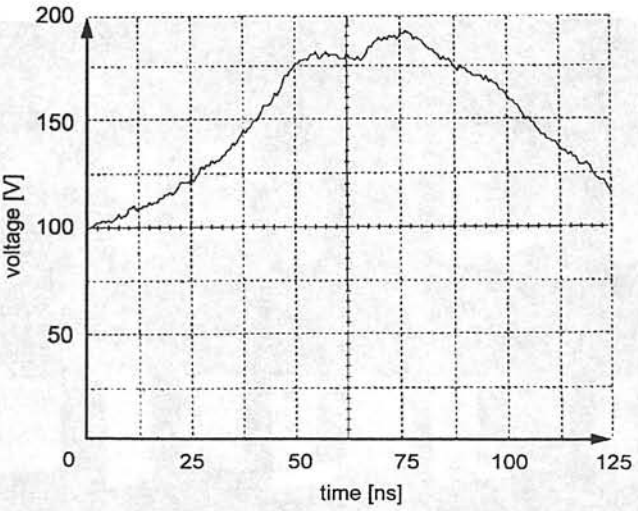

Figure 9. Reignition with an inflexion in slope before the voltage maximum (Figure 8) with an extended time base.

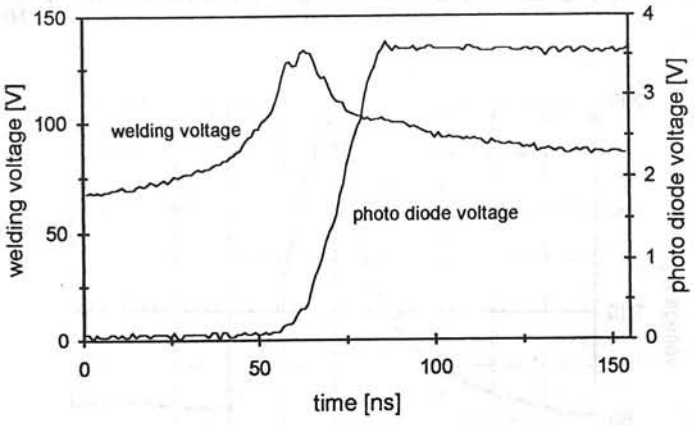

Figure 10. Welding voltage and arc light signal from a reignition after a short circuit in MAG welding.

In short-arc welding of steel an explosion of the molten metal bridge, at the end of the short-circuit, leads to a very fast and high voltage peak, sometimes up to 200 V. During the brief voltage peaks, there are different kinds of slope-up curves. In addition to voltage continuously rising, there are also cases with inflexions in the upward slope. From recordings of the arc light intensity it can be assumed that an inflexion in the slope is caused by a reignited gas discharge.

References

1. Chace, W.G.: A brief survey of exploding wire research. In: Exploding Wires, pp. 7-16, Chapman & Hall, London (1959).
2. Rehfeldt, D., u.a.: Untersuchungen zum Metall-Schutzgasschweißen mittels Ultrahochgeschwindigkeitskinematografie und schneller Erfassung elektrischer Schweißparameter. Schw. & Schn., 41 (1989), H. 3, S. 139–141.
3. Zaruba, I.I.: Electrical explosion as the cause of metal spatter. Avtom. Svarka, 23 (1970), No. 3, pp. 14–18.

Electrode Melting in Arc Welding

E. Halmøy

University of Trondheim – Norwegian Institute of Technology and
SINTEF, Welding Center
Trondheim, Norway

Abstract

A quantitative model for the melting rate in gas metal arc welding is reviewed and compared with data for submerged arc and shielded metal arc welding. For positive electrode polarity the same simple model is, for practical purposes, applicable to all these methods. For negative polarity the similarity is weaker. The physical explanations for this simplicity are discussed and found partly lacking and partly contradictory.

1. Introduction

The melting of electrodes in arc welding is a fascinating physical process which is also of great technical importance. Physically it is poorly understood. Technically, however, it seems to be very simple and predictable. Indeed, despite the great differences in electrode type and dimension, shielding gas and/or flux, current and voltage, type of droplet transfer etc. the melting rate is surprisingly easy to model mathematically and predict quantitatively. It depends in a simple way on just a couple of parameters and is independent of the others.

The purpose of this paper is to demonstrate this simplicity and also to point out our lack of physical understanding of why it is so simple. First an overview is given of the most important factors affecting the melting rate for gas metal arc welding with carbon steel electrodes, which has been most thoroughly studied. These results are then compared with other arc welding methods to demonstrate the similarities. Aluminum will also be discussed briefly. It should be noted that this paper does not pretend to be a comprehensive review of all phenomena or all major contributions concerning the melting of welding electrodes.

The first known quantitative study of the melting rate was published as early as 1930 by Leif Lefring of the Norwegian Institute of Technology [1]. This work established the simple fact that the mass melting rate M [kg/hour] was proportional to the current I [A], and the melting speed v [mm/s] was proportional to the current density j [A/mm^2]

The voltage appeared to have no effect. Naturally this study was limited to covered electrodes or SMAW, which was the only arc welding method used at that time. Because the current densities are generally low in SMAW, ohmic heating of the electrode was insignificant, hence the first power relationship. The only heating took place at the tip of the electrode. Such a simple relationship was, of course, what engineers would wish for, i.e.:

$$M = c_0 I \tag{1}$$

where c_0 is a constant.

Submerged arc welding (SAW) became available later in the thirties. Again the ohmic heating is usually insignificant, and 'Lefring's Law' remained useful.

2. The melting rate for gas metal arc welding (GMAW)

The next major development happened in the 1950s with the advent of gas metal arc welding. The pioneering study was published by Lesnewich in 1958 [2]. Because of thin wire electrodes and consequently higher current densities ohmic heating now became important. For one type of positive steel electrode Lesnewich established a relationship of the form

$$M = (0.017 + 0.37A)\, I + \frac{3{,}69 \cdot 10^{-8}}{A^{1.26}} LI^2 \text{ [lb/hr]} \tag{2}$$

where L [in] is the electrode extention or stick-out and A [in^2] is the cross-sectional area of the wire. In practice $0.37A \ll 0.017$. The first term is therefore practically proportional to the current I.

The most obvious physical interpretation of equation (2) would appear to be that the first term represents the arc heating at the end while the second term is the ohmic heating along the electrode. This is nearly the form to be expected if the end heating were similar to that of the covered electrodes, equation (1), and the stick-out behaved like a wire of length L with a constant resisitivity ρ. For such a simple system the melting rate would have been given by:

$$M = c_1 I + c_2 \frac{\rho}{A} LI^2 \tag{3}$$

It was in fact surprising that the resistive term in equation (2) was proportional to I^2, since the resistivity of steel increases by an order of magnitude from room temperature to the melting point. The average resistivity should then increase as more current is passed through the wire. The apparent $A^{-1.26}$ dependence in equation (3) may be related to this varying resistance.

The first term has approximately the form of equation (l) but the constant $c_1 < c_0$. It was found by doing welding trials at finite extension and extrapolating the results to $L = 0$. As will be shown below, this leads to too low an estimate of the anode heating.

Lesnewich also measured the melting rate for *negative* electrodes. For clean wires the cathode heating was also nearly proportional to the current, but approximately twice as high as the anode heating. When activated with cesium to lower the work function of the electrode, the anode melting rate was unchanged. The cathode melting rate, however, was strongly reduced at high currents. These results are shown in Figure 1 (from ref. [2]).

The anode heating was found to be independent of shielding gas composition. For cathode heating a small influence (< 10%) was observed. Both rates were independent of the arc voltage.

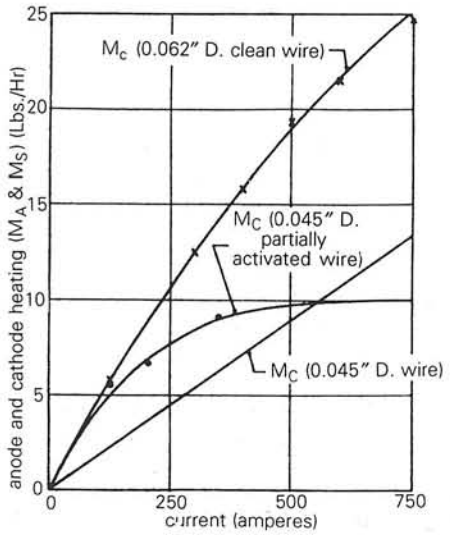

Figure 1. Anode and cathode melting rates for GMAW. Ref. [2].

A more detailed model of the GMAW electrode melting rate was developed 20 years later [3]. The temperature dependent resistivity was accurately measured as a function of the heat content (i.e. the temperature) of the wire by means of a simple experiment. It was found that the heat content H_L [J/mm^3] caused by the resistance was a non-linear function of Lj^2/v where v is the wire feed rate (or melting rate). For sufficiently high values of H_L this function could be linearized to the form:

$$H_L = \rho_L \frac{Lj^2}{v} - b \qquad (4)$$

Here ρ_L is the nearly constant resistivity of steel at temperatures above ca. 800°C and b is a constant depending on the room temperature resistivity. Welding experiments verified the following equation where ϕ [V] and H_0 [J/mm^3] are constants:

$$H_L + \phi \frac{j}{v} = H_0 \tag{5}$$

Substituting the linearized expression (4) into equation (5) yields a useful linearized equation for the wire melting speed:

$$v = \frac{1}{H_0 + b}(\phi j + \rho_L L j^2) \tag{6}$$

The mass melting rate is then, when m is the mass density:

$$M = \frac{m}{H_0 + b}(\phi I + \rho_L \frac{L}{A} I^2) \tag{7}$$

For a standard carbon steel solid wire electrode the numerical values were found by experiments to be:

$$H_0 = 11.1 \text{ J/mm}^3,\ b = 4{,}0 \text{ J/mm}^3,\ \phi = 3.5 \text{ V and } \rho_L = 1.2 \cdot 10^{-3} \text{ ohm mm}$$

It is important to remember that these linearized equations are valid only when the ohmic heating is not too small. Numerically this requires that $H_L > 4$ J/mm^3 which corresponds to $Lj > 3.3 \cdot 10^3$ (A/mm) or to $j/v < 2.0$ (As/mm^3). This criterion is satisfied for most practical GMAW with free flight drop transfer. In this regime equation (6) has been verified for several electrode diameters and different carbon steel electrode materials. The latter affects mainly the parameter b. For the common solid electrodes b does not vary much. Equation (7) has the same dependence on I, L and A as equation (3) which assumes constant resistivity. The nonlinearity of the real resistivity is taken care of by the parameter b.

For decreasing values of current density equation (7) becomes increasingly inaccurate. For this non-linear regime, i.e. for $H_L < 4$, the following equation fits the experimental data and equation (5) quite accurately [4]:

$$v = 2.89 \cdot 10^3 \frac{j}{9.07 \cdot 10^3 - Lj} \quad \text{[mm/s]} \tag{8}$$

Unlike equation (6) this equation (8) does not have a physically intuitive form, nor does it fit very well for electrodes with very different values of b. It should, however, be valid even as L approaches zero. For $L = 0$ the contribution to the wire melting speed due to the anode heating alone is equal to:

$$v = 0.32\, j \quad \text{[mm/s]} \tag{9}$$

For steel the mass density is $m = 7.8 \cdot 10^{-6}$ kg/mm^3 and the mass melting rate is:

$$M = 8.9 \cdot 10^{-3} I \quad \text{[kg/hr]} \tag{10}$$

Note that the same values for v and M at $L = 0$ are also, of course, obtained from equations (6) and (7) by taking both $b = 0$ and $L = 0$. A simple substitution of only $L = 0$ into equation (6) will yield $v = 0.23\, j$ mm/s which is significantly lower than equation (9).

Curve fitting may be a tricky and deceptive affair. The numerical values for H_0 and ϕ above were fitted to the normal operating regime of GMAW. By extrapolation to $H_L = 0$ other numerical values in equation [9] may fit better, i.e. $v/j = 0.33$–0.34. Lesnewich's value measured from Figure 1 is $v/j = 0.29$.

Equation (5) and experimental points are shown in Figure 2. The dashed straight lines represent the linearized equation (6).

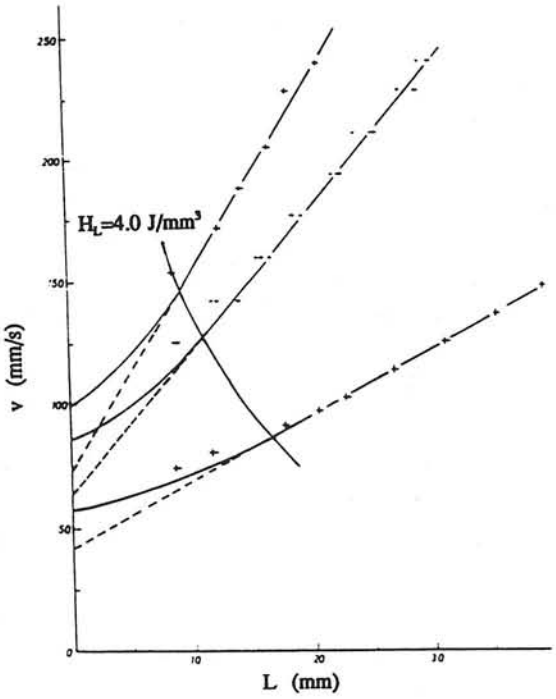

Figure 2. GMAW melting rate. Electrode positive. Ref. [3].

The GMAW model has also been verified for flux-cored arc welding (FCAW), first by Ushio et al. in 1984 [5]. For low melting speeds a small deviation due to heat loss to the flux was observed. The current is conducted through the steel tube, the annular

section of which corresponds to A. However, for fluxes containing a large proportion of iron powder a small fraction of the current may also pass through the core. Flux-cored wires usually have a lower room temperature resistivity than the standard solid wires. The parameter b will then be greater.

Pulsed GMAW is also well described by the same model as for smooth DC. This has been extensively studied especially by the group at Cranfield Institute of Technology (summarized in ref. [6]). When using equations (6) and (7) arithmetic mean values, i.e. j_m or I_m, should be used in the first term and the mean of the square, i.e. $(j^2)_m$ and $(I^2)_m$ for the second term.

Pulsed GMAW is frequently used at fairly low current densities in order to maintain spray transfer with low average current. This means that the ohmic heating may be in the non-linear regime. An equation such as equation (8) may then be better than equation (6) for the wire melting speed.

3. Comparison with other arc welding methods

3.1. Covered electrodes (SMAW)

A comprehensive study of the thermal processes in covered electrodes of several types with both positive and negative polarity was published by Waszink and Piena in 1985 [7]. Although the ohmic heating generally was found to be small, it was measured and subtracted to estimate the melting rate due to anode/cathode heating alone. This work confirmed the linear relationship of equation (1). Being primarily concerned with the thermal processes at the anode/cathode ref. [7] does not present the actual data for the melting rates, except for one case (a basic 3.25 mm ∅ electrode at 133 A). In terms of equation (9) the result is $v = 0.33\,j$.

For a large number of other electrodes, rutile and basic ones of various diameters, Waszink and Piena present calculated values of the power input to the molten drop which is the sum of the power used in melting the electrode and an estimated power loss by conduction into the flux covering . The latter is a rather complicated thermal estimate, which is difficult to verify. For high current densities, however, the correction is less than 10% anyway. It is possible to calculate backwards from the listed data to the measured, uncorrected melting rates. Figure 3 shows the calculated power input to the drop for rutile electrodes of diameters from 1.75 to 6.0 mm with both positive and negative polarities. These points will also correspond to an uncorrected value of $v/j = 0.33$. A weak increase in corrected power input per ampere with increasing diameter is also found, in qualitative agreement with equation (2) for GMAW. The effect may appear to be within the uncertainty of the data points. Note in

Figure 3 that the power input and hence the melting rates are practically equal for positive and negative electrodes. If anything, it is slightly lower for the negative. This is contrary to Lesnewich's results for GMAW.

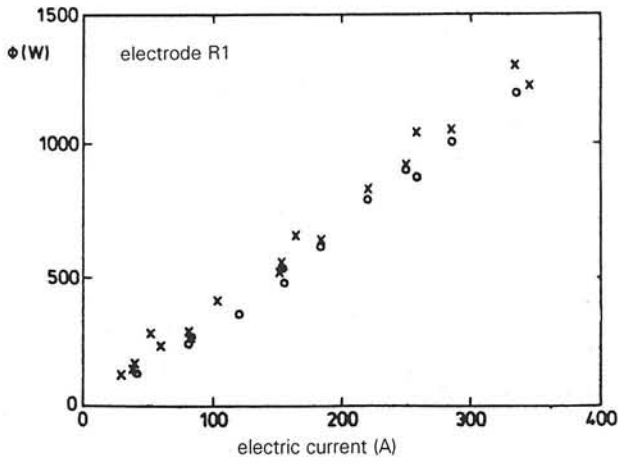

Figure 3. Power input through the electrode tip. Rutile SMA electrodes. x positive, o negative. Ref. [7].

Ohmic heating will never be of great practical importance in SMAW. The flux cover will be destroyed if the core temperature exceeds 500–600°C. This means a difference in melting rate between the start and the end of, at most, about 20%, or less than 10% for the average rate. Due to the slow rate of ohmic heating much of the heat generated in the core is lost to the surroundings in SMAW, unlike the case of GMAW.

3.2. Submerged arc welding (SAW)

The most recent and very detailed measurements of the melting rates for SAW were published by Tusek and Kralj in 1992 [8]. Their paper contains data for single, double and triple electrodes. Here we shall compare only the relevant results for single electrode SAW. Figure 4 from ref. [8] shows the mass melting rates for $I = 350$ A positive polarity and $L = 25$ mm for four different diameters. At 3 mm ∅ and thicker the melting rate levels off, indicating that the ohmic heating becomes negligible. On this graph are plotted data points (marked with +) calculated from the GMAW model as represented by equations.(6) and (8). The agreement is quite good especially for the larger diameters. This shows that the melting rates, for all practical purposes, are identical for SAW and GMAW. The discrepancy at the smallest diameter may be due to inaccuracies or the fact that wire resistivities may be different. The curves will rise very steeply as the diameter is further reduced. For double and triple electrodes the melting rates are obviously not simply multiples of the single electrode rate, but significantly higher.

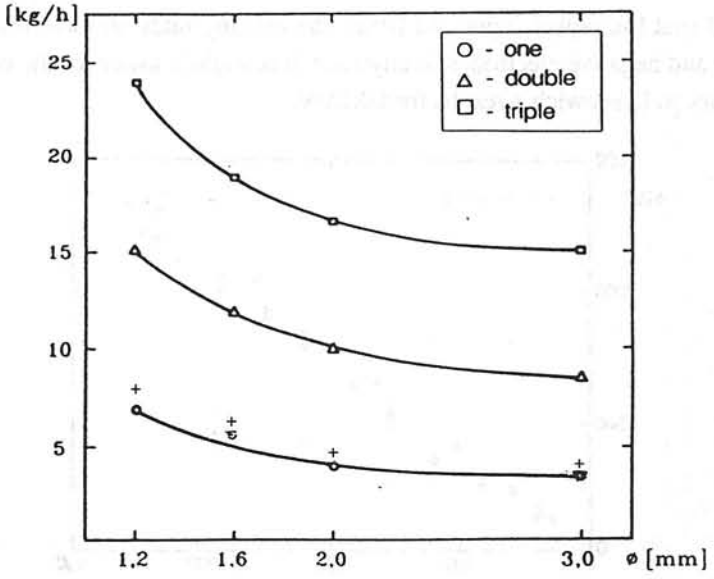

Figure 4. SAW melting rates for multiple positive electrodes vs. diameter. I = 350 A, L = 25 mm. Ref. [8]. The crosses (+) are calculated values obtained from equations (6) and (8).

Tusek and Kralj [8] also compare the melting rates for positive and negative electrodes as functions of the stick-out for triple wire SAW with 2 mm and 3 mm diameters. At $L = 0$ the melting rate for electrode negative is about 33% higher than for electrode positive. This difference is in qualitative agreement with, but significantly smaller than, the factor 2 reported by Lesnewich [2] for GMAW.

In an earlier report Tusek [9] also reports measuring an effect of the polarity upon the heating in the electrode extension. It is proposed that this is due to the Thomson effect. A simulated experiment on a piece of wire with a temperature drop of several hundred degrees and a current density $j = 19$ A/mm^2 gives a voltage difference between the two polarities of about 15% of the total voltage. Relatively speaking this is not negligible. However, at such a low current density the stick-out heating is rather unimportant anyway. Waszink [10] has estimated the Thomson effect for GMAW and found it negligible. In ref. [9] the voltage drop along the electrode extension was measured directly for both polarities. It was found that "in welding with electrode positive polarity the heating of the electrode extension is faster than that at electrode negative polarity, with all other welding conditions being kept the same". The latter condition seems impossible to fulfill for the following reason.

Consider an equation such as equation (6) relating the three variables L, j and V. If values for any two of the three are selected, the third is also fixed. Refs. [2] and [8]

show that the quantity ϕ/H_0 is greater for negative than for positive polarity. If the first term in equation (6) is increased, the second term, which represents the heating in the electrode extension, will have to decrease in order for the melting speed v to remain constant. A closer study of the explicit equations for the stick-out voltage [11], which are derived from equations (6) and (8), show that if any pair of the variables j, v and L is kept constant while ϕ/H_0 is increased, the voltage V_L must decrease. The voltage equations are:

$$V_L = H_0 \frac{v}{j} - \phi \tag{11}$$

or

$$V_L = \frac{H_0}{H_0 + b} \rho_L L j - \frac{b}{H_0 + b} \phi \tag{12}$$

It therefore seems unnecessary to invoke the Thomson effect to explain the observations reported in ref. [9].

3.3. GMAW of aluminum

In the case of GMAW of aluminum the resistivity is so small that the ohmic heating in the electrode extension is negligible. As long as the arc length is not too short the wire melting rate is proportional to the current as in the case of steel. For low arc voltages, which means short arc lengths, however, the current will decrease when the wire speed is kept constant, i.e. the melting efficiency is greater. This effect was reported by Lesnewich [2] and studied more carefully by Kiyohara et al. [12] as illustrated in Figure 5. At low arc voltage the anode is actually below the surface of the work piece. This is equivalent to sticking the wire into a hot furnace, which seems to be a rather simple and plausible explanation. For steel electrodes this effect is too small to be noticed.

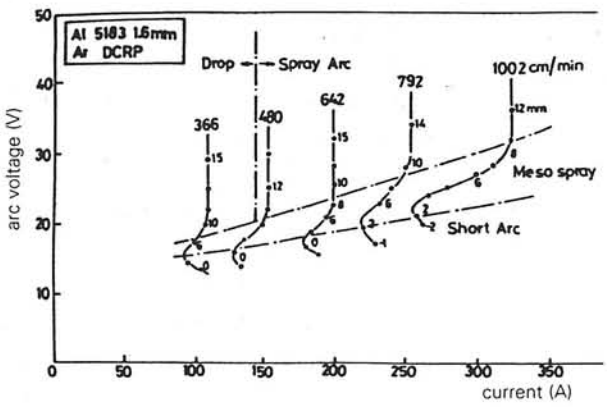

Figure 5. GMAW of aluminum. From ref.[10].

Since the ohmic heat input H_L is negligible in aluminum GMAW, it cannot be used to calibrate and estimate the total heat input to the electrode, unlike in the case of steel electrodes.

3.4. Hyperbaric welding

The increased pressure in dry, hyperbaric habitats for the welding of sub-sea pipelines has a strong effect on the voltage drop in the arc column, but only a weak effect on the melting rate. An example from a study of flux-cored arc welding at pressures up to 30 bars by Hoffmeister et al. [13] is shown in Figure 6. Given the scattering of the data points one might be forgiven for suggesting that the melting rate is hardly affected by the ambient pressure.

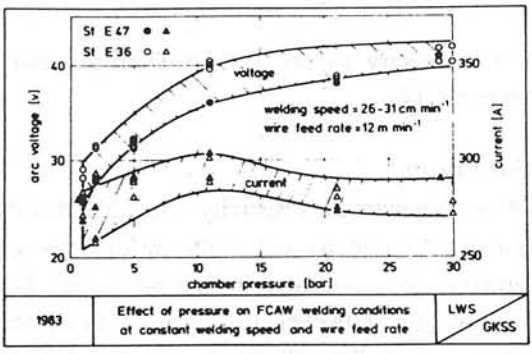

Figure 6. Hyperbaric FCAW. From ref. [11].

4. Discussion

It seems rather well established that the melting rate for all the common arc welding methods with current carrying consumable electrodes obey the same 'law'. It is the sum of two terms:

1. An electrode term (anode or cathode) which is proportional to the current and practically independent of anything else. For the anode the numerical values are practically equal for GMAW, SMAW and SAW.
2. Ohmic heating in the electrode extension which, either negligible or dominant, linear or non-linear, can be calculated using Ohm's law.

The second term presents no mystery. The first, however, is poorly understood physically. The simple relationship covers nearly an order of magnitude range in electrode diameter and current, about two orders of magnitude in droplet volume, different metal compositions (for steel) and arc atmospheres (shielding gases and fluxes). Of course, there *are* variations. All the references quoted here and most others report deviations or 'wiggles' on the curves. What is lacking, though, is a simple explanation for the simple overall relationship. Once the simplicity is well understood, the details and deviations may be easier to explain.

A formal but simple explanation is, of course, that the power is produced in a constant potential drop ϕ at or close to the droplet. When the droplet then reaches a constant heat content H_0 it drops off the electrode. The melting speed would then be $v = (\phi/H_0)j$ which leads to equation (5) if ohmic heating is included. We then need to understand why ϕ and H_0 are constants and know what their real values are, not just the ratio between the two.

The heat content H_0 is most likely to remain constant if it corresponds to either the melting or the boiling temperature. The value of $H_0 = 11.1$ J/mm^3 in equation (6) is only slightly higher than the value of $H_0 = 10.2$ J/mm^3 needed to heat and melt the steel. The latter value was also used in ref. [7] to calculate the power produced. Actual measurements of the temperature after the droplets have passed through the arc, on the other hand, indicate constant temperatures at the boiling point [14] or at 2400°C [15]. Which is it?

The constancy of ϕ for anode heating is also understandable. A widely used model for the heat produced at the anode [16] may be written as:

$$vH_0 = [\phi_e + \frac{3}{2}\frac{kT}{e} + V_a] \cdot j \tag{13}$$

For the cathode the corresponding equation is

$$vH_0 = [V_c - \phi_e + \frac{3}{2}\frac{kT}{e}] \cdot j \tag{14}$$

where ϕ_e is the electronic work function, V_a and V_c the anode and cathode potentials and 3kT/2e the thermal energy of the plasma electrons in standard notation. The latter term is small compared to the other two, both of which are generally assumed to be independent of the current. On the anode, at least, the work function must give a definite contribution to the heating, because the potential drop is actually inside the metal. For pure iron $\phi_e = 4.4$ V and for the common alloying element manganese $\phi_e = 3.8$ V at room temperature and maybe 0.3 V lower at the boiling point. The value of $\phi_e = 3.5$ V found above is less than these values, which indicates that an anode potential of the order of $V_a = 2$ V does not contribute to the melting. Higher values of ϕ give better agreement with the measurements of droplet temperatures in refs. [14] and [15], but disagree with the model given by equation (6).

If ϕ_e is the dominant contribution, one would expect it to decrease when cesium is added. Lesnewich [2] found that it did not for the anode heating, but rather for the cathode heating, where the role of the work function may be less obvious. According to equation (14) a reduction in ϕ_e will increase the melting rate, which appears contradicted by Lesnewich's measurements.

Since it is generally assumed that $V_c > V_a$, this may explain why the cathode melts faster than the anode for GMAW [2] and for SAW [8]. Then, why is the same not true for SAW [7]?

The melting potential ϕ must be located at the surface, while H_0, is the heat content in the bulk of the electrode tip or droplet, large or small. If both are indeed constants it would probably imply that losses, such as that due to evaporation, are either negligible or also constant. Furthermore, the heat transfer through the molten metal must be nearly a thermal short circuit regardless of size, shape and current distribution of the droplet. The heat and fluid flow in the electrode tip has been studied theoretically by Waszink, e.g. [7]. A continuation of this work should perhaps focus on why the heat transfer is so efficient over such a wide range of conditions.

Clearly, there are important gaps in our knowledge of the basic physical processes taking place at the tip of the electrode. This is unlikely to worry the practical world of the welding industry. Indeed, our present knowledge has provided a very simple practical model of the melting process, which undoubtedly has been of considerable value in the development of improved methods, equipment and procedures. Members of the Study Group Physics of Welding are unlikely to remain satisfied with the present state of our knowledge. When we know more, perhaps we shall further improve the state of the art of welding.

References

1. Lefring, L. 'Einfluss der Schweissstrombedingungen bei der elektrischen Lichtbogenschweissung von Weichem Flussstahl', Forschungsarbeiten auf dem Gebiete des Ingenieurwesens, VDI, Berlin, Heft 332:1-53. 1930.
2. Lesnewich, A. 'Control of Melting Rate and Metal Transfer in Gas-Shielded Metal Arc Welding, Part 1: Control of Electrode Melting Rate'.Welding Journal Research Supplement, Vol. 37(8), p.343s-353s. 'Part II: Control of Metal Transfer'. 37(9), p.418s-425s. 1958.
3. Halmøy, E. 'Wire melting rate, droplet temperature and effective anode melting potential'. Proc. lit. Conf. on Arc Physics and Weld Pool Behaviour. p.49-57, The Welding Institute, London. 1979.
4. Halmøy, E. 'Current-Voltage Process Characteristics In Gas Metal Arc Welding'. Proc. ASME Winter Annual Meeting, Allanta, GA, PED-Vol.51, p.17-27. Dec. 1991.
5. Ushio, M., Raja, A. and Matsuda, F. 'Melting characteristics of flux cored wire'. Transactions of JWRI, Vol.13, No. 1, p.1-6. 1984.
6. Norrish, J. 'Advanced Welding Processes', chpt.7, Institute of Physics Publishing. 1992.
7. Waszink, J.H. and Piena, M.I. 'Thermal Processes in Covered Electrodes'. Welding Journal Research Supplement, Vol.64 (2), p.37s-48s. 1985
8. Tusek, J. and Kralj V. 'Mathematical modeling of the melting rate in triple electrode submerged are welding'. IIW Doc. 212-811-92. Sept. 1992.
9. Tusek, J. 'The effects of polarity on electrode extension heating in submerged arc welding'. IIW Doc. 212-791-91. June 1991.
10. Waszink, J.H. and van den Heuvel, G.J.P.M. 'Measurements and calculations of the resistance of the wire extension in arc welding'. Proc. Int. Conf. on Arc Welding and Weld Pool Behaviour'. p.227-239, The Welding Institute, London. 1979.

11. Halmøy, E. 'Electrode wire heating in terms of welding parameters'. The Physics of Welding, 2nd ed., J.F. Lancaster ed., Pergamon Press. 1986.
12. Kiyohara, M., Okalla, T., Wakino, Y. and Yamamoto, H. 'On the stabilization of GMA welding of aluminum'. Welding Journal, Vol.56 (3), p.20-28. 1977.
13 Hoffmeister, H., Huismann, G. and Schafstall, H.G. 'Effect of Pressure and Process Parameters on Weld Joint Properties of St E 36 and St E 47 Irry FCA-MAG Welds'. Underwater Welding, p.239-246, Pergamon Press. 1983.
14. Acinger, K. Sipek, L. and Smås, E. 'Temperature, metal vapour density, and energy balance in an argon-shielded welding arc with iron electrodes', Report no. 7~ 10, Electron and Plasma Physics. The Royal Inst. of Techn., Stockholm. 1970.
15. Jelmorini, G. Tichelaar, G.W. and van den Heuvel, G.I.P.M. 'Droplet temperature measurements in arc welding'. IIW Doc. 212-411-77. 1977.
16. Lancaster, J.F. 'Metal Transfer and Mass Flow in the Weld Pool', Chapter 7 in The Physics of Welding, 2nd ed., I.F. Lancaster ed., Pergamon Press. 1986.

Weld Pool Phenomena

S.A. David, J.M. Vitek, T. Zacharia and T. DebRoy*

Oak Ridge National Laboratory, Oak Ridge, U.S.A.

* Penn State University, University Park, U.S.A.

Abstract

During welding, the composition, structure and properties of the welded structure are affected by the interaction of the heat source with the metal. The interaction affects the fluid flow, heat transfer and mass transfer in the weld pool, and the solidification behavior of the weld metal. In recent years, there has been a growing recognition of the importance of the weld pool transport processes and the solid state transformation reactions in determining the composition, structure and properties of the welded structure. The relation between the weld pool transport processes and the composition and structure is reviewed. Recent applications of various solidification theories to welding are examined to understand the special problems of weld metal solidification. The discussion is focused on the important problems and issues related to weld pool transport phenomena and solidification. Resolution of these problems would be an important step towards a science based control of composition, structure and properties of the weld metal.

1. Introduction

During welding, as the heat source interacts with the metal, melting, solidification, and various solid state transformation reactions influence the structure and properties of the welded product. In the weld pool, metal undergoes vigorous circulation driven by surface tension, buoyancy and, when electric current is used, electromagnetic forces. In non-autogenous welding, where filler metals are used, additional physical processes add to the complexity of the weld pool phenomena. The fluid flow and heat transfer affect the size and shape of the weld pool, the cooling rate, the kinetics and the extent of various solid state transformation reactions [1–7]. The weld pool geometry influences dendrite and grain growth selection processes [7–11]. The distribution of nitrogen, oxygen and hydrogen between the weld pool and its surroundings significantly affects the weld metal composition and properties. In addition, vaporization of alloying elements, and transport of elements into and from the weld pool greatly influence the microstructure, composition and properties of weld metal.

In recent years, significant progress has been made in understanding how the various physical processes in the weld pool influence the development of the weld pool and the macro and microstructures of the welded region. Much of the recent research on the weld pool phenomena has attempted to gain an understanding of fluid flow and heat transfer in the weld pool. Significant progress has also been made in understanding both weld pool solidification behavior and solid state transformations in the weld metal and the heat affected zone. It should be noted that a fundamental understanding of some of these topics is still evolving and significant challenges lie ahead for those studying weld pool phenomena and its relationship to microstructure and properties. However, solution of the important problems and issues related to weld pool physical phenomena is necessary, if not essential, for eventual science based control of the structure and properties of the weld metal. In this paper, a selection of recent research results from the authors' laboratories is discussed to highlight how the various weld pool phenomena are related to the composition and structure of the weld metal and the heat affected zone.

2. Weld pool dynamics

a. Weld pool geometry

Since the early efforts of heat transfer calculations, significant advances have been made in the calculation of weld pool heat transfer and geometry. Weld pool fluid flow and heat transfer are now recognized to be critical in the development of the weld pool shape and size, and its macro and microstructures. Therefore, it is critical to understand the dynamics of the weld pool. Mathematical modeling is now commonly used to simulate the development of weld pool geometry and cooling rate. Most of these models now address coupled conduction and convection heat transfer problems to predict weld pool geometry and cooling rate. Of the various modes of heat transfer, convection plays a critical role in determining the weld penetration, shape and size. Convection in the weld pool is driven by surface tension, buoyancy, and, when electric current is used, electromagnetic forces. The presence of a significant temperature gradient on the weld pool surface leads to a spatial gradient of interfacial tension. The spatial gradient, known as the Marangoni stress, contributes to convection in the weld pool. Buoyancy effects are a result of the spatial variation of density of the liquid as a function of temperature and composition. Since large variations in temperature are present in the weld pool, the corresponding density gradients produce convective flow. Electromagnetic effects are a consequence of the interaction between the divergent current path in the weld pool and the magnetic field it generates.

Previous work has concentrated on the convective heat transfer and, in particular, the effect of the spatial gradient of surface tension on the weld penetration. A critical

variable that controls the weld penetration is the nature and amount of surface active element in the alloy. Recent work has shown that consideration of a temperature coefficient of surface tension dependent on temperature and composition is important for the calculation of fluid flow in the weld pool and its shape. The calculated surface tension for the iron-oxygen alloys as a function of temperature and oxygen content is shown in Figure 1 [12-14]. However, depending on the interplay between various driving forces, the convective flow can be simple, or more complex with a number of convective cells, as shown in Figure 2 [12-14]. For simplicity, most of the earlier models have addressed stationary arc welds with a flat weld pool surface. In recent years, the models have been refined to incorporate realistic weld pool conditions such as free deformable weld pool surface and moving heat source [15-18].

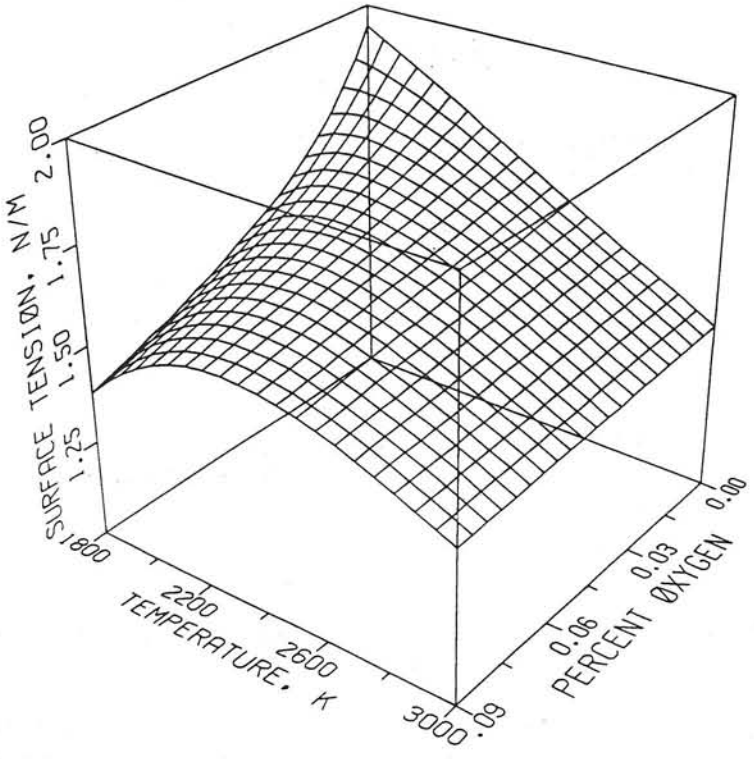

Figure 1. Surface tension of iron-oxygen alloy as a function of temperature and oxygen concentration.

Recently, a multidimensional computational model was developed to analyze heat and fluid flow in a thin plate full penetration linear weld [19]. The model considers the solid plus liquid mushy zone as a porous media in the calculation of convective heat transfer. Figure 3 shows the top and central view of the weld pool flow field for the specimen moving with a constant speed [19]. Figure 4 shows a transverse section of a gas tungsten arc (GTA) spot-weld overlaid with the calculated weld profile for a

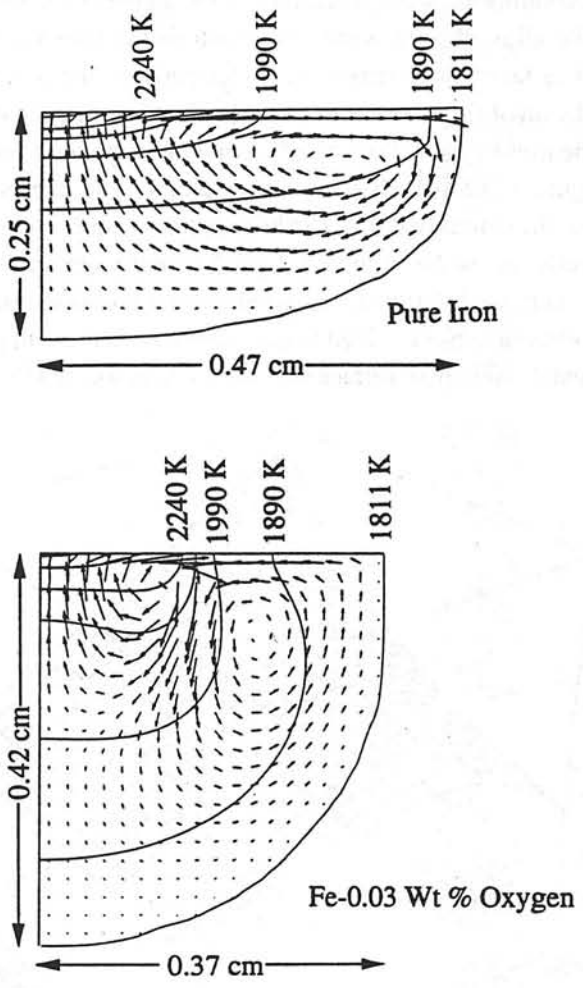

Figure 2. Velocity and temperature fields for two different cases: a. for pure iron and b. iron with 0.03 wt % oxygen.

welding current of 150 A. Although the correlation is reasonable, further work is underway to improve these models. Mathematical modeling is a powerful tool to understand the heat transfer, fluid flow and development of weld pool geometry. However, in view of the complexities of the welding process, attempts to understand them through numerical simulation must involve concomitant, well designed experimental work to validate the models.

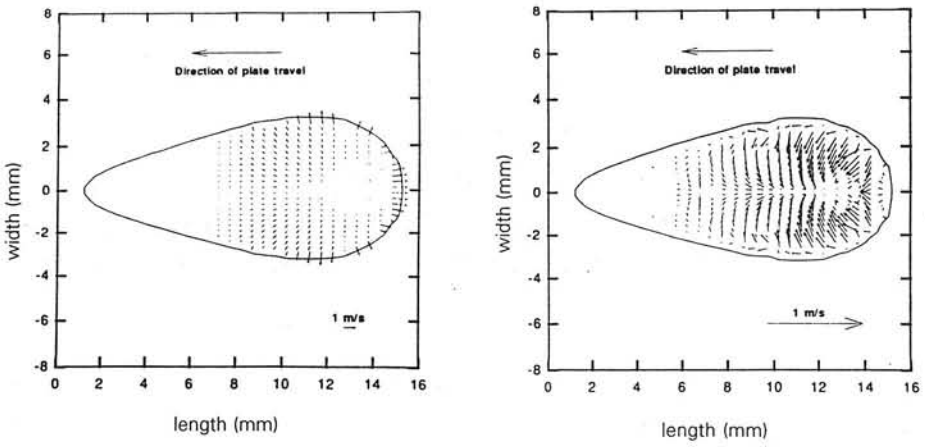

a *b*

Figure 3. a. Top view of the flow field on the surface of the specimen moving with a constant speed of 4.23 mm/s (10 ipm) in the negative x-direction. b. Central plane view (horizontal section) of the weld pool flow field for the specimen moving with a constant speed of 4.23 mm/s (10 ipm) in the negative x-direction.

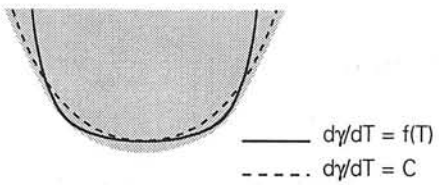

Figure 4. Transverse section of the GTA weld overlay with the calculated weld pool profiles for a welding current of 150 A.

b. Vaporization of elements from weld pool surface

During the interaction of the heat source with the metal, the weld pool surface temperatures are much higher than the liquidus temperature of the weld metal. When very high power density heat sources such as lasers and electron beams are used, the temperature can even exceed the boiling point [20–22]. Consequently, pronounced vaporization of alloying elements take place. Such loss of elements from the weld pool often results in a change in the composition of the weld metal and is a serious problem in the welding of many important engineering alloys [23–30]. Figure 5 shows the change in the manganese concentration during laser welding of various grades of high manganese steels [25]. Similar composition changes have been observed for the welding of Al-Mg alloys.

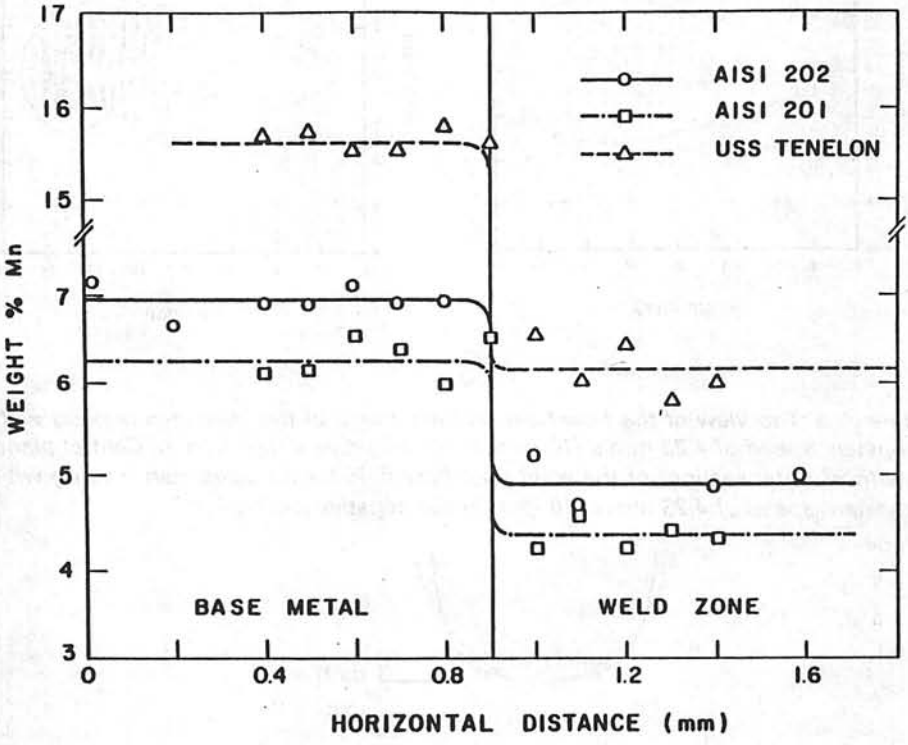

Figure 5. Concentration of manganese versus distance in the base metal and in the weld zone for continuous wave carbon dioxide laser welding. Laser power: 560 Watts, welding speed 3.5 x 10^{-3} m/s, shielding gas flow rate: 10^{-4} m^3/s, and sample thickness: 7 x 10^{-4} m.

DebRoy et al. [24,27,28] have developed a comprehensive model to understand the vaporization of elements and the composition change of the weld metal. They have calculated vaporization rates using computed weld pool surface temperatures. The weld pool fluid flow and heat transfer were coupled with the velocity distribution functions of the vapor molecules at various locations above the weld pool surface to calculate the rates of vaporization of various alloying elements. The procedure allowed for the calculation of both the evaporation and the condensation fluxes based on the application of conservation of mass, momentum and energy equations to both the liquid and the vapor phases. The mass transfer rates due to both concentration and pressure gradients just above the pool surface were considered. When using very high

power density for welding, the pressure gradient driven mass transfer can be an important factor. The calculated vaporization rates [28] for iron and manganese are compared with the experimental data and the values obtained from the Langmuir equation [31] in Figure 6. The experimental data and the model predictions are consistent with one another. Straightforward calculations using the Langmuir equation do not account for the condensation of vapors. As a result, the rates calculated from the Langmuir equation are much higher than the experimentally observed values. Although the computed vaporization rates using the model proposed by DebRoy et al. [24,27,28] predicts acceptable results, the accuracy is achieved by including more realistic and detailed description of the physical processes, and consequently, by doing more complex calculations.

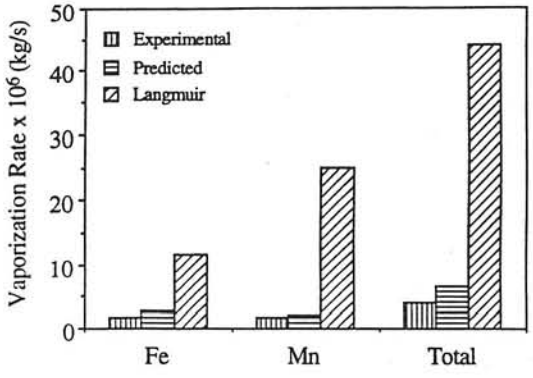

Figure 6. Comparison of the vaporization rates calculated from the Langmuir equation and from the model with experimentally determined values for AISI 201 stainless steel. Laser power: 3000 W, scanning speed: 15.24 x 10^{-3} m/s, argon flow rate: 5.5 x 10^{-4} m^3/s.

c. Oxygen, nitrogen and hydrogen in the weld pool

During welding, hydrogen, nitrogen and oxygen may dissolve in the weld metal, whereupon they escape to form pinholes or bubbles, or they combine with elements in the alloy to form inclusions. In steels, hydrogen induces cracking, nitrogen increases the yield strength and the tensile strength, but reduces the ductility, and oxygen promotes inclusion formation [32]. In arc welding, the consumables can contribute to the weld metal impurity concentrations, and slag-metal reactions have a strong influence in determining the concentrations of impurities [33-35]. However, in laser welding, the concentrations of hydrogen, nitrogen and oxygen in the weld metal are affected by the interaction between the weld pool and the surrounding shielding gas environment. Oxygen and nitrogen contents as high as 0.7 and 0.2 wt% respectively have been obtained in the weld metal during arc welding [36]. These concentration levels were far greater than those in the base and filler metals.

In a diatomic gas environment, the equilibrium concentration in a metal of a species such as hydrogen is given by Sieverts' law, which states that the concentration is proportional to the square root of the partial pressure at any given temperature [31]. However, in most welding processes, the weld metal is exposed to a plasma environment. The gas phase contains neutral atoms and ions, excited molecules and atoms, and electrons. Under these conditions, the concentrations of these species in the metal are significantly higher than those calculated [32,37,38] from Sieverts' law [31]. The transformation of ordinary molecular species to excited neutral atoms and ions in the gas phase leads to enhanced solution of the species in the metal.

Gedeon and Eagar [37], in their study of hydrogen dissolution, clearly indicated the prominent effect of atomic hydrogen gas in determining the hydrogen concentration in the weld metal. They proposed that a model for hydrogen dissolution in the weld metal must take into account the mechanism of hydrogen absorption in the weld pool, hydrogen rejection from the solidifying front, and hydrogen diffusion away from the weld pool. Since the diffusivity of hydrogen is much higher than that of nitrogen or oxygen, the problem of nitrogen or oxygen diffusion away from the weld pool is not likely to be significant [32].

The properties of the plasma such as the electron density and the energy affect the formation of various atomic, ionic and excited neutral species from the diatomic molecules. The gas atoms in the plasma are formed by a series of reactions involving inelastic collisions of the diatomic molecules with electrons [39]. The enhanced solubility is consistent with the formation of the atomic species from the molecules. Determination of the nature and the concentration of the various species within the plasma is the key to quantitative understanding of the enhanced solution of nitrogen, oxygen and hydrogen in the weld metal.

Efforts to develop a fundamental understanding of the partition of species such as hydrogen, nitrogen and oxygen between the weld pool and its environment are just beginning. Bandopadhyay et al. [39] studied the plasma – enhanced nitrogen solubility in pure tantalum and niobium at 2243 K. Samples of these metals were equilibrated under helium – nitrogen mixtures. The results of their study with tantalum are presented in Figure 7. The plot shows a much greater nitrogen solubility in the presence of a plasma than without for the same level of diatomic nitrogen in the source gas. From the optical emission spectra of the plasma, they determined that the plasma contained nitrogen molecules and atoms in both neutral and ionized states. The enhanced solubility was attributed to the presence of atomic nitrogen in the plasma. Work is now underway to relate the properties of the plasma with the concentrations of species in the plasma.

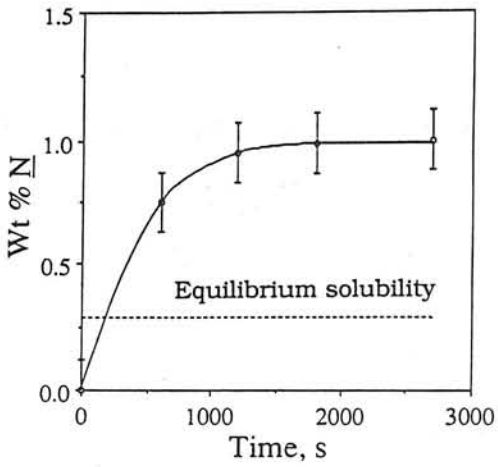

Figure 7. Weight percent nitrogen versus time for dissolution of nitrogen in tantalum at 2243 K. Partial pressure of nitrogen in the plasma source gas: 1.12 Pa.

3. Weld pool solidification

Development of microstructure in the fusion zone (FZ), also known as weld metal, depends on the solidification behavior of the weld pool. Considering the FZ as a mini casting, parameters important in determining cast microstructures in castings such as growth rate (R), temperature gradient (G), undercooling (ΔT) and alloy composition play significant roles in determining the development of microstructure in welds. In welding, where the molten puddle is translated through the material, the cooling rate and thermal gradient vary considerably across the FZ. Consequently, the microstructure that develops varies considerably within the weld metal. Geometrical analyses have been developed that relate welding speed to the actual growth rates of the solid as a function of location in the weld pool [40,41,7–11]. Figures 8 and 9 show schematically the influence of G and R on the microstructural variations within the weld metal. Most of our current knowledge of the weld pool solidification is derived from an extrapolation of the knowledge of freezing of castings, ingots and single crystals at lower thermal gradients and growth rates [7]. The development of FZ microstructures can be understood by considering classical concepts of nucleation and growth theories.

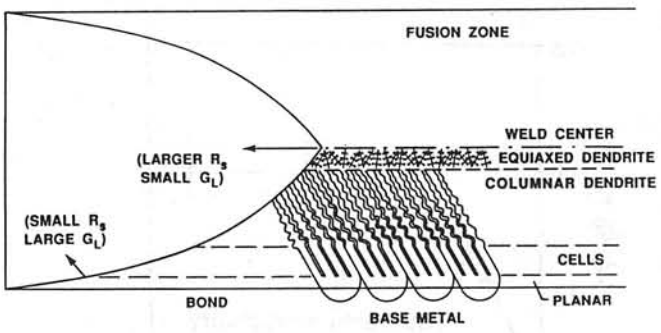

Figure 8. Schematic drawing of structural variation of weld microstructure across fusion zone (modified from ref. 3).

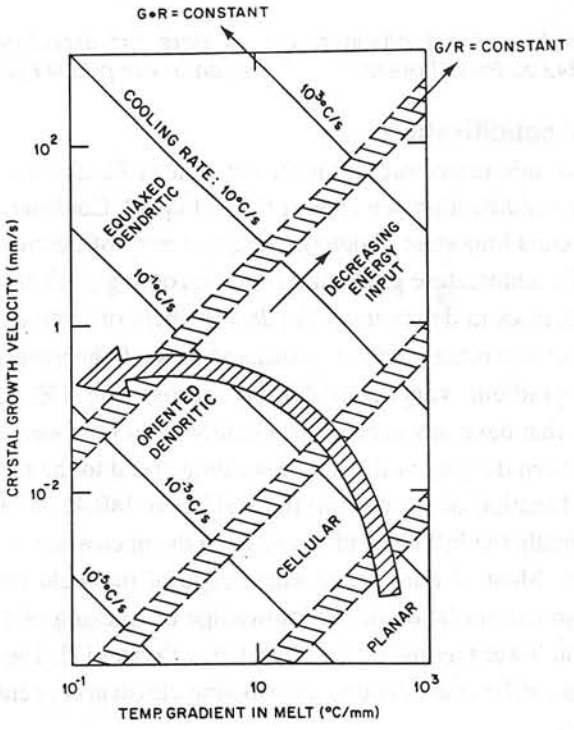

Figure 9. Variation of weld microstructure as function of temperature gradient, growth rate and combination of these variables ($G_L < G/R$). The arrow indicates the range of microstructures and growth conditions encountered in a weld.

a. Nucleation

In welds, solidification proceeds from the pre-existing solid substrate and hence there is little or no nucleation barrier. In the case of autogenous welding, solidification

occurs spontaneously by epitaxial growth. In cases where filler metal is used, epitaxial growth may still occur. However, the more classical case of heterogeneous nucleation may also apply. In addition to heterogeneous nucleation on the solid base material, innoculants have been successfully used to promote nucleation. Finally, dynamic methods such as stirring and oscillations have been used to dislodge dendrite fragments from the solidification front and these fragments act as nuclei for growth of additional grains of different orientations.

b. Growth

As in castings or single crystal growth, the stability of the solid/liquid interface is critical in determining the microstructural characteristics of the weld metal. The microscopic shape of the interface is determined by the conditions in the immediate vicinity of the interface. These conditions determine whether the growth occurs by planar, cellular, or dendritic growth. Theories for interface stability under conditions of equilibrium at the interface for normal solidification or under extreme nonequilibrium conditions prevalent during rapid solidification have been developed [42,43]. These theories can be extended to weld pool solidification.

There are three cases of solidification commonly referred to in literature [42–44]. These three cases can be considered for weld pool solidification. Case I is equilibrium solidification with complete solid and liquid diffusion. This case does not generally apply to welding situations. Case II assumes little or no diffusion in the solid while complete mixing in the liquid by convection and diffusion is presumed. This case is applied to lateral growth of dendrites and describes microsegregation effects in weld microstructures. Case III assumes no diffusion in the solid and limited diffusion in the liquid, with no convection. This case applies for planar growth and allows for the buildup of a solute boundary layer ahead of the solid/liquid interface. Case III is used as the basis for descending morphological stability and microstructural development in welds.

In Case III, the effect of solute redistribution and buildup at the solid/liquid interface on the morphological stability of the solidification front has been described elsewhere [42,43], by considering the concept of constitutional supercooling. The criterion for constitutional supercooling for plane front instability can be mathematically stated as

$$G_L/R < -\frac{M_L C_0(1-K)}{KD_L} \tag{1}$$

or, equivalently,

$$G_L/R < \frac{\Delta T_0}{D_L} \tag{2}$$

where

G_L is the thermal gradient in the liquid at the solidification interface,
R is the solidification front growth rate,
M_L is the slope of the equilibrium liquidus line,
C_0 is the overall alloy composition,
K is the equilibrium partition coefficient,
D_L is the solute diffusion coefficient in liquid, and
ΔT_0 is the equilibrium solidification temperature range at composition C_0.

If this criterion is met, the plane front is unstable and dendritic growth is promoted. If

$$G_L/R > \frac{\Delta T_0}{D_L},$$

the plane front will be stable.

The plane front stability criterion is shown graphically in Figure 10. For steady state plane front growth, the solute composition profile is shown in Figure 10a. The corresponding temperature profile for the equilibrium liquidus temperature is shown in Figure 10b and 10c. Depending on the actual thermal gradient in the liquid, the plane front will remain stable (Figure 10b) or it will become unstable (Figure 10c). As the growth conditions depart from planar stability (defined by Equation 1), the interface morphology will change from planar to cellular to dendritic. If the conditions are favorable, the dendrites will exhibit secondary and tertiary arms in crystallographically predetermined preferred growth directions. The concept of constitutional supercooling is very useful for broadly understanding the development of microstructure and the influence of process parameters on these microstructures in welds, but it is not sufficient to describe precisely or in detail the morphological stability at the solidification front. More rigorous analyses by Mullins and Sekerka [45] and others [46–50] have been developed to evaluate additional conditions for plane front solidification.

c. Solute redistribution

During alloy solidification, it is well established that extensive solute redistribution occurs. Solute redistribution during weld pool solidification is an important phenomenon resulting in segregation that can significantly affect weldability, microstructure and properties. A limited amount of theoretical and experimental work has been done to describe the solute redistribution during weld pool solidification. These studies are extensions of different models proposed to describe the solute redistribution that occurs during solidification of castings and single crystals.

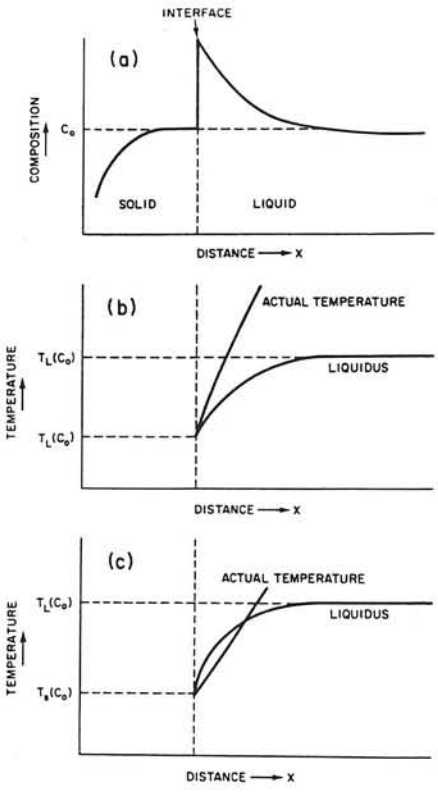

Figure 10. Development of constitutional supercooling during plane front alloy solidification: a. composition profile and solute enrichment layer ahead of steady state planar solidification, b. conditions for plane front stability, and c. condition for unstable plane front and compositional supercooling.

In describing solute redistribution under dendritic growth conditions, consideration should be given to redistribution both at the dendrite tip and in the interdendritic regions. The solute redistribution at the dendrite tip is determined, to a large extent, by the dendrite tip undercooling, which is made up of four components: thermal undercooling, kinetic undercooling, constitutional undercooling, and undercooling due to tip curvature. In welding, the first two contributions can be ignored. However, since the microstructures are much finer in scale in welds than in castings, the contribution to the total tip undercooling due to the curvature effect is very significant [7]. The effect of increased undercooling at the dendrite tips would be to solidify at a composition closer to the overall alloy composition and thus reduce the extent of microsegregation. Dendrite tip undercoolings in welds have been estimated by measuring core compositions in two different alloy systems, Al-Cu and Fe-Nb after GTA welding [51]. The estimated dendrite tip undercoolings have been found to be significant. Considering the solute redistribution in the interdendritic regions, it may

be sufficient to extend the solidification model for microsegregation in castings to welds. The model based on Case II solidification described earlier is more appropriate than a Case III model for descending microsegregation in welds. The composition of the solid is given by the Scheil equation [52]. This equation was further modified to account for diffusion in the solid during solidification [53,54]. This particular model was used by Brooks and Baskes to describe microsegregation in Al-Cu and Fe-Nb welds.

d. Grain structure

As mentioned earlier, growth often occurs by epitaxial growth from the partially melted grains in the base metal. Therefore the FZ grain structure is predominately determined by the base metal grain structure and the welding conditions. In addition, crystallographic effects can have a strong influence on the development of the grain structure. Crystallographic effects will influence grain growth by favoring the growth along particular crystallographic direction, namely the easy growth direction [42,55]. For cubic metals, the easy growth directions are <100>. Conditions for growth are optimum when one of the easy growth directions coincides with the heat flow direction. Welding conditions and heat flow significantly influence the FZ grain structure, in that they determine the weld pool shape and the heat flow directions..

Since the solid/liquid interface is essentially perpendicular to the heat flow direction, the pool shape influences the optimum growth direction. Recent work [9-11] has examined the effect of growth crystallography and dendrite selection process on the development of FZ microstructures using Fe-15Ni-15Cr alloy single crystals. A geometrical analysis has been developed that provides a three-dimensional relationship between travel speed, solidification velocity and dendrite growth velocity. The results of these calculations for two welds of two different orientations are shown in Figure 11. The two angles, θ and ϕ, are used to describe the solidification front orientation, and hence the weld pool shape. The range, in terms of θ and ϕ, over which different dendrite growth directions are stable are shown. Also shown are the dendrite growth velocities, normalized in the welding speed. These relationships have been used to analyze and explain the microstructural features of Fe-15Ni-15Cr alloy single crystal welds. Also from the observed dendritic arrangements, a three-dimensional reconstruction of the weld pool is possible, as shown in Figure 12. This analysis has been extended to evaluate the competitive dendritic growth behavior in bicrystal welds [56].

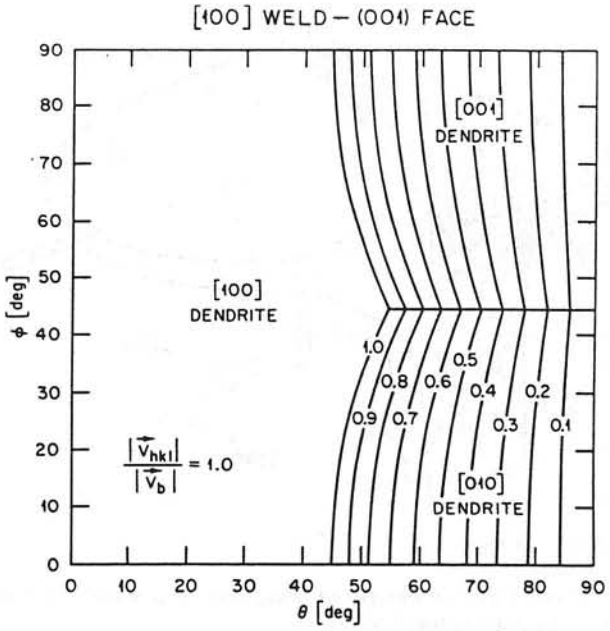

Figure 11. a. Velocity isopleth map of the minimum dendrite tip velocity $|V_{hkl}|$, normalized to the beam velocity $|V_b|$, as a function of the orientation angles θ and ϕ of the solidification front normal n for a weld in the [100] direction. Only half of the weld pool is represented. $0 \leq \phi \leq 90°$.

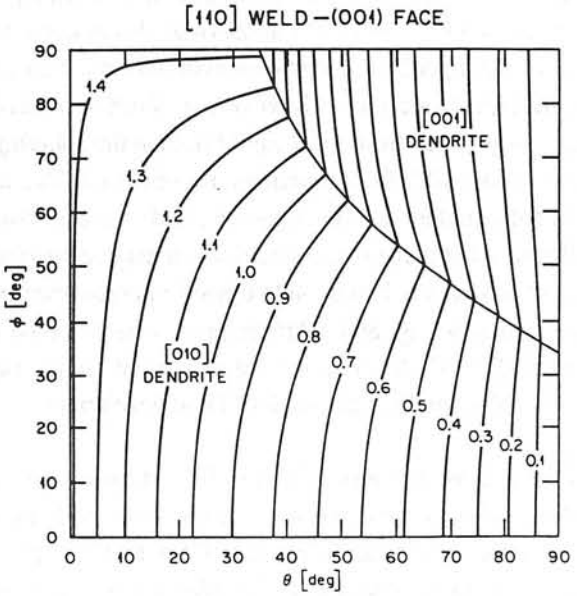

b. Isopleth map of the minimum dendrite tip velocity $|V_{hkl}|$, normalized to the beam velocity $|V_b|$, as a function of the orientation angles θ and ϕ of the solidification front normal n for a weld in the [110] direction. Only half of the weld pool is represented. $0 \leq \phi \leq 90°$.

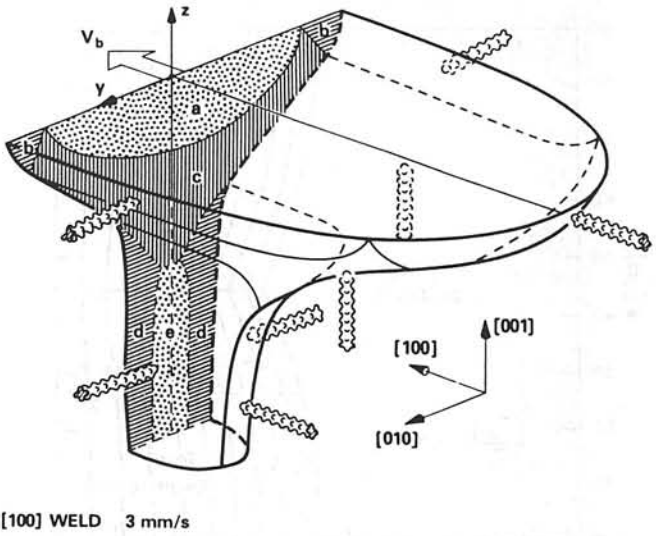

Figure 12. Reconstructed three dimensional diagram of a weld pool showing the development of weld microstructural features.

e. Rapid solidification effects

Depending on the process, weld metal cooling rate may vary from 10 to 10^3 °C/sec for conventional welding processes such as submerged arc (SA), gas tungsten arc (GTA) and electroslag welding from 10^3 to 10^6 °C/sec for high energy density processes such as laser and electron beam welding. In all of the previous discussions describing the solidification behavior of weld pool, an underlying assumption is that equilibrium is maintained at the solid/liquid interface. However, in situations involving rapid solidification, significant departures from local equilibrium at the solid/liquid interface may occur. As a result, nonequilibrium structures are obtained. The magnitude of these departures is not fully understood and characterized. Another consequence of rapid solidification effects is that plane front solidification may become stable at rapid growth rates. Significant progress is being made toward interrelating heat extraction rate to nucleation rate, undercooling, and solute trapping effects in the formation of unique microstructures [57-59]. Weld pool solidification under rapid cooling conditions needs to be examined in the light of all of these developments.

Recent work by several investigators [58–63] has shown that, under rapid solidification conditions such as those present during laser welding or even EB welding, metastable microstructures can be produced. Such observations have been made on rapidly solidified stainless steel welds. A wide variety of steel compositions has been examined, and the effect of laser welding on the resultant microstructures clearly demonstrates many of the structural modifications possible under rapid cooling conditions. The effects are related to both rapid solidification and suppression of solid

state transformation during post solidification cooling.

Summary

This paper describes our current understanding of the weld pool phenomena. The interaction of the heat source with the metal during welding affects the fluid flow, heat transfer and mass transfer in the weld pool and the solidification behavior of the weld metal. It is clear that much progress has been made in our fundamental understanding of the weld pool phenomena. However, considerable work still needs to be performed in our fundamental understanding of the weld pool phenomena, modeling and experimental verification of these models.

Acknowledgment

The authors gratefully acknowledge Dr. S. Babu and R. Prader for reviewing the manuscript. This research was sponsored by the Division of Materials Sciences, U. S. Department of Energy, under contract DE-AC05-84OR21400 with Martin Marietta Energy Systems, Inc.

References

1. G. M. Oreper and J. Szekely, *J. Fluid Mech.*, 147, 53 (1984).
2. S. Kou and Y. Le, *Metall. Trans*, 14A, 2243 (1983).
3. J. Szekely, 'Advances in Welding Science and Technology,' Ed. S. A- David, 3, ASM International (1987).
4. A. Paul and T. DebRoy, 'Advances in Welding Science and Technology,' Ed. S. A. David, 29, ASM International (1987).
5. C. Chan, J. Mazumder, and M.M. Chen, *Metall.Trans.*, 15A, 2175 (1984).
6. T. Zacharia, S.A. David, J.M. Vitek, and T. DebRoy, *Metall. Trans.*, 20A, 957 (1989).
7. S.A. David and J.M. Vitek, *Intl. Materials Rev.*, 34 (5), 213 (1989).
8. S.A. David and T. DebRoy, *Science,* 257, 497-502 (1992).
9. M. Rappaz, S.A. David, J. M. Vitek and L.A. Boatner, *Metall. Trans. A.*, 20A, 1125-38 (1989).
10. M. Rappaz, S.A. David, J. M. Vitek and L.A. Boatner, *Metall. Trans. A.*, 21A, 1767-82 (1990).
11. S.A. David, J.M. Vitek, M. Rappaz, and L.A. Boatner, *Metall. Trans. A.*, 21A, 1753-66 (1990).
12. T. DebRoy, 'Interfacial Phenomena in the Numerical Analysis of Weldability,' presented at the Proceedings of the Second International Seminar on Numerical Analysis of Weldability, H. Cerjak, Ed., 10-11 May 1993.
13. P. Sahoo, T. DebRoy and M.J. McNallan, *Metall. Trans.*, 22B, 483-491 (1988).
14. K. Mundra and T. DebRoy, unpublished research, Department of Materials Science and Engineering, Penn. State University, University Park, PA, 1993.
15. S. Kou and Y. H. Wang, *Weld. J.*, 65 (3), 63s (1986).
16. E. Friedman, *Weld. J.*, 57, 161s (1978).
17. A. Paul and T. DebRoy, *Metall. Trans.* B., 19B, 851-858 (1988).
18. T. Zacharia, A.H. Eraslan and D.K. Aidun, *Weld. J.*, 67, 53s-62s (1988).
19. T. Zacharia, S.A. David, and J.M. Vitek, 'International Trends in Welding Science and Technology' Eds. S.A. David and J.M. Vitek, 27, ASM International, Materials Park, Ohio (1993).
20. V.A. Batanov, F.V. Bunkin, A.M. Prokhovov and V.B. Fedorov, Soviet Physics -*JETP*, 36,311–322 (1973).
21. C.J. Knight, *AIAA Journal,* 17, 519–523 (1979).
22. C.L. Chan and J. Mazumder, *J. Appl. Phy.*, 62, 4579-4586 (1987).

23. P.A.A. Khan and T. DebRoy, *Metall. Trans. B.*, 15B, 641–644 (1984).
24. T. DebRoy, S. Basu and K. Mundra, *J. Appl. Phys.*, 70, 1313–1319 (1991).
25. M.M. Collur, A. Paul and T. DebRoy, *Metall. Trans. B.*, 1813, 733–740 (1987).
26. P.A.A. Khan, T. DebRoy and S.A. David, *Weld. J.*, 67, 1s–7s (1988).
27. K. Mundra and T. DebRoy, *Weld. J.*, 72 (1), 1s–9s (1993).
28. K Mundra and T. DebRoy, *Metall. Trans. B.*, 24B, 145–155 (1993).
29. R. Miller and T. DebRoy, *J. Appl. Phy.*, 68, 2045–2050 (1990).
30. G.J. Dunn, C.D. Allemand and T.W. Eagar, *Metall. Trans. A.*, 17A, 1851–1863 (1986).
31. R.D. Pelhke, *Unit Processes in Extractive Metallurgy*, Elsevier, New York (1979).
32. A. Banerjee, T. DebRoy, C. Onneby and M. Small, 'International Trends in Welding Science and Technology,' S.A. David and J. Vitek, Eds., ASM International, Materials Park, OH, 39–44 (1993).
33. C.S. Chan and T.W. Eagar, *Weld. J.*, 59, 93s (1980).
34. C.S. Chan and T.W. Eagar, *Metall. Trans. B.*, 12B, 539–47 (1981).
35. J.E. Indacochea, M. Blander, N. Christensen and D.L. Olson, *Metall. Trans. B.*, 16B, 237–45 (1985).
36. S. Kou, 'Welding Metallurgy,' John Wiley and Sons, New York, 61–63 (1987).
37. S.A. Gedeon and T.W. Eagar, *Weld. J.*, 69, 264s–271s (1990).
38. M. Uda and S. Ohno, Trans. *Nat. Res. Inst. Metals*, 15, 20–28 (1973).
39. A. Bandopadhyay, A. Banerjee and T. DebRoy, *Metall. Trans. B.*, 23B, 207–214 (1992).
40. W.F. Savage, *Weld World*, 18, 89 (1980).
41. G.J. Davies and J.G. Garland, *Int. Met. Rev.*, 10, 83 (1975).
42. M.C. Flemings, 'Solidification Processing,' New York, McGraw–Hill (1974).
43. W. Kurz and D.J. Fisher, 'Fundamentals of Solidification,' Aedermannsdorf, Switzerland, Trans. Tech. Publications (1986).
44. H. Biloni, 'Physical Metallurgy, Part I,' 478, R.W. Cahn and P. Haasen, eds. Elsevier, New York (1983).
45. W.W. Mullins and R.F. Sekerka, *J. Appl. Phys.*, 35, 444 (1964).
46. R. Trivedi, *Acta Metall.*, 18, 287 (1970).
47. W. Kurz and D.J. Fisher, *Acta Metall.*, 29, 11 (1981).
48. W. Kurz, B. Giovanola, and R. Trivedi, *Acta Metall.*, 34, 823 (1986).
49. R. Trivedi and W. Kurz, *Acta Metall.*, 34, 1663 (1986).
50. J.S. Langer and H. Muller–Krumbhaar, *Acta Metall.*, 26, 1681 (1978).
51. J.A. Brooks and M.I. Baskes, 'Advances in Welding Science and Technology,' 93, ed. S.A. David, Metals Park, OH, ASM International (1987).
52. E. Scheil, *Z. Metall.*, 34, 70 (1942).
53. D.H. Brody and M.C. Flemings, *Trans. AIME*, 236, 615 (1966).
54. W. Kurz and W. Clyne, Metall. Trans., 12A, 965 (1981).
55. W.F. Savage, C.D. Lundin and A. Aronson, *Weld. J.*, 44, 175 (1965).
56. J.M. Vitek, S.A. David, L.A. Boatner and M. Rappaz, 'International Trends in Welding Science and Technology,' eds. S.A. David and J.M. Vitek, 167, ASM International, Materials Park, Ohio (1993).
57. M.J. Aziz, *J. Appl. Phys.*, 53, 1158 (1982).
58. S.A. David and J.M. Vitek, 'Lasers in Metallurgy,' 2247–554, K Mukherjee and J. Mazumder, Warrendale, PA (1981).
59. J.M. Vitek, A. DasGupta, and S.A. David, *Metall. Trans. A.*, 14A, 1833–41 (1983).
60. S.A. David, J.M. Vitek, and T.L. Hebble, *Weld. J.*, 66 (1), 289s (1987).
61. S. Katayama and A. Matsunawa, *Proc. ICALEO*, 60–67 (1984).
62. J.W. Elmer, S.M. Allen, and T.W. Eagar, *Metall. Trans. A.*, 2117–131 (1989).
63. J.A. Brooks, M.I. Baskes, and F.A. Greulich, *Metall. Trans. B.*, 915–24 (1991).

This volume contains the papers presented at a seminar held in honour of Prof. J.F. Lancaster on 1 September 1993 in order to mark the occasion of his retirement as Chairman of Study Group 212 (Physics of Welding) of the International Institute of Welding.

Prof. Lancaster was Chairman of Study Group 212 from 1965 to 1992.
During the long period of his chairmanship he was the driving force behind the many activities of the Study Group. He organised numerous meetings, stimulated many discussions on a variety of topics within the area of physics of welding and succeeded in bringing and keeping together a group of experts in the field from many different countries. He made Study Group 212 what it is today: a unique scientific forum for the physics of welding.

The members of Study Group 212 offer this volume to Prof. Lancaster in recognition of his stimulating activities in the field of physics of welding over a period of many years.

ISBN 90 6562 149 0
Delftse Uitgevers Maatschappij